Wegener Center for Climate and Global Change
University of Graz

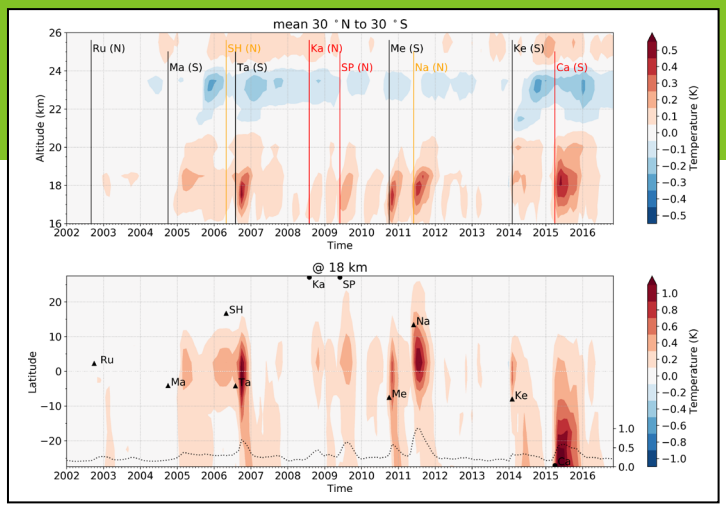

Scientific Report No. 86-2020

Signals of recent volcanic eruptions in vertically resolved atmospheric temperature

Matthias Stocker

May 2020

Financially supported by

The **Wegener Center for Climate and Global Change** is an interdisciplinary, internationally recognized research and graduate education institute of the University of Graz that is pooling the University's expertise in Climate, Environmental and Global Change. It brings together research teams and scientists from fields such as geophysics and climate physics, meteorology, economics, geography, and regional sciences. At the same time close links are maintained and further developed with many national and international cooperation partners. The research interests range from monitoring, analysis, and modeling of climate and environmental change to the investigation of climate change impacts and the analysis of the human dimensions of these changes related to mitigation, adaptation, and loss&damage. (more information at www.wegcenter.at)

This report is the result of a Master thesis work completed in March 2020.

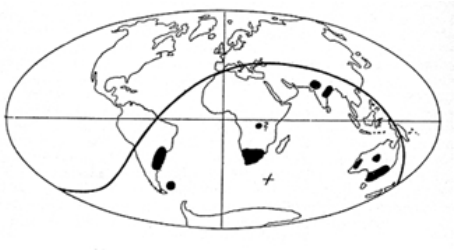

Alfred Wegener (1880–1930), after whom the Wegener Center is named, was founding holder of the University of Graz Geophysics Chair (1924–1930). In his work in the fields of geophysics, meteorology, and climatology he was a brilliant scientist and scholar, thinking and acting in an interdisciplinary way, far ahead of his time with this style. The way of his ground-breaking research on continental drift is a shining role model – his sketch on the relations of continents based on traces of an ice age about 300 million years ago (left) as basis for the Wegener Center Logo is thus a continuous encouragement to explore equally innovative ways:
paths emerge in that we walk them (Motto of the Wegener Center).

Wegener Center Verlag • Graz, Austria

ISBN 978-3-9504717-5-5

May 2020

Contact: Matthias Stocker
matthias.stocker@sbg.at

Wegener Center for Climate and Global Change
University of Graz
Brandhofgasse 5
A-8010 Graz, Austria
www.wegcenter.at

Master thesis
to obtain the degree Master of Sciences
at the University of Graz

Signals of recent volcanic eruptions in vertically resolved atmospheric temperature

STOCKER Matthias, BSc

March 20, 2020
Edited: May 26, 2020

Supervisor
Assoc. Prof. Mag. Dr. Andrea K. Steiner
Co-Supervisor
Mag. Dr. Florian Ladstädter

Wegener Center for Climate and Global Change, Austria
University of Graz, Austria

This thesis was submitted in March 2020 and edited in May 2020. Minor changes have been made to the figure captions in Part III, Ch. 5 to make them more specific.

Abstract

Explosive volcanic eruptions, such as Pinatubo in 1991, can inject sulfur dioxide, ash and other aerosols into the stratosphere causing temperature changes and affecting climate in the short term. Recently, also small post-2000 volcanic eruptions and their effects have come into research focus. While the effects of large eruptions are relatively well known, the impacts of smaller eruptions are hard to quantify because their signals are easily masked by natural variability.

In this thesis, the temperature signals from small volcanic eruptions between 2002 and 2016 are quantified, by using new vertically resolved aerosol data and precise temperature observations from radio occultation. Applying regression analysis, we find that conventional indices used to account for natural variability, such as the El Niño–Southern Oscillation and the Quasi-Biennial Oscillation, leave large temperature residuals. This further complicates a precise quantification of the small volcanic temperature signals.

Therefore, we use here novel variability indices, which are vertically resolved and derived directly from radio occultation temperature. Additionally, we account for collinearity between these indices and the aerosol index for a precise quantification of the volcanic temperature signals.

Results show characteristic space-time signals that can be clearly associated with specific volcanic eruptions. In the lower stratosphere, robust warming signals are observed, while in the mid-stratosphere also cooling signals of some eruptions appear, possibly from upwelling of ozone poor air. We find that the volcanic contribution to the stratospheric temperature trend 2002 to 2016 is up to 20%, depending on latitude and altitude. Therefore, we conclude that detailed knowledge of the vertical structure of volcanic temperature impacts is crucial for comprehensive trend analysis in order to separate natural from anthropogenic driven temperature changes.

Zusammenfassung

Explosive Vulkanausbrüche, wie des Pinatubo 1991, können Schwefeldioxid, Asche und andere Aerosole bis in die Stratosphäre einbringen und Temperaturänderungen verursachen sowie das Klima kurzfristig beeinflussen. Seit Kurzem stehen auch die Auswirkungen kleiner Vulkanausbrüche, die sich seit dem Jahr 2000 ereignet haben, im Fokus der Forschung. Während die Auswirkungen großer Eruptionen vergleichsweise gut erforscht sind, sind jene kleinerer Eruptionen nur schwer zu quantifizieren, da ihre Signale oft durch natürliche Variabilität überlagert werden.

In dieser Arbeit werden die Temperatursignale kleinerer Vulkanausbrüche zwischen 2002 und 2016 anhand von neuen, vertikal aufgelösten, Aerosoldaten und präzisen Temperaturbeobachtungen aus der Radio-Okkultation detektiert. Mittels Regressionsanalyse wurde festgestellt, dass bei Verwendung konventioneller Indizes zur Charakterisierung der natürlichen Variabilität, wie El Niño–Southern Oscillation und Quasi-Biennale Oszillation, ein großes Residuum bleibt. Dies erschwert eine genaue Quantifizierung der vulkanischen Temperatursignale.

Daher werden in dieser Arbeit neue, vertikal aufgelöste, Variabilitätsindizes verwendet, welche direkt aus den Temperaturmessungen berechnet werden. Auch wird die Kollinearität zwischen diesen Indizes und den Aerosolen berücksichtigt zur genauen Quantifizierung der vulkanischen Temperatursignale

Unsere Ergebnisse zeigen charakteristische Signale im Temperaturfeld, welche eindeutig Vulkanausbrüchen zugeordnet werden können. In der unteren Stratosphäre detektieren wir robuste Erwärmungssignale während in der mittleren Stratosphäre auch Abkühlungssignale nach bestimmten Eruptionen auftreten. Der Temperaturtrend in der unteren Stratosphäre wird im Zeitraum von 2002 bis 2016 durch Vulkanausbrüche um bis zu 20% beeinflusst. Daraus schließen wir, dass für eine umfassende Analyse von Klimatrends auch der Einfluss von kleinen Vulkanen miteinbezogen werden muss.

Acknowledgments

First of all I would like to express my sincere gratitude to my supervisor, Assoc. Prof. Mag. Dr. Andrea Steiner, for giving guidance and support but also for her patience throughout the course of this thesis. She made it possible for me to pursue my own ideas, but led me in the right direction whenever this was necessary. I really appreciate that Prof. Steiner's office door was open any time I needed advice. I have greatly benefited from her broad experience and expertise.

I would like to extend my sincere gratitude to my co-supervisor, Mag. Dr. Florian Ladstädter, for all the instructive discussions, insightful comments and constructive feedback. I very much appreciate that he was always willing to listen to all of my questions. Thank you Andrea and Florian, I really enjoyed the working atmosphere!

Many thanks to Hallgeir Wilhelmsen for all the informative conversations and the useful programming advice. Furthermore, I honestly thank the whole Wegener Center for Climate and Global Change (WEGC) team who kindly assisted and supported me in many ways.

I am also grateful to the WEGC EOPAC team for providing the OPSv5.6 RO data and also the NASA Langley Research Center Atmospheric Sciences Data Center for providing the GloSSAC aerosol data, which formed the basis for this thesis. The Austrian Science Fund (FWF) is acknowledged for the financial support under Research Grant P27724-NBL (VERTICLIM).

A special thank you goes to my office colleagues Patrick, Veronika, Max, Florian, Stefanie and Melissa for all the fun discussions and small-talk which made the office an enjoyable workplace.

Last but not least I am particularly grateful to my parents Vera and Gottfried for their kind support and encouragement over the years.

Contents

Preface

This master thesis is based on the following peer-reviewed publication as well as on additional results that were generated during the research process but not published.

Stocker, M., Ladstädter, F., Wilhelmsen, H., & Steiner, A. K. (2019).“Quantifying Stratospheric Temperature Signals and Climate Imprints From Post-2000 Volcanic Eruptions”. *Geophysical Research Letters*, 46, pp. 12,486–12,494. DOI: 10.1029/2019GL084396

Part I introduces the research topic and communicates necessary background knowledge. Additionally, an overview on used methods and data sets is provided. This part ends with an overview and discussion of the main results. Part II presents the main research results in form of a published paper. Supplementary results not published are presented in Part III. Acronyms, figures and tables along with the bibliography are provided at the end of this thesis.

Part I.

Synopsis

1. Introduction

Volcanism has influenced Earth's shape on many timescales and was one of the key processes involved in the evolution of the atmosphere (Kasting and Catling 2003; Mather 2015). Massive eruptions such as that of the Tambora in 1815 or the Krakatoa in 1883 caused far reaching devastation and changed climate on a global scale (Wirakusumah and Rachmat 2017; Schaller et al. 2009). Following the Tambora, which was the largest eruption humans have ever experienced, global temperatures dropped by about 2.5 °C and in some places even by 10 °C. This caused the year 1816 to be the year without summer, leading to food shortages and epidemics all over Europe and the United States (Wirakusumah and Rachmat 2017).

Volcanic activity is an ongoing geophysical process and its effects have to be taken into account whenever the climate system is assessed. Major eruptions such as that of El Chichón in 1982 and Pinatubo in 1991 are known to have substantially affected tropospheric as well as stratospheric temperature, dynamics, and chemistry (Randel et al. 2009; Free and Seidel 2009; Aquila et al. 2013).

More recently smaller eruptions have also become of research interest as they most likely led to a steady increase in stratospheric Aerosol Optical Depth (AOD) during the last decade (Vernier et al. 2011). They have also been found to substantially affect stratospheric temperature (Mehta et al. 2015; Biondi et al. 2017) and a contribution of those eruptions to the 21st century warming hiatus has also been discussed (Santer et al. 2015).

In the troposphere, it is the volcanic ash that causes local weather changes (Robock 2015). In the stratosphere, sulfate aerosols formed by volcanic emissions absorb and back-scatter solar radiation and affect surface temperature as well as stratospheric temperature and dynamics (Robock 2000; Aquila et al. 2013).

This study aims to quantify signals from small post-2000 volcanic eruptions and to clarify their role in the temperature variability of the upper troposphere and lower stratosphere. This is done using the potential of newly available vertically resolved aerosol data (Thomason 2017) in combination with precise temperature observations from radio occultation.

The knowledge gained can help to distinguish between anthropogenic and natural influences on temperature variability more effectively. It can also contribute to the validation and further improvement of climate models. Moreover the insights can give a better understanding of how stratospheric geoengineering would affect stratospheric temperature and dynamics.

Chapter 2 provides an overview of the atmospheric structure and introduces main atmospheric variability modes. A discussion of how volcanic aerosol emissions

interact with the climate system is given in Ch. 3. This is followed by a description of the data sets used (Ch. 4) and the methods applied (Ch. 5) to determine the volcanic temperature imprints. A summary and concluding remarks are given in Ch. 6. In Part II the main results of this thesis are presented in form of a peer reviewed publication. Finally, supplementary results not published are presented in Part III.

2. Atmospheric Structure and Dynamics

This chapter provides a brief overview of the atmospheric structure and of major atmospheric variability modes. Since the different phenomena are fairly complex, only the basic concepts as well as aspects relevant for this study are discussed. However, interested readers can find detailed information in the literature cited (in particular review papers).

2.1. The Structure of the Atmosphere

The atmosphere's thickness corresponds to only 1% of the Earth's radius and it developed around 400 million years ago as we experience it today (Barry et al. 2004). Atmospheric dry air consists of 99% nitrogen and oxygen. Less than 1% is composed of climate-relevant components such as greenhouse gases and reactive gases such as nitrogen and sulfur species (Barry et al. 2004). With the exception of ozone and water vapour all of the gaseous components are relatively well mixed up to a height of approximately 80 km to 100 km. This is why this part of the atmosphere is also called the homosphere (Barry et al. 2004). In addition to the gaseous components the atmosphere also contains small particles known as aerosols which will be further discussed in Sect. 3.1.

On the basis of the vertical temperature gradient the atmosphere can be separated into four layers, which are referred to as troposphere, stratosphere, mesosphere and thermosphere (see Fig. 2.1).

The troposphere, which contains about 75% of the total atmospheric mass, is characterized by a strong decrease in temperature with altitude (about $6.5\,\mathrm{K\,km^{-1}}$) (Barry et al. 2004). Most of the atmospheric water is located in the troposphere, which in connection with strong vertical winds leads to cloud formation and precipitation (Kraus 2004). The upper limit of the troposphere is called the tropopause and is commonly determined either as the altitude where the temperature is minimal (cold point tropopause) or the lapse rate is reduced to $2\,\mathrm{K\,km^{-1}}$ (World Meteorological Organization (WMO) definition for the laps rate tropopause). Depending on the latitude and season it is located at a height of approximately 17 km in the tropics and 8 km in polar regions. Especially in the tropics the tropopause can also be seen as a transition layer to the stratosphere (tropical tropopause layer TTL) which has characteristics of both, stratosphere and troposphere (Fueglistaler et al. 2009).

In contrast to the troposphere, the stratosphere contains only 10% of the atmospheric mass. However, it holds most of the stratospheric ozone, which absorbs UV radiation and leads to an increase in temperature with increasing

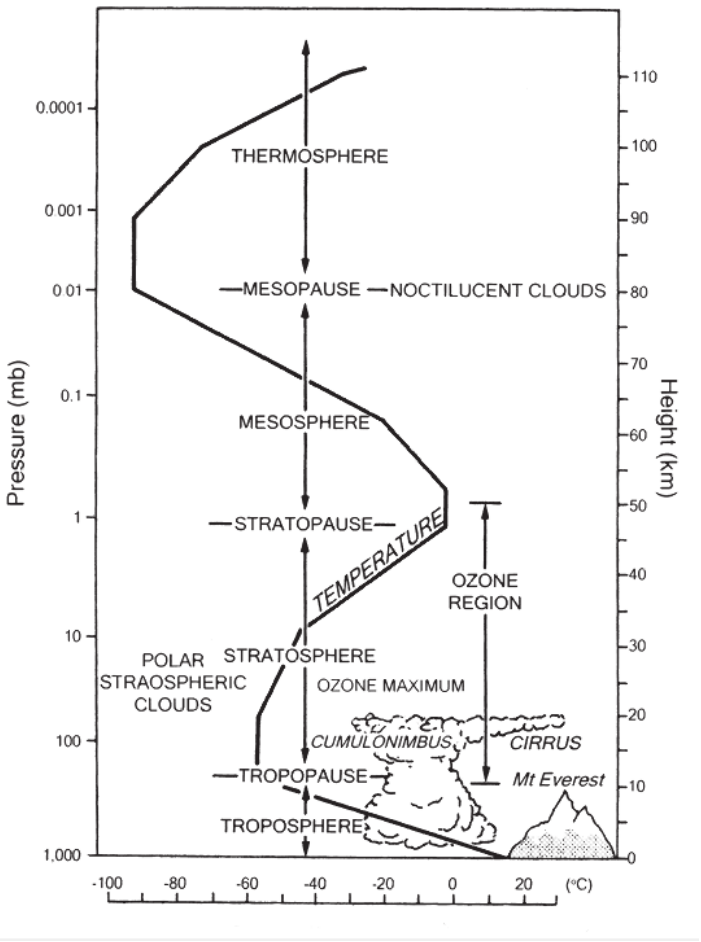

Figure 2.1.: Vertical structure of the Earth's atmosphere as a function of temperature. Adapted from Barry et al. (2004).

altitude. Maximum temperature is reached at the stratopause at an altitude of approximately 50 km. Since there is little water present in the stratosphere only few clouds such as nacreous clouds appear (Kraus 2004; Barry et al. 2004).

Above the stratosphere is the mesosphere, where temperatures begin to drop again until with approximately 140 K the lowest temperature in the atmosphere is reached at the mesopause. The mesopause marks the upper limit of the homosphere (Kraus 2004; Barry et al. 2004).

In the mesosphere the temperature increases again due to the absorption of extreme UV radiation by molecular and atomic nitrogen and oxygen. The upper mesosphere and lower thermosphere region is also known as ionosphere, where cosmic rays, X-rays and UV radiation cause photoionization (Seinfeld and Pandis 1997; Barry et al. 2004).

2.2. El Niño–Southern Oscillation (ENSO)

The El Niño–Southern Oscillation (ENSO) has its origin in the southern Pacific and represents one of the most prominent variability modes affecting climate on a global scale (Scaife et al. 2019).

As shown in Fig. 2.2, basically three phases of the ENSO can be distinguished. During regular years trade winds blowing from the east bring warm surface water off the coast of Southeast Asia, which leads to an east-west gradient in the sea surface temperature and also in the sea surface pressure. This pressure difference leads, seen from the south, to a clockwise zonal circulation, known as Walker circulation, which causes convective activity in the western Pacific and maintains the easterly trade winds. Depending on the change in condition, deviations from this regular state are called El Niño or La Niña and take place irregularly in cycles of 2 to 7 years. During La Niña more warm water is dammed up in Southeast Asia due to stronger trade winds, causing a stronger temperature gradient and a further increase in the regular circulation pattern. El Niño, in contrast, is characterized by a warmer surface water in the eastern Pacific causing a lower temperature gradient and weaker trade winds. This change in the regular circulation pattern, in turn, leads to strong convective activity in the central and eastern Pacific region. (Scaife et al. 2019; Domeisen et al. 2019)

One of the most common proxies used to account for this ENSO variability is the Niño 3.4 index, which is defined as the 5 month running mean Sea Surface Temperature (SST) anomalies in the Pacific region from 5°N to 5°S and 170°W to 120°W (Trenberth 2020; Domeisen et al. 2019). Positive SST anomalies account for El Niño and negative for La Niña signals, provided they are 0.4 K above or below the long-term mean over a period of at least 6 months (Trenberth 2020).

ENSO events have been found to significantly alter tropospheric weather, rainfall patterns and temperatures even outside the tropical region (Timmermann et al. 2018). Those remote interactions are know as teleconnections which can even reach the stratosphere (Domeisen et al. 2019). For instance Free and Seidel (2009)

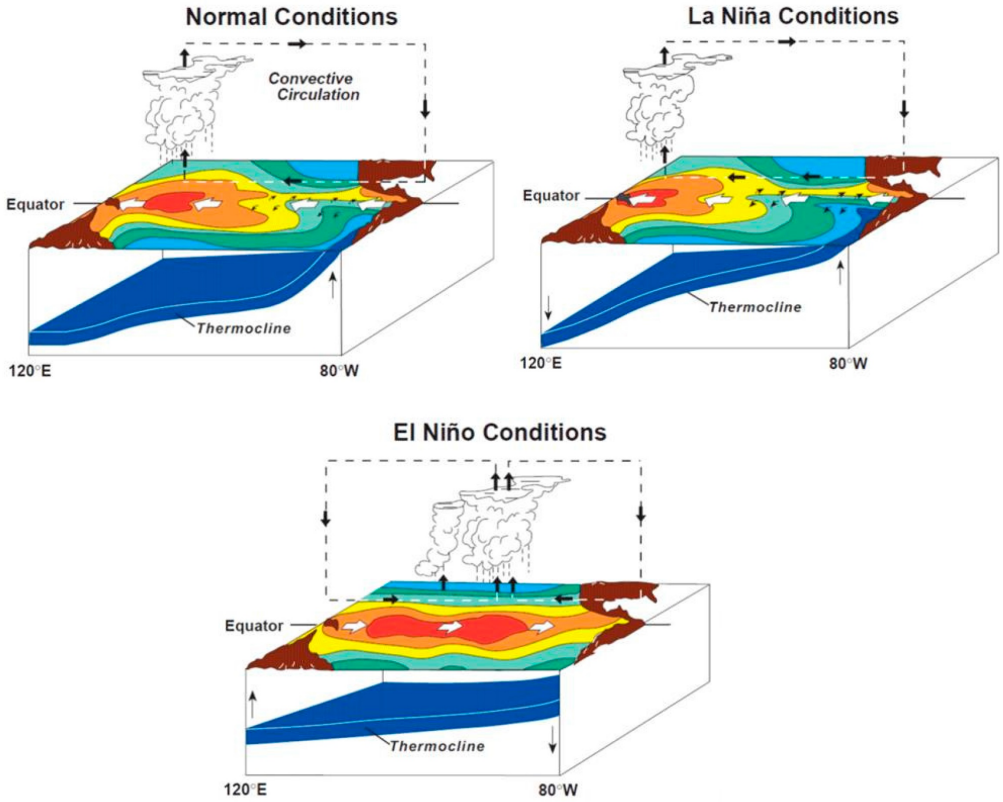

Figure 2.2.: Schematic illustration of the different ENSO phases. Adapted from Scaife et al. (2019). Licensed under CC BY 4.0.

observed that, besides a comparatively warm troposphere during El Niño, the tropical lower stratosphere is cooled while the polar stratosphere is warmed. By influencing the tropical convection, the ENSO additionally affects the generation of atmospheric waves, which have been found to alter the phases of the Quasi-Biennial Oscillation (QBO) as well as the strength of the Brewer–Dobson Circulation (BDC). Especially El Niño signals appear to have a strengthening effect on the BDC. This affects the ozone concentration in the lower stratosphere and hence can also be an explanation for the observed ENSO induced temperature changes (Domeisen et al. 2019, & references therein).

2.3. The Quasi-Biennial Oscillation (QBO)

While ENSO is the leading variability mode in the troposphere the variability in the tropical stratosphere is dominated by a downward propagating wind pattern known as QBO.

Observation of the volcanic cloud after the eruption of the Krakatoa in 1883 led to the conclusion that constant easterly winds must be dominant in the stratosphere. However, in the 1950s, radiosonde data revealed that in the stratosphere a pattern oscillating between easterly and westerly winds prevails, which moves from the mid stratosphere towards the tropopause with a speed of approximately 1 km per month (Baldwin et al. 2001). The oscillation is called quasi-biennal since one full period takes approximately 28 months (Baldwin et al. 2001).

The occurrence of the QBO can be explained by a broad range of vertically propagating waves (gravity, inertia-gravity, Rossby-gravity, Kelvin), which originate in the troposphere and transport momentum (both, easterly and westerly) to the stratosphere. These waves break in the transition zones between the winds and cause the wind maxima to move downwards (Geller et al. 2016; Baldwin et al. 2001).

In general, the easterly winds are stronger, while the westerlies propagate downwards faster. Near the tropopause the westerly phase is prolonged while at higher altitudes it is the other way round (Naujokat 1986). The leading QBO signal is pronounced around the equator from approximately 12°N to 12°S. Additional out of phase signals can be observed at higher latitudes in both hemispheres (Baldwin et al. 2001).

The transitions from easterly to westerly wind are called westerly shear and are accompanied by positive temperature anomalies, while the transitions from westerly to easterly (easterly shear) are characterized by negative temperature anomalies (Randel et al. 1999; Baldwin et al. 2001; Wilhelmsen et al. 2018).

Apart from its influence on the stratospheric temperature variability, the QBO is particularly relevant because it influences the distribution of trace gases such as ozone as well as aerosols in the stratosphere (Trepte and Hitchman 1992; Baldwin et al. 2001).

A frequently used proxy which is used to account for QBO variability are stratospheric wind speeds measured above Singapore at different pressure levels.

2.4. The Brewer-Dobson Circulation (BDC)

The BDC refers to a global circulation pattern in which air masses are transported into the tropical stratosphere, where they rise further before they are ultimately transported to high latitudes where they sink and reach the troposphere again (Butchart 2014). It is often referred to as stratospheric meridional- or mean meridional circulation and is essential for the distribution of trace gases but also aerosols (Bönisch et al. 2014; Butchart 2014). This is also reflected by the fact that the theory behind it was originally developed to explain the discrepancy between low ozone concentrations in the tropics compared to higher concentrations in the polar regions (Bönisch et al. 2014).

The BDC can be divided into two circulation branches, a shallow branch and a deep branch (Plumb 2002). The latter is driven by planetary scale waves and extends vertically into the mesosphere but has a comparatively slow and less pronounced mass flow. The lower branch, in contrast, is maintained by planetary and synoptic scale waves and carries comparatively large air masses poleward at an altitude of about 20 km to 22 km (Birner and Bönisch 2011; Bönisch et al. 2014).

In the tropical lower stratosphere, the BDC is characterized by an upwelling of air. This area is also called tropical pipe and, depending on the vertical speed of the ascending air masses, acts as a barrier that prevents the exchange of different atmospheric constituents between the tropics and subtropics (Plumb 1996; Flury et al. 2013).

As already discussed, the upwelling within the tropical pipe can be influenced by ENSO events (Domeisen et al. 2019, & references therein) but it also depends on the phase of the QBO (see Fig. 2.3).

Flury et al. (2013) investigated the influence of the QBO on the tropical pipe and lower branch of the BDC using water vapour measurements. They note that in the westerly shear zone below the westerly maximum the transport out of the tropical pipe towards higher latitudes is enhanced, while the vertical transport within the pipe is reduced. During the QBO easterly shear the process is reversed and also the mixing barrier seems to be shifted to lower altitudes.

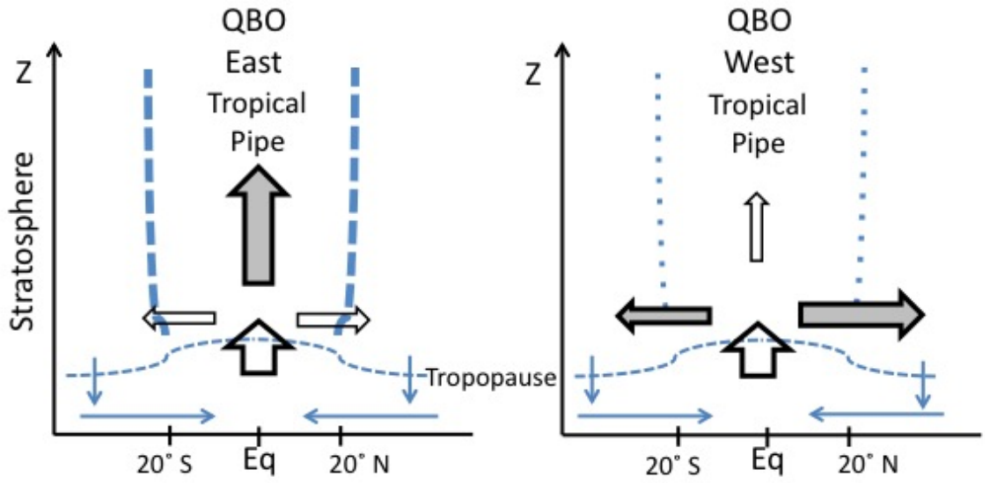

Figure 2.3.: Schematic illustration of the QBO induced changes on the BDC. Reprinted from Flury et al. (2013). Licensed under CC BY 3.0.

3. Volcanoes and Aerosols

This chapter provides an overview of how volcanic eruptions affect the climate system. Therefore, basic aerosol properties are discussed and an introduction to volcanic activity is given. Additionally, processes controlling how volcanic aerosol emissions interact with the climate system are highlighted. Although volcanic activity is a source of natural CO_2 emissions the focus of this study is on volcanic aerosols which are especially relevant in the stratosphere.

3.1. Aerosols

Aerosols and their impacts on the climate system are still among the largest uncertainties in our current understanding and quantification of climate change (Boucher et al. 2013). Aerosols are small, solid or liquid phase particles that can be of natural but also anthropogenic origin. The main anthropogenic aerosol sources are combustion of fossil-fuels, bio-fuels, biomass or human land use whereas the natural sources are sea spray caused by waves and wind, dust from deserts or organic particles from the biosphere and aerosols from volcanic eruptions. The highest aerosol concentration is found in the tropospheric boundary layer (Bourgeois et al. 2018), however, substantial amounts are also transported to the stratosphere (Boucher et al. 2013).

In the troposphere, aerosols are commonly associated with air pollution which can pose health risks (e.g. particulate matter, pollen etc.). Yet aerosols are particularly relevant for the weather system as they act as condensation nuclei, which play a key role in the formation of clouds (Boucher et al. 2013). It has been shown that aerosols from volcanic eruptions can change cloud properties, such as their ability to reflect sunlight or the rainfall pattern which controls the distribution of water resources (Rosenfeld and Woodley 2001; Boucher et al. 2013).

In the troposphere, the aerosols' lifetime is about one day to a week since most of them are easily "washed out" by rain. The stratospheric aerosols, in contrast, last up to several years (Robock 2000). The vast majority of the stratospheric aerosols are liquid phase sulfate particles, which primarily originate from natural sources such as the oceanic and terrestrial biosphere, but also volcanic eruptions (Murphy et al. 2013; Kremser et al. 2016). They are formed from precursor gases such as sulfur dioxide (SO_2) or carbonyl sulphide (OCS) and dimethyl sulfide (DMS) which are oxidized to sulfuric acid (H_2SO_4) by different processes. In the Upper Troposphere–Lower Stratosphere (UTLS) region the reaction with OH dominates and H_2SO_4 is formed within a few days to some weeks. In the presence of H_2O vapor, the gaseous H_2SO_4 ultimately forms sulfate aerosols by gas to particle

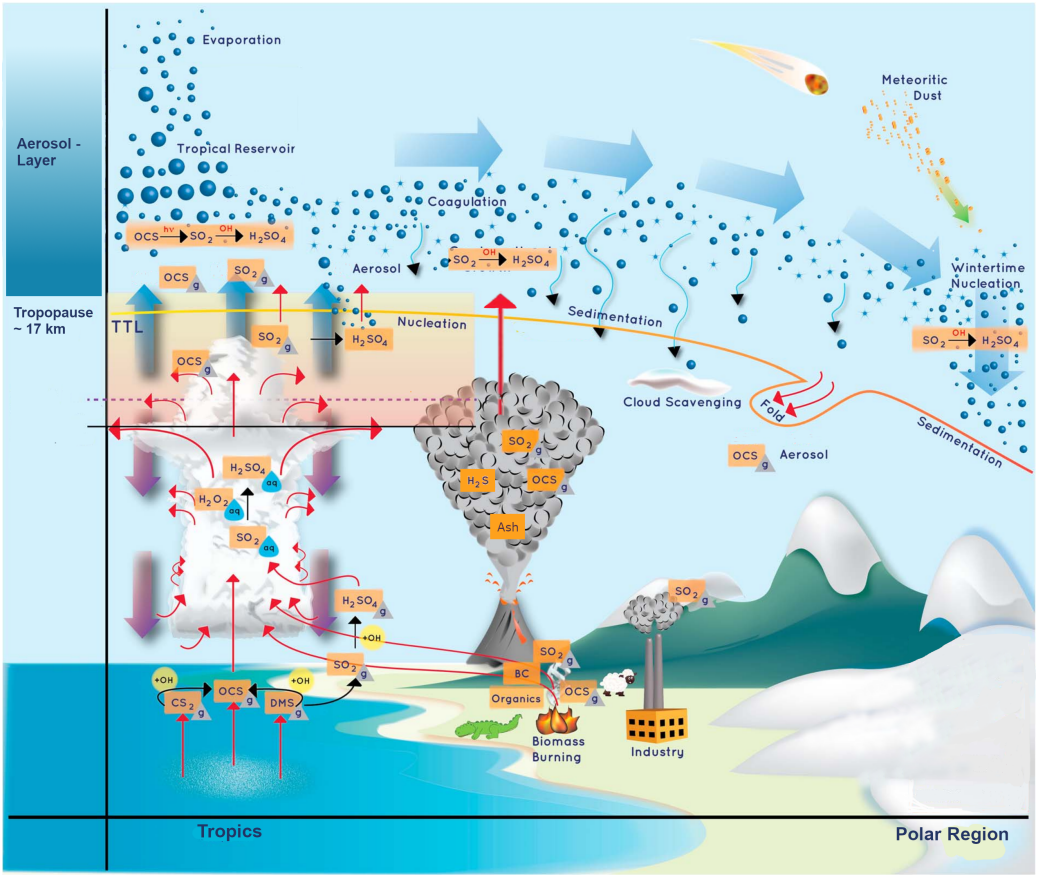

Figure 3.1.: Schematic illustration of the sulfur transport to the stratosphere as well as the processes governing the stratospheric sulfate formation and distribution. Adapted from Kremser et al. (2016).

conversion (binary homogeneous nucleation) (Kremser et al. 2016; Langmann 2014; Pitari et al. 2016; Mirabel and Jaecker-Voirol 1988).

Tropospheric OCS and DMS, which are mainly released by the oceans, as well as the non-volcanic SO_2 and some tropospheric aerosols, reach the stratosphere by slow radiative driven ascent across the tropical tropopause. Sometimes they are also directly injected by overshooting clouds such as pyrocumulonimbus clouds that form above forest fires (Kremser et al. 2016; Murphy et al. 2013; Barkley et al. 2008; Vernier et al. 2009).

During volcanically quiescent periods OCS/DMS and non-volcanic SO_2 are relevant sources of stratospheric sulfur. In volcanically active periods, eruptions that emit SO_2 and to a lesser extent H_2S directly to the stratosphere clearly dominate the stratospheric sulfate formation (Kremser et al. 2016).

In the lowermost stratosphere, to some extent, other particles which originate in the troposphere are also relevant. Other species such as dust from meteorites, soot or black carbon (from e.g. biomass burning) and volcanic ash are also present,

however, only in small quantities and most of them are quickly removed by sedimentation (Murphy et al. 2013). An overview of the sulfate formation and transport within the troposphere and stratosphere is given in Fig. 3.1.

3.1.1. The Stratospheric Aerosol Layer

Most of the stratospheric aerosols are found in the lower to mid-stratosphere at altitudes between the tropopause and 20 km to 25 km (Junge et al. 1961). More recent studies such as Hommel et al. (2015) and Vernier et al. (2011) indicate that for the last two decades the maximum aerosol mixing ratio in the tropics is rather found at altitudes between 25 km and 30 km.

This lower stratospheric aerosol layer was first discovered by Junge et al. (1961) and therefore is often referred as the "Junge Layer". Basically, the Junge Layer covers a wide range of latitudes but Trepte and Hitchman (1992) who studied the tropical stratospheric circulation using aerosol data, could show that in the lowermost tropical stratosphere the meridional transport of aerosols towards mid-latitudes is strong, while at higher altitudes the aerosols accumulate in the tropical region.

The lower boundary of the stratospheric aerosol layer is the tropopause, where most of the larger aerosols that are not easily lofted to higher altitudes are removed. The top of the layer is located around 32 km to 35 km where the aerosol mixing ratio rapidly decreases as the stratospheric temperature is high enough so that the sulfate aerosols begin to evaporate (Kremser et al. 2016). Within the deep branch of the Brewer–Dobson Circulation (BDC) the gaseous sulfate is transported to the polar regions, where the temperature is low enough for sulfate droplets to form again (Kremser et al. 2016).

Hommel et al. (2015) modelled the influence of the Quasi-Biennial Oscillation (QBO) on the Junge Layer and found that the altitude of the maximum mixing ratio as well as the top height and thickness of the aerosol layer are influenced by the phase of the QBO. This was already reported by Trepte and Hitchman (1992). An instructive illustration of this behaviour can also be found in Vernier et al. (2011). Hommel et al. (2015) found the strongest QBO influence at the top of the layer, where the aerosols begin to evaporate. Additionally they found that in the lower part of the aerosol layer there is increased upwelling of SO_2 during the QBO easterly phase.

3.2. Volcanoes

Depending on their magnitude, volcanic eruptions can emit huge amounts of trace gases such as CO_2 as well as aerosols and aerosol forming substances (Kremser et al. 2016; Timmreck 2012). Besides volcanic ash the main chemical compounds released by volcanic eruptions are water vapour (H_2O), carbon dioxide (CO_2), sulfur dioxide (SO_2) and hydrogen sulfide (H_2S) (Textor et al. 2004). While the emissions of CO_2 and H_2O are negligible compared to other anthropogenic and

natural sources (Textor et al. 2004), volcanic SO_2 emissions as described in Sect. 3.1 have the potential to significantly influence the climate system, especially when reaching the stratosphere.

According to Textor et al. (2004), the chemical composition of the volcanic plume mainly depends on the conditions during the eruption as well as on the type of magma. Basaltic magma is rich in sulfur and CO_2 and is typically erupted by volcanoes near divergent oceanic plate boundaries. Most of these eruptions are effusive, which means that the magma slowly flows out of the volcano. This results from the basaltic magma having a low viscosity which in turn allows the dissolved gaseous volatiles to escape so that only low pressure can build up. Therefore, basaltic eruptions rarely reach higher altitudes (Textor et al. 2004).

In contrast to basaltic eruptions, eruptions where felsic (rhyolite) and intermediate (andesite) magma is ejected, are highly explosive which makes them more likely to reach the stratosphere.

Since those eruption types contain a lot of SiO_2, their viscosity is high, which makes it difficult for the gaseous volatiles to escape. Hence, those eruptions are more explosive as high pressure can build up. Andesitic eruptions are most common and typically occur at converging plate boundaries where the oceanic plate is subducted (e.g. Andes – Calbuco volcano, Philippines – Pinatubo volcano) (Textor et al. 2004).

Although petrological measurements of magmas from explosive rhyolithic and andesitic eruptions indicate that there is relatively low sulfur dissolved, remote sensing measurements show that they too can emit large amounts of SO_2 (Langmann 2014). This is a phenomenon known as "excess sulfur" and may be explained by the formation of sulfur-rich "gas bubbles" in the magma chamber which are supplied by gas saturated basaltic magma lower in the mantle (Wallace 2001; Langmann 2014).

3.2.1. The Volcanic Explosivity Index

A widely used measure for the magnitude of an eruption is the Volcanic Explosivity Index (VEI). The VEI was introduced by Newhall and Self (1982) as an estimate for the magnitude of historic volcanic eruptions and is based on a logarithmic scale ranging from 0 for non explosive eruptions to 8 for "cataclysmic" eruptions. It is based on volcanological data exclusively and does not incorporate atmospheric data such as opacity or temperature (Newhall and Self 1982). The main criteria used for the classification as well as some representative eruptions for each VEI level are listed in Fig. 3.2.

As stated by Robock (2015) one major problem with using the VEI to study the atmospheric impacts of volcanoes is that it is strongly based on the ejected amount of tephra. The climate impact, however, mainly depends on the input of sulfur into the stratosphere which is not directly used for the VEI classification.

Nevertheless, the VEI is a first indication of whether an eruption has the potential to reach the stratosphere. However, to correctly estimate the climatic impacts of

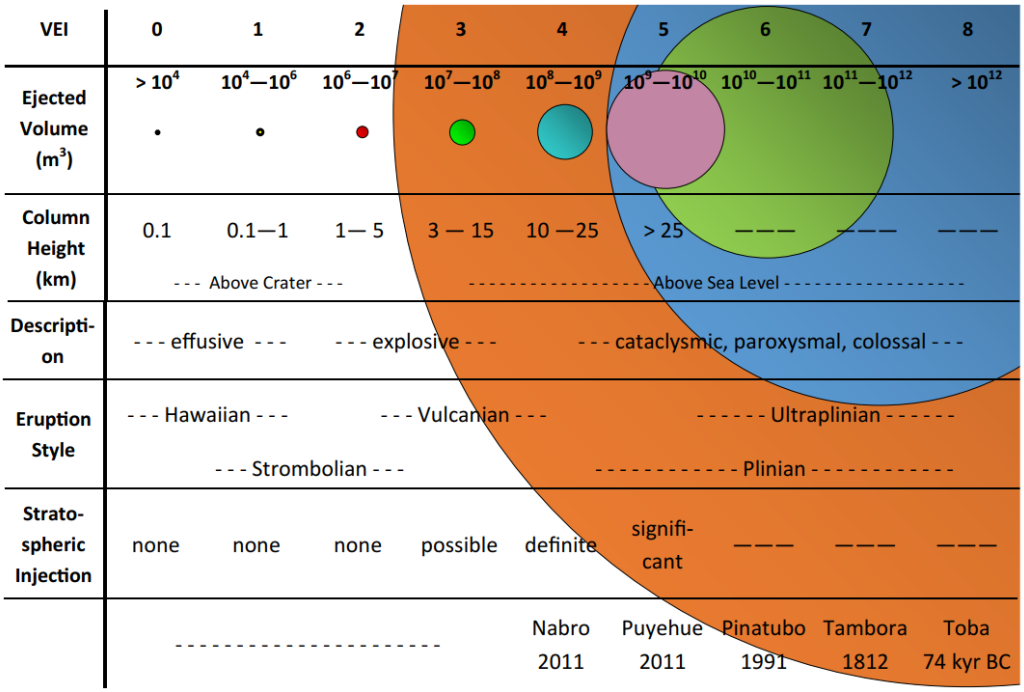

Figure 3.2.: The Volcanic Explosivity Index (VEI) as well as the main classification criteria. Based on Newhall and Self (1982).

an eruption, additional factors such as the maximum altitude of the SO_2 "cloud" or the emitted SO_2 mass have to be considered (Newhall and Self 1982; Robock 2015).

3.2.2. Post-2000 Volcanic Eruptions

The Pinatubo in 1991 represents the last eruption that both, volcanologists and atmospheric scientists, characterize as major eruption. It was assigned a 6 out of 8 on the VEI scale and emitted about 20 Mt of SO_2 directly to the mid-stratosphere (Global Volcanism Program 2013). This resulted in a stratospheric warming of up to 2 K and a global tropospheric cooling of up to 0.6 K for the following years (Parker et al. 1996; Robock 2000). Following the Pinatubo no major eruptions that substantially altered the stratospheric aerosol levels occured until 2002, when a series of minor volcanic eruptions started (Vernier et al. 2011) (Table 3.1). As shown in Fig. 3.3 a majority of them took place along the Pacific Ring of Fire, where the oceanic plate is subducted e.g. at the Andean Volcanic Belt, the Alleutian Volcanic Arc as well as in Southeast Asia (Sunda Arc etc.). Some eruptions such as the Eyjafjallajökull in 2010 or the Nabro in 2011 occured along continental and oceanic Rift Zones. Almost every eruption during this period that reached stratospheric altitudes had a VEI of 4. However, after the Soufrière Hills eruption as substantial amount of sulfur did reach the stratosphere although it was classified

Table 3.1.: Eruptions between 2002 and 2017 with a minimum VEI of 4[a]. Eruptions reaching the stratosphere are in bold.

Name	Start date	VEI	SO_2 mass	Altitude	Country
Ruang (Ru)	09-25-2002	4	80 kt	22 km	Indonesia
Reventador	11-03-2002	4	84 kt	17 km	Ecuador
Manam (Ma)	10-24-2004	4	152 kt[b]	24 km[b]	P. N. Guinea
Tavurvur (Ta)	08-11-2006	4	300 kt	18 km	P. N. Guinea
Chaitén	05-02-2008	4	14 kt	17 km	Chile
Okmok	07-12-2008	4	150 kt	15 km	Alaska
Kasatochi (Ka)	08-07-2008	4	2000 kt	15 km	Alaska
Sarychev P. (Sp)	06-11-2009	4	1200 kt	17 km	Russia
Eyjafjallajokull	03-20-2010	4	466 kt	9 km	Iceland
Merapi (Me)	10-26-2010	4	300 kt	17 km	Indonesia
Grimsvötn	05-21-2011	4	300 kt	12 km	Iceland
Puyehue	06-04-2011	5	200 kt	14 km	Chile
Nabro (Na)	06-13-2011	4	3650 kt	18 km	Eritrea
Tolbachik	11-27-2012	4	200 kt	10 km	Russia
Sinabung	09-15-2013	4	20 kt	7 km	Indonesia
Kelut (Ke)	02-13-2014	4	200 kt	19 km	Indonesia
Calbuco (Ca)	04-22-2015	4	400 kt	20 km	Chile
Wolf	05-25-2015	4	200 kt	7 km	Ecuador

[a]Data from the Global Volcanism Program (2013).
[b]Main emission event during the eruption.

a VEI of only 3. The sulfur emission following the Puyehue in 2011, which had a VEI of 5, was in contrast negligible and did not reach altitudes above 14 km. More detailed information about post-2000 eruptions >VEI 4 can be found in Table 3.1.

Despite the fact that compared to the Pinatubo, the sulfur input to the stratosphere from post-2000 eruptions was up to three orders of magnitude smaller, they most likely led to a steady increase in the stratospheric aerosol load (Vernier et al. 2011).

Studies that addressed the atmospheric impacts of specific post-2000 eruptions found that some eruption such as the Mt. Chaitén eruption in 2008, the Eyjafjallajökull in 2010 as well as the Puyehue eruption in 2011 caused significant negative tropospheric temperature signals (Wang and Alexander 2009; Okazaki and Heki 2012; Biondi et al. 2017). Significant warming in the lower stratosphere of 0.8 K to 1.2 K (Mehta et al. 2015) has been found for the Tavurvur and Soufriére Hills while for the Nabro which emitted by far the highest amount of SO_2 since the Pinatubo eruption a maximum stratospheric warming signal of 4 K (up to 10 K for individual Radio Occultation (RO) profiles) (Biondi et al. 2017) was detected.

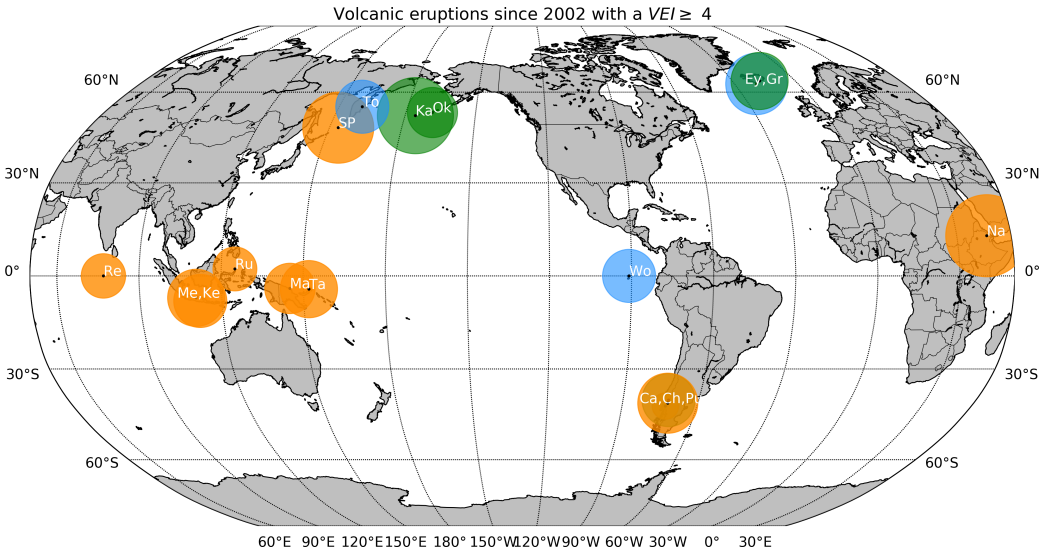

Figure 3.3.: Eruption locations. The size of the circular areas indicates the emitted SO_2 mass (logarithmic scale). Colors indicate the emission altitude (blue $\leq$ 10 km, green $\leq$ 15 km, orange $>$ 15 km. Data from the Global Volcanism Program (2013).

3.3. Volcanic Impacts on the Atmosphere

Similar to greenhouse gases and aerosols from other natural and anthropogenic sources, volcanic aerosol emissions can influence the climate system by affecting the atmospheric energy balance. They directly scatter and absorb incoming and outgoing radiation and indirectly influence the radiative balance by changing cloud properties as well as chemical processes in the atmosphere but also by altering the atmospheric circulation (Robock 2000; Samset 2016). The most important volcano-atmosphere interactions are summarized in Fig. 3.4.

Minor explosive or even strombolian style eruptions are restricted to the troposphere and can change cloud properties such as cloud albedo or cloud lifetime. Thereby the increased aerosol concentration following an eruption leads to smaller cloud droplets which reflect solar radiation more efficiently. Additionally, the volcanic ash from such eruptions directly alters the transport of radiation in the atmosphere. However, due to the ashes' short residence time, those tropospheric direct and indirect effects are rather local and only affect regions downwind of the volcano (Ebmeier et al. 2014; Samset 2016; Langmann 2014).

Highly explosive eruptions which emit aerosols to the stratosphere, in contrast, can have climatic effects on a global scale as the aerosols are spread globally or at least hemispherically, depending on the prevailing stratospheric wind regimes at the time of the eruption (Robock 2000).

Based on their size, which is described by the area-weighted effective radius (r_{eff}), the volcanic sulfate droplets efficiently scatter light in the visible region but also absorb incoming solar and outgoing terrestrial longwave radiation. Long-

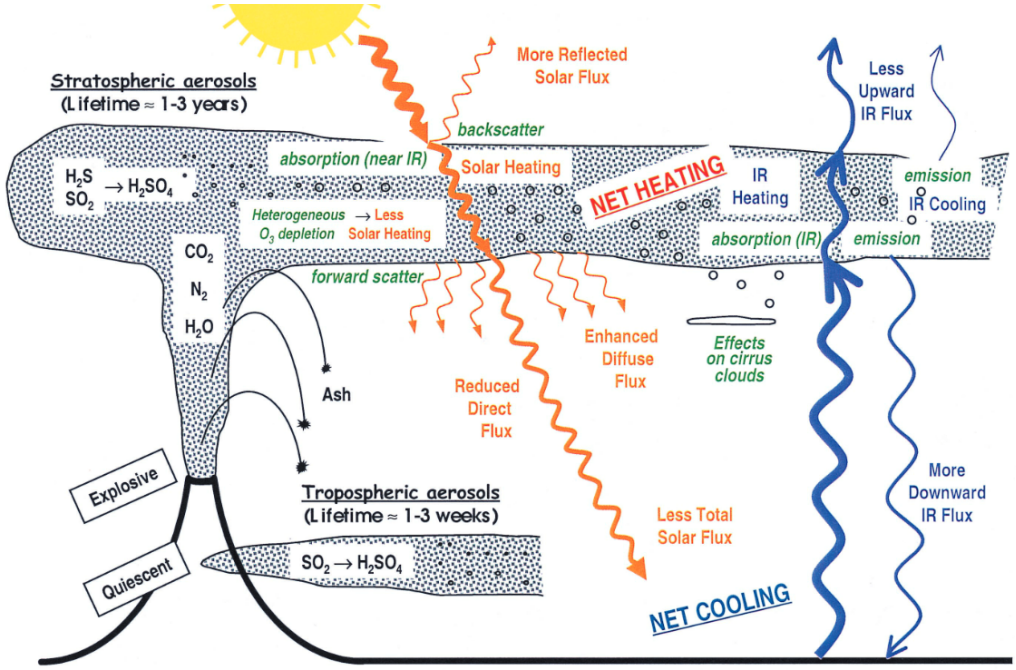

Figure 3.4.: Overview of the most important volcanic effects on the atmosphere. Reprinted from Robock (2000) with permission. Copyright 2000 by the American Geophysical Union.

wave absorption is stronger for large particles whereas the albedo effect caused by scattering of shortwave radiation only slightly depends on the particle size (Lacis et al. 1992).

Increased shortwave scattering reduces direct solar radiation reaching the surface, leading to an increased planetary albedo and hence causing a cooling at the surface. Absorption of terrestrial and solar longwave radiation in turn causes a heating of the stratospheric aerosol cloud and also increases the downward flux of longwave radiation (Robock 2000; Lacis et al. 1992; Pitari et al. 2016).

Lacis et al. (1992) found that for particle sizes larger than $r_{eff} \approx 2\mu$m the albedo effect can be compensated by the increased downward emission of longwave radiation from the volcanic cloud. However, such large aerosols are quickly sedimented which makes an overall warming at the surface rather unlikely.

Besides their effects on the radiative flux, volcanic aerosols can also affect stratospheric dynamics and chemistry, thereby affecting the concentration of important chemical species such as ozone (Robock 2015; McCormick et al. 1995; Aquila et al. 2013).

On the one hand, the radiatively heated volcanic cloud can enhance the tropical upwelling and bring low ozone concentration layers to higher altitudes, which in turn reduces the ozone concentration at these altitudes (Robock 2015; McCormick et al. 1995). Depending on the magnitude of the eruption those dynamical changes can even be strong enough to affect the pattern of the QBO (Pitari et al. 2016).

On the other hand, the volcanic aerosols offer a surface for heterogeneous chemical reactions which destroy N_2 and form OH and ClO which in turn are responsible for the destruction of ozone (Aquila et al. 2013). Such ozone depletion due to aerosol–chemical reactions is most effective at high latitudes with low temperatures (e.g. responsible for the ozone hole) but is also strong within the volcanic cloud (Robock 2015). Aquila et al. (2013), who investigated the Pinatubo case, found that directly after the eruption the ozone reduction is mainly caused by increased upwelling while about two years after the eruption the chemical ozone depletion is more relevant.

As ozone strongly absorbs UV radiation, it is one of the main causes for stratospheric warming and also prevents harmful radiation from reaching the surface. A reduced ozone concentration therefore causes stratospheric cooling but also increases the amount of UV radiation reaching the surface (Robock 2015; McCormick et al. 1995). Free and Lanzante (2009) argue that such a negative temperature feedback caused by an ozone reduction, as described by Aquila et al. (2013), is responsible for the comparatively low stratospheric warming signals observed after the Pinatubo outbreak compared to model studies.

For large eruptions such as the Pinatubo those radiative, dynamical and chemical effects in general lead to a net warming of the lower stratosphere and a net cooling at the surface (Robock 2000; Robock 2015; McCormick et al. 1995).

4. Data

Aerosols emitted to the stratosphere are distributed horizontally and vertically by different atmospheric processes. To account for this distribution and to investigate their effects, data sets which offer a sufficient horizontal but also vertical resolution are needed. In this study newly available vertically resolved aerosol data together with temperature data from Radio Occultation (RO) measurements, which offer an exceptional vertical resolution but also a sufficient horizontal resolution, are utilized.

4.1. Temperature Data From Radio Occultation

Global Navigation Satellite System (GNSS) RO is an active limb sounding technique, where radio-waves originating from GNSS satellites are used for remote sensing the atmosphere (Steiner et al. 2011; Anthes 2011).

When the radio signals propagate through the atmosphere they are refracted, resulting in a difference in amplitude and phase (also referred to as excess phase) of the signal compared to a signal that does not travel through the atmosphere. The refracted signal is then received by a reciever on a satellite flying in a Low Earth Orbit (LEO) (Kursinski et al. 1997).

As during an occultation event the receiver and the transmitter move towards each other (rising occultation) or away from each other (setting occultation), the atmosphere is scanned vertically. Using the resulting amplitude and excess phase data, together with precise information of the position and velocity of the spacecrafts the influence of a kinematic Doppler shift is removed and subsequently, bending angle (α) profiles are calculated. The radio waves also propagate through the ionosphere. Thus, in order to obtain atmospheric measurements, the ionospheric influence has to be eliminated. For this purpose, bending angle profiles that come from two different GNSS frequencies are combined linearly (Vorob'ev and Krasil'nikova 1994). Using an inverse Abel integral on the remaining atmospheric bending angle profiles, refractivity profiles are calculated. These in turn form the basis for deriving key atmospheric parameters such as density, pressure and temperature, which are calculated using the Smith-Weintraub formula, hydro-static equation and equation of state.

The key properties of the RO method are high accuracy (less than 1 K) and precision (less than 0.05 K) (Scherllin-Pirscher et al. 2011), and all weather capability. The measurements from different satellites can be combined without inter-calibration (Foelsche et al. 2011; Angerer et al. 2017). The resolution of the profiles ranges from approximately 60 km to 300 km horizontally and 0.1 km to

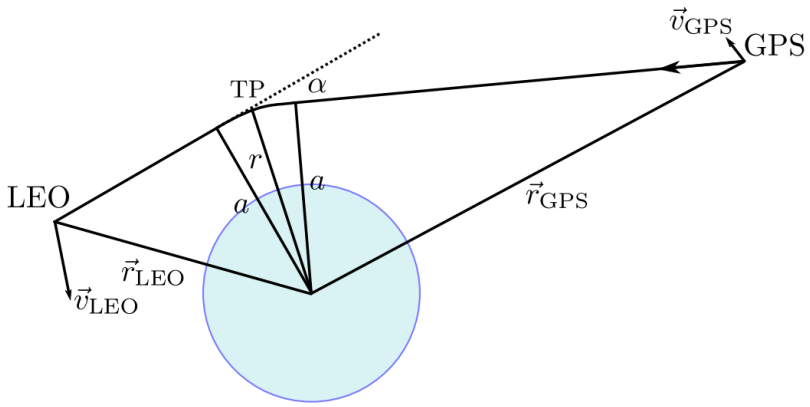

Figure 4.1.: Schematic illustration of the geometry during an RO event. TP represents the tangent point, r the tangent point radius and α the bending angle. Originally drawn by Pirscher (2010), reprinted from Schwärz et al. (2013).

1.5 km vertically in the troposphere and stratosphere, respectively (Gorbunov et al. 2004; Kursinski et al. 1997). Due to their high vertical resolution and the fact that the quality of the RO measurements is best in the Upper Troposphere–Lower Stratosphere (UTLS) region (Foelsche et al. 2011; Steiner et al. 2011), temperature data from RO are a favorable choice for studying volcanic temperature signals.

In this study, monthly mean temperature data from Wegener Center for Climate and Global Change (WEGC) Occultation Processing System version 5.6 (OPSv5.6) processed RO profiles are used. The processed RO profiles were brought onto 5° latitude bands. A description of the WEGC RO Occultation Processing System (OPS) procedure is provided by Schwärz et al. (2016) and Angerer et al. (2017).

4.2. Aerosol Data

A measure for the amount of aerosols in the atmosphere is the Aerosol Optical Depth (AOD), which is commonly used to determine the impact of aerosols on the climate system. With respect to the extinction law of Beer-Lambert the AOD provides information about how much of the vertically incident solar radiation is absorbed and scattered by aerosols (DWD 2020; Seinfeld and Pandis 1997). This can be written as,

$$\frac{I(\lambda)}{I_0(\lambda)} = e^{-\tau(\lambda)} \tag{4.1}$$

where $\tau(\lambda)$ is the wavelength dependent AOD. $I(\lambda)$ and $I_0(\lambda)$ denote the intensity of the solar radiation at the surface and the top of the atmosphere, respectively.

The AOD typically refers to the aerosol concentration of the atmospheric layer from 15 km upwards as e.g. provided by Sato et al. (1993). Therefore, it is often referenced as Stratospheric Aerosol Optical Depth (SAOD). The SAOD is used in studies dealing with tropospheric temperature effects of volcanoes (Solomon et al. 2011), as well as in studies dealing with stratospheric temperature effects (Mehta et al. 2015). Ridley et al. (2014) argue that the SAOD which neglects volcanic aerosols below 15 km, can lead to a misjudgment of temperature variability caused by volcanoes, especially at high latitudes. This may pose a problem when analysing tropospheric temperature signals (Ridley et al. 2014). For the examination of stratospheric temperature signals, however, the key problem is that SAOD does not provide any information about the vertical evolution of volcanic plumes.

In this work, we therefore used the new Global Space-based Stratospheric Aerosol Climatology (GloSSAC) data set (Thomason et al. 2018; Thomason 2017), which provides the Volume Extinction Coefficient (VEC) as function of altitude and latitude.

A Global Space-based Stratospheric Aerosol Climatology

The GloSSAC is a continuous gap free aerosol climatology constructed from measurements of different space-born instruments such as SAGE, OSIRIS, CALIPSO and also ground- or balloon based instruments. It covers the time-range from 1979 to 2016 and focuses on monthly mean VEC on 5° latitude bands between 80°N and 80°S. In the vertical it covers the atmospheric layer between the tropopause and 40 km with a resolution of 500 m (Thomason et al. 2018).

By definition, the VEC with the unit km^{-1} corresponds to the attenuation of monochromatic light due to scattering or absorption in a medium. It is related to the AOD of a specific atmospheric layer between altitudes $z0$ and $z1$ by:

$$\tau_\lambda = \int_{z0}^{z1} \beta_\lambda(z) dz \,. \tag{4.2}$$

Hereby τ denotes the AOD and β the altitude dependent VEC (Sokolik 2009).

Besides other aerosol properties such as area density, the focus of this data set is on the VEC at wavelengths of 525 nm and 1020 nm. Tropospheric data are also included but only where available. Although Thomason et al. (2018) note that the measurements from the different instruments show inhomogeneity and in some cases the VEC for 525 nm and 1020 nm, respectively, had to be empirically derived, the final GloSSAC data are robust and have been subjected to strict quality controls (Thomason et al. 2018).

In addition to the VEC a measure for the stratospheric background which represents the stratospheric aerosol levels when they are unaffected by volcanic eruptions is included in the data-set. It consists of the average of the monthly VEC of the years 1999 to 2002, excluding 2002.

In this study, consistent with other studies on volcanic signals, data for a wavelength of 525 nm are used. Further information about the data preprocessing

for both, the aerosol and temperature data is provided in the methods section of the paper presented in Part II.

5. Detecting Volcanic Temperature Imprints

This chapter covers the steps and methods used to determine the volcanic temperature imprints as well as the resulting temperature trend. The calculations are based on a multiple linear regression analysis of the Radio Occultation (RO) temperature anomalies. Volcanic aerosols together with other major atmospheric variability modes are considered as predictor variables. In the first section, different indices which can be used to account for natural variability are discussed (Sect. 5.1). This is followed by a brief description of the multiple linear regression analysis (Sect. 5.2). The last section presents a possible approach to deal with the statistical problem of collinearity between the regressors (Sect. 5.3).

5.1. Accounting for Natural Variability

As outlined in Ch. 2, stratospheric temperature variability in the tropics, aside from aerosols and trace gases such as ozone, is determined by two major atmospheric phenomena that need to be considered when attempting to calculate the temperature imprints of volcanic eruptions.

These phenomena are the El Niño–Southern Oscillation (ENSO) and the Quasi-Biennial Oscillation (QBO). The ENSO is dominant in the troposphere but to a certain extent also affects the stratosphere. The QBO is the leading circulation pattern in the stratosphere. Other modes such as the solar cycle can also affect stratospheric temperatures. However, prior studies such as Mehta et al. (2015) found that the solar cycle is less relevant compared to QBO or ENSO variability.

Commonly, QBO and ENSO are characterized by indices, e.g. the Niño 3.4 Sea Surface Temperature (SST) for describing ENSO variability and e.g. the 50 hPa and 30 hPa winds for representing QBO variability. These indices are not vertically resolved and in order to get the corresponding temperature signatures for different altitude levels an unknown time lag, especially for the QBO, has to be considered (Wilhelmsen et al. 2018).

One way to improve this is to create the QBO indices from the Principal Components (PCs) of the QBO wind field (cf. Mehta et al. 2015; Randel et al. 1999) or even to create the variability indices directly from the temperature field, using Empirical Orthogonal Function (EOF) analysis.

Wilhelmsen et al. (2018) presented two such EOF based methods where the atmospheric variability indices are created from the RO temperature anomalies. In the first method they derived one-dimensional variability indices from the

temperature anomalies that can be applied to any altitude level. Here a similar approach is used to create variability indices from the QBO wind field. These indices generated from either the wind field or the RO temperature anomaly field, are sufficiently detailed to detect signals from larger volcanic eruptions. Unfortunately, they are less effective for detecting signals of small eruptions as they leave high residual variability that is comparable to the volcanic signal amplitude.

For the second method Wilhelmsen et al. (2018) created indices separately for each altitude level. Those vertically resolved indices derived from RO temperature anomalies leave only small residual variability. Therefore they are more suitable for a regression analysis where small volcanic signals shall be detected.

5.1.1. Variability Indices Based on Empirical Orthogonal Function Analysis

As described by Hannachi et al. (2007), EOF analysis extracts the major variability patterns from higher dimensional space-time fields, such as the QBO wind field as well as the highly resolved Global Navigation Satellite System (GNSS) RO temperature data. Thereby the data are reduced into a smaller number of space components (EOFs) and time components (PCs) from which the EOF analysis attempts to create linear combinations that explain most of the variance present in the input data (Hannachi et al. 2007).

Based on this EOF approach, Wilhelmsen et al. (2018) introduced two methods of how natural variability indices can be created from RO temperature anomalies. In the first classical method they stacked the longitude (ϕ), latitude (ψ), and altitude (h) dimension of the input data in order to get a two-dimensional space-time matrix X (Eq. 5.1) that only has one space dimension ($\mathrm{s}_{\phi,\psi,h}$) and a time dimension (t). In this work, a similar approach is used to create the PCs from the QBO wind field, which (compared to the temperature anomaly field) only has one vertical dimension and a time dimension.

For the second method, Wilhelmsen et al. (2018) stack the longitude (ϕ) and latitude (ψ) dimension and perform an EOF analysis separately for each altitude level. This enables to produce vertically resolved indices. Since those indices are far more detailed than the wind or temperature indices from the classical method, they leave little residual variability, provided that the input field is horizontally well resolved.

$$X = \begin{pmatrix} x_{s_1,t_1} & x_{s_1,t_1} & \cdots & x_{s_1,t_n} \\ x_{s_2,t_1} & x_{s_2,t_2} & \cdots & x_{s_2,t_n} \\ \vdots & \vdots & \ddots & \vdots \\ x_{s_m,t_1} & x_{s_n,t_1} & \cdots & x_{s_m,t_n} \end{pmatrix} \tag{5.1}$$

Following Hannachi et al. (2007) the EOFs and PCs are the results of the eigenvalue problem Eq. (5.2),

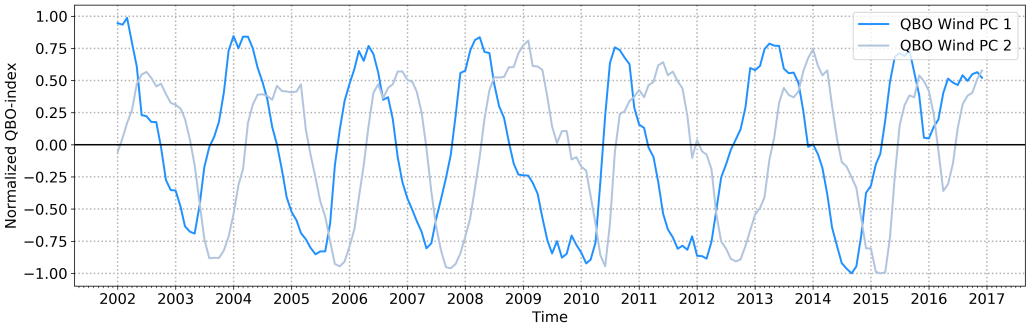

Figure 5.1.: QBO-wind indices derived from the Singapore wind anomalies using EOF analysis.

$$S\vec{u} = \lambda^2 \vec{u} \tag{5.2}$$

where S denotes the covariance matrix which is given as,

$$S = \frac{1}{n} X^{\mathrm{T}} X \tag{5.3}$$

and $\vec{u}_i$ are the eigenvectors representing the EOFs of the covariance matrix and λ_i^2 are the accompanying eigenvalues. The PCs who represent the variability indices are then given by Eq. (5.4) and λ_i which is a measure for the explained variance of the corresponding PC:

$$\mathrm{PC}_i = X\vec{u_i}\,. \tag{5.4}$$

To create the final PCs, Wilhelmsen et al. (2018) scale the PCs using the eigenvalues.

$$\mathrm{PC}_i^{\mathrm{final}} = \frac{\mathrm{PC}_i}{\sqrt{\lambda_i}}\,. \tag{5.5}$$

The resulting PCs from the classical EOF analysis of the QBO wind field are shown in Fig. 5.1.

5.2. Multiple Linear Regression

In atmospheric sciences linear regression analysis is a common method to determine the relation between a variable of interest, called dependent variable, and one or more predictor variables that determine its evolution (Storch and Zwiers 1999).

As already mentioned, in this study the variable of interest is the temperature that is assumed to depend on different atmospheric processes described by their corresponding indices.

The simplest form of a linear regression is a line equation that models the relation between the variable of interest and one predictor variable. It can be written as,

$$y_i = \beta_0 + \beta_1 x_i + \epsilon_i \tag{5.6}$$

where y_i represents the i^{th} observation of the dependent variable, β_0 some constant offset, β_1 the slope of the fitted line and x_i the i^{th} observation of the predictor variable. The random error ϵ_i can be written as,

$$\epsilon_i = y_i - \underbrace{(\beta_0 + \beta_1 x_i)}_{\hat{y}_i} \tag{5.7}$$

where $\hat{y}_i$ represents the modeled value of y_i (Karl et al. 2006). Commonly the values are calculated by the least squares approach where the regression coefficients β are chosen so that the residual variance, which is the sum of squared errors, is minimal (Storch and Zwiers 1999):

$$RV = \sum_{i=0}^{N} (y_i - \hat{y}_i)^2 = \sum_{i=0}^{N} \epsilon_i^2 \rightarrow \min . \tag{5.8}$$

If the independent variable x was the time such a regression would simply calculate the linear trend in the temperature data (Karl et al. 2006).

Since the temperature variability can not only be explained by a linear trend other influencing factors have to be taken into account. Therefore a more general approach such as the multiple linear regression can be used.

Similar to Eq. (5.6) a regression model can be written as a linear combination of the different predictor variables x_p,

$$y_t = \beta_0 + \beta_1 x_{t,1} + \beta_2 x_{t,2} + \cdots + \beta_p x_{t,p} + \epsilon_t \tag{5.9}$$

where $p = 1 \ldots n$ and t the time (Karl et al. 2006). In matrix notation this can be expressed as,

$$\vec{Y} = X\vec{b} + \vec{E} \tag{5.10}$$

where $\vec{Y}$ contains the observations of the dependent variable, $\vec{b}$ the coefficients and $\vec{E}$ the error terms. X is called the design matrix and is given as (Storch and Zwiers 1999):

$$X = \begin{pmatrix} 1 & x_{1,1} & \cdots & x_{p,1} \\ \vdots & \vdots & & \vdots \\ 1 & x_{1,i} & \cdots & x_{p,i} \\ & & & \end{pmatrix} . \tag{5.11}$$

Similar to Eq. (5.8) the regression coefficients are estimated so that the sum of squared errors is minimal (Storch and Zwiers 1999):

$$SSE = \vec{E}^T \vec{E} \rightarrow \min . \tag{5.12}$$

For this study, it is assumed that the stratospheric temperature mainly depends on the QBO and ENSO phases as well as the aerosol concentration. Therefore they are considered as predictors and are represented by their corresponding indices.

5.2.1. Generalized Least Squares Regression

To allow for an accurate estimation of the regression coefficients, the Ordinary Least Squares (OLS) approach requires that the individual error terms ϵ_i are random variables independent of each other. Unfortunately this is not the case for most meteorological time series data. If the time steps are small enough, e.g. the temperature at a specific time t depends on the temperature at time $t-1$. In statistics such dependencies are called autocorrelation or serial correlation (Storch and Zwiers 1999; Karl et al. 2006). Most climate data are autocorrelated and they are commonly considered to follow a First-order Autoregressive process (AR(1)) (Storch and Zwiers 1999; Karl et al. 2006; Santer et al. 2000). Whether autocorrelation is present can be tested by using the Durbin-Watson statistics as well as plotting the autocorrelation function (ACF) (Dettling 2016).

Autocorrelation of the regression residuals violates one of the classical OLS assumptions (Gauss-Markov assumptions) and leads to an underestimation of the standard errors. As a consequence the t-statistics for significance testing are invalid (Storch and Zwiers 1999; Karl et al. 2006). To avoid this, several approaches can be used. A comparatively simple approach is given by Karl et al. (2006) and Santer et al. (2000) where they use an adapted sample size for their statistical calculations.

Here, a Generalized Least Squares (GLS) model which considers the effects of an AR(1) process is used. Since it is assumed that the error term contains an AR(1) structure it can be written as,

$$\epsilon_t = \rho \epsilon_{t-1} + \mu_t , \tag{5.13}$$

where ρ is the correlation coefficient between the error term and itself lagged by one time-step, and μ_t is the "true" random error (Dettling 2016). Using the transformation,

$$y_t^{'} = y_t - \rho y_{t-1} \quad \text{and} \quad x_t^{'} = x_t - \rho x_{t-1} , \tag{5.14}$$

a problem which fulfills the Gauss-Markov assumptions can be created (Dettling 2016):

$$y_t^{'} = \beta_0^{'} - \beta x_t^{'} + \mu_t . \tag{5.15}$$

Using the autocovariance matrix of the error terms $\sigma^2\Sigma = \sigma^2 S^{-1} S$ where Σ contains the correlation between the errors, this transformation can also be done in matrix notation and leads to (Dettling 2016):

$$\vec{Y'} = X' \vec{B} + \vec{E'} \tag{5.16}$$

The GLS regression coefficients $\hat{\beta}$ as well as the covariance matrix containing the effective standard errors are then given by (Dettling 2016; Storch and Zwiers 1999):

$$\begin{aligned} \hat{\beta} &= (X^T \Sigma^{-1} X) X^T \Sigma^{-1} \vec{Y} \\ \mathrm{Var}(\hat{\beta}) &= (X^T \Sigma^{-1} X)^{-1} \sigma^2 \end{aligned} \tag{5.17}$$

Since the coefficient ρ and the error-covariance matrix are unknown they have to be estimated. According to Dettling (2016), one way to do this is the iterative Cochrane-Orcutt procedure where at first the residuals are calculated using an OLS regression. In the following an appropriate model (AR(1), depending on the autocorrelation structure) is fitted to the regression residuals and the error-covariance matrix is estimated. Using Eq. (5.17) the generalized coefficients are estimated. This procedure is repeated until convergence (Dettling 2016). In practice, however, the coefficients are usually calculated numerically using the Maximum Likelihood principle.

A satisfying explanation of this procedure is beyond the scope of this work, therefore, the interested reader is referred to Storch and Zwiers (1999) or Dettling (2016), where a detailed description of this process can be found. In this study the calculations were performed in the programming language Python using the GLSAR function from the statsmodels[1] module.

5.3. Dealing With Collinearity

As discussed in Sect. 5.1.1, vertically resolved variability indices, which are created using the second method from Wilhelmsen et al. (2018) are favorable for detecting small volcanic signals, since they leave little residual variability. However, when performing a linear regression with those indices together with the aerosol anomalies as explanatory variables, the effect of the aerosols and hence the signals of volcanic eruptions are small and statistically not significant. This contrasts with findings from other studies such as Mehta et al. (2015) or Biondi et al. (2017).

Wilhelmsen et al. (2018) already noted the variability indices created from the vertically resolved temperature anomaly field do not only cover QBO or ENSO signals, but all other main modes of variability including e.g. ozone or aerosol-induced temperature changes. Additionally, the QBO phases modify the strength of the stratospheric circulation which in turn controls the vertical and latitudinal distribution of the stratospheric aerosols. Consequently, the aerosol data also

[1] Statsmodels: https://www.statsmodels.org/stable/index.html

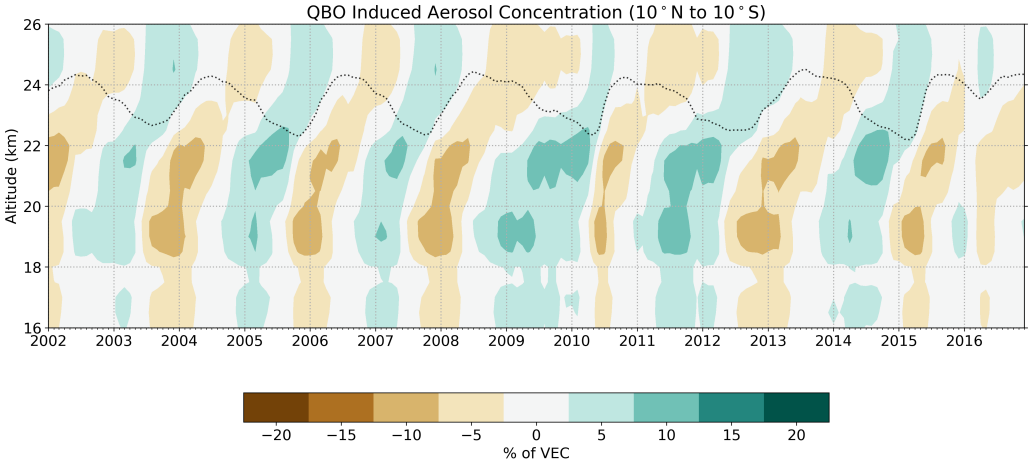

Figure 5.2.: Reconstructed QBO-induced aerosol concentration for the central tropical region (mean 10°N to 10°S). The dashed line represents the 30 hPa Singapore wind.

include a QBO variability pattern (Hommel et al. 2015; Trepte and Hitchman 1992). Geoengineering studies such as Niemeier and Schmidt (2017) have shown, that to a certain extent the aerosols themselves can also affect the stratospheric circulation (Pitari et al. 2016). However, for the small eruptions considered in this study such an effect should be comparatively low.

Together, these interconnections result in a non-zero correlation between the aerosol index and the other predictors which reduces the explanatory power of the aerosols. In statistics this problem is known as collinearity between regressors (Santer et al. 2001).

Although the correlations turned out to be comparatively weak, a majority of the aerosols' influence on the stratospheric temperature is "absorbed" by the PCs describing the QBO and ENSO.

To avoid such collinearity, here, we remove the QBO signal (Fig. 5.2) from the aerosol data in a first step. Hereby EOF based one-dimensional indices derived from the QBO wind field as shown in Fig. 5.1 are utilized. Highest QBO influence is found at altitudes between 18 km and 22 km. Fig. 5.2 also shows similarities with the atmospheric tape recorder signal, which is a measure of the strength of the tropcial pipe (Flury et al. 2013).

In a second step, the remaining QBO-free volcanic aerosol signal is removed from the original temperature anomalies via linear regression (Sect. 5.1).

This regression model omits the QBO, which could cause the regression results to be biased. Fortunately such a bias only occurs when the omitted predictor (in this case the QBO) is correlated to a predictor included in the regression model (in this case are the aerosols). Since we removed the QBO signal in advance from the aerosols, primarily the uncorrelated volcanic pattern remains. After QBO removal the correlation between the residual aerosol anomalies at 23 km and the 30 hPa QBO wind is reduced to R $\approx$ -0.1. Since the strength of the regression

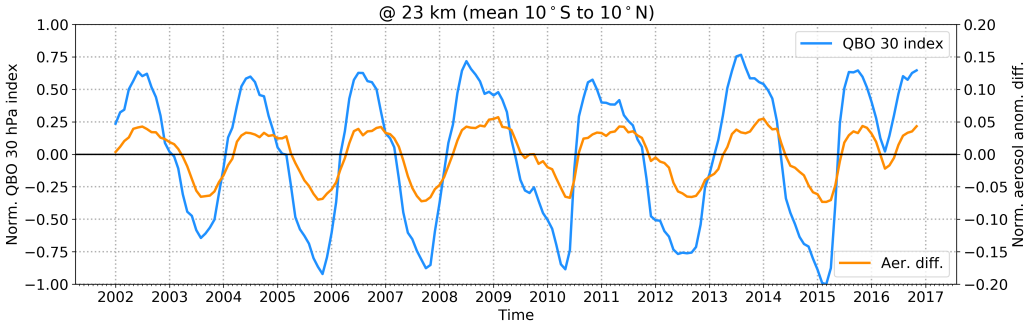

Figure 5.3.: Difference in the aerosol anomalies (QBO-cleared vs. regular) compared to the QBO 30 hPa index at 23 km (mean 10°N to 10°S).

bias is directly proportional to the strength of the correlation (Hanck et al. 2019), any bias that could remain should be considerably small. The resulting difference between the aerosol anomalies and the QBO-cleared aerosol anomalies are shown in Fig. 5.3.

Finally, we used the resulting temperature anomalies to compute vertically resolved variability indices by using method two from Wilhelmsen et al. (2018). These new variability indices do no longer include volcanic signals. A description of this process is also given in the methods section of the paper presented in Part II. The resulting aerosol-free temperature variability indices are presented in Sect. 3 of the supplementary results.

6. Summary and Conclusions

Explosive volcanic eruptions are a relevant aspect of the climate system since they dominate the stratospheric aerosol levels, affect surface temperatures and in particular temperatures in the lower stratosphere. Detailed knowledge of volcanic temperature imprints is vital, especially for the differentiation of natural and anthropogenic temperature changes.

This thesis provided an overview of how volcanoes interact with the climate system in Part I. In Part II and Part III the focus was put on the impacts of post-2000 volcanic eruptions on stratospheric temperature. For this purpose, in contrast to other studies, a combination of vertically high resolved temperature and aerosol data was used, which account for the vertical evolution of the volcanic plumes.

The main scientific results presented in Part II and Part III showed that the combination of both, highly resolved Radio Occultation (RO) temperature data together with Global Space-based Stratospheric Aerosol Climatology (GloSSAC) aerosol data are favorable for detecting signals of small eruptions. Even smaller signals, such as those of forest fires, could be detected. This might be relevant, particularly in view of widespread forest fires, which will occur more frequently due to climate change (University of East Anglia 2020), and therefore could become a more relevant source of stratospheric aerosols.

For the accurate detection of small volcanic signals, other natural variability modes have to be precisely accounted for. In this study this was done by using the potential of variability indices derived directly from RO temperature data (Wilhelmsen et al. 2018). These vertically resolved indices, compared to regular Quasi-Biennial Oscillation (QBO) and El Niño–Southern Oscillation (ENSO) indices, lead to less residual variability. However, due to the complex interplay between the different variability modes and the aerosol concentration the creation of indices which do not include volcanic aerosol variability was found to be a challenging task.

The main findings of this work were published in Stocker et al. (2019). The results exhibit distinct warming signals in the lower stratosphere that can clearly be associated with specific post-2000 volcanic eruptions. Especially the Tavurvur, Nabro and Calbuco eruptions caused a substantial warming in the lower stratosphere of the order of up to 0.5 K in the tropical mean. This is in line with findings from earlier studies such as Mehta et al. (2015). In addition to the lower stratospheric warming, small cooling signals in the mid-stratosphere were found for some eruptions. There is strong evidence that these signals result from enhanced upwelling of ozone poor air within the tropical pipe caused by the volcanic erup-

tions. However, since QBO and ENSO can also affect the vertical transport within the Brewer–Dobson Circulation (BDC), the results do not allow for a definite interpretation. Investigating a possible volcanic influence on the vertical transport within the BDC may be subject of future research.

Finally it was demonstrated that, compared to major variability such as QBO and ENSO, the volcanic signals do not largely contribute to the overall variability in the stratospheric temperature. Nevertheless they can, depending on latitude and altitude, substantially affect the short-term linear trend by up to 20%.

Although the signals observed in the mid-stratosphere may need further investigation, the results presented in this study can help to separate natural climate variability from anthropogenic influences in climate trend detection and further improve climate models (Stocker et al. 2019).

Part II.

Published Paper

Geophysical Research Letters

RESEARCH LETTER
10.1029/2019GL084396

Quantifying Stratospheric Temperature Signals and Climate Imprints From Post-2000 Volcanic Eruptions

Matthias Stocker[1], Florian Ladstädter[1,2], Hallgeir Wilhelmsen[1,3], and Andrea K. Steiner[1,2]

[1]Wegener Center for Climate and Global Change (WEGC), University of Graz, Graz, Austria, [2]Institute for Geophysics, Astrophysics, and Meteorology/Institute of Physics, University of Graz, Graz, Austria, [3]FWF-DK Climate Change, University of Graz, Graz, Austria

Key Points:
- The imprints of minor volcanic eruptions on stratospheric temperature are precisely quantified
- Vertically high resolved aerosol and temperature observations facilitate the accurate detection of volcanic signals in space and time
- Minor volcanic eruptions clearly affect the short-term temperature trend in the lower stratosphere

Correspondence to:
A. K. Steiner,
andi.steiner@uni-graz.at

Citation:
Stocker, M., Ladstädter, F., Wilhelmsen, H., & Steiner, A. K. (2019). Quantifying stratospheric temperature signals and climate imprints from post-2000 volcanic eruptions. *Geophysical Research Letters*, *46*, 12,486–12,494. https://doi.org/10.1029/2019GL084396

Received 2 JUL 2019
Accepted 20 SEP 2019
Accepted article online 29 OCT 2019
Published online 3 NOV 2019

Abstract Small volcanic eruptions and their effects have recently come into research focus. While large eruptions are known to strongly affect stratospheric temperature, the impacts of smaller eruptions are hard to quantify because their signals are masked by natural variability. Here, we quantify the temperature signals from small volcanic eruptions between 2002 and 2016 using new vertically resolved aerosol data and precise temperature observations from radio occultation. We find characteristic space-time signals that can be associated with specific eruptions. In the lower stratosphere, robust warming signals are observed, while in the midstratosphere also cooling signals of some eruptions appear. We find that the volcanic contribution to the temperature trend is up to 20%, depending on latitude and altitude. We conclude that detailed knowledge of the vertical structure of volcanic temperature impacts is crucial for comprehensive trend analysis in order to separate natural from anthropogenic temperature changes.

1. Introduction

Volcanic eruptions can substantially influence the climate system (Kremser et al., 2016; Robock, 2000, 2015; Timmreck, 2012) through the emission of trace gases, volcanic ash, and aerosol forming substances, such as sulfur dioxide (SO_2). In the troposphere, the volcanic ash causes local weather changes (Robock, 2015). In the stratosphere, sulfate aerosols formed by volcanic SO_2 emissions absorb and backscatter solar and terrestrial radiation and also enhance chemical reactions, for example, ozone depletion. This affects surface temperature as well as stratospheric temperature and dynamics (Aquila et al., 2013; Robock, 2000, 2015). Those sulfate aerosols are among the main components of the stratospheric aerosol layer (Kremser et al., 2016). Besides aerosol chemistry and physics, their distribution in the stratosphere is governed by large-scale processes such as the Brewer Dobson Circulation and the Quasi-biennial Oscillation (QBO; Baldwin et al., 2001; Kremser et al., 2016; Timmreck, 2012; Trepte & Hitchman, 1992).

The last major volcanic eruptions were those of El Chichón in 1982 and Pinatubo in 1991. They emitted tremendous amounts of SO_2, and their consequences have been addressed in several studies (e.g., Aquila et al., 2013; Free & Lanzante, 2009; Randel et al., 2009). They were found to strongly affect tropospheric as well as stratospheric temperature and chemistry. Following the Pinatubo eruption, a global tropospheric cooling of up to 0.6 K (Parker et al., 1996) and a stratospheric warming of 2 K (Robock, 2000) were detected. In the lowermost stratosphere, model studies showed an even stronger warming due to the Pinatubo aerosols compared to the observed one (Free & Lanzante, 2009). Moreover, Aquila et al. (2013) modeled a drop of approximately 8% in tropical stratospheric ozone concentration directly after the eruption.

Recently, a series of smaller volcanic eruptions that started in 2002 has been of research interest. Those eruptions most likely led to a steady increase in stratospheric aerosol optical depth (AOD) during the last decade (Mehta et al., 2015; Vernier et al., 2011). Also, a contribution of those eruptions to the 21st century warming hiatus has been discussed (Santer et al., 2015).

Not all of the small eruptions reach the stratosphere, depending on the latitude of the eruption, the explosivity, the emitted SO_2 mass (Robock, 2000), and also the emission height. Only aerosols reaching the stratosphere have a sufficient lifespan (up to 3 years) to affect climate (Robock, 2015).

Table 1
Eruptions Between 2002 and 2017 With a Minimum VEI of 4

Name	Start date	VEI	SO_2 mass (kt)	SO_2 altitude (max.; km)	Latitude	Country
Ruang (Ru)	09-25-2002	4	80	22	2.3°N	Indonesia
Reventador	11-03-2002	4	84	17	0.077°S	Ecuador
Manam (Ma)	10-24-2004	4	152[a]	24[a]	4.08°S	Papua New Guinea
Rabaul (Tavurvur; Ta)	08-11-2006	4	300	18	4.271°S	Papua New Guinea
Chaitén	05-02-2008	4	14	17	42.833°S	Chile
Okmok	07-12-2008	4	150	15	53.43°N	United States (Alaska)
Kasatochi (Ka)	08-07-2008	4	2,000	15	52.177°N	United States (Alaska)
Sarychev Peak (Sp)	06-11-2009	4	1,200	17	48.092°N	Russia
Eyjafjallajökull	03-20-2010	4	466	9	63.633°N	Iceland
Merapi (Me)	10-26-2010	4	300	17	7.54°S	Indonesia
Grímsvötn	05-21-2011	4	300	12	64.416°N	Iceland
Puyehue-Cordón Caulle	06-04-2011	5	200	14	40.59°S	Chile
Nabro (Na)	06-13-2011	4	3,650	18	13.37°N	Eritrea
Tolbachik	11-27-2012	4	200	10	55.832°N	Russia
Sinabung	09-15-2013	4	20	7	3.17°N	Indonesia
Kelut (Ke)	02-13-2014	4	200	19	7.93°S	Indonesia
Calbuco (Ca)	04-22-2015	4	400	20	41.33°S	Chile
Wolf	05-25-2015	4	200	7	0.02°N	Ecuador

Note. Eruptions reaching the stratosphere are in bold. Data are from the Global Volcanism Program (2013).
[a]Main emission event during the eruption.

The Volcanic Explosivity Index (VEI), which describes the magnitude of the eruption, is a first indication of whether the eruption can cause stratospheric temperature changes. For post-2000 volcanoes, eruptions that reached the stratosphere typically had a minimum VEI of 4 (Table 1). Yet, not all of the >VEI 4 eruptions reached the stratosphere. The Puyehue in 2011, for example, had a VEI of 5, but most of the emitted aerosols were not transported to altitudes above 14 km. Data for these indicators used here are taken from the Global Volcanism Program (2013) database, "Volcanoes of the World."

The impact of specific smaller eruptions on atmospheric temperature has been addressed by Wang et al. (2009), who investigated the Mount Chaitén eruption in 2008, and Okazaki and Heki (2012), who studied the Eyjafjallajökull eruption in 2010 and the Puyehue eruption in 2011. They found significant negative tropospheric temperature signals induced by those eruptions using novel radio occultation (RO) satellite data. Biondi et al. (2017) also employed RO data to observe the volcanic clouds of the Puyehue and the Nabro eruptions in 2011. For Puyehue they found tropospheric cooling signals, while for Nabro considerable stratospheric warming was detected. Mehta et al. (2015) examined eruptions between 2001 and 2010 using RO and found small but significant warming in the upper troposphere-lower stratosphere region for the Soufrière Hills and Tavurvur eruptions, which occurred in quick succession.

However, the accurate quantification of temperature signals of such small eruptions is challenging. The emitted SO_2 mass of these eruptions (Table 1) is up to three orders of magnitude smaller than that of, for example, Pinatubo (20 Mt), illustrating the difficulty. Previous studies relied on AOD data as a proxy for the identification of volcanically induced temperature signals. Yet the AOD does not account for a vertically resolved distribution of the volcanic aerosols, which are lofted within the "tropical pipe" (Flury et al., 2013; Kremser et al., 2016; Vernier et al., 2011).

In this study, we quantify the stratospheric volcanic temperature signals in space and time for post-2000 volcanoes. We use the potential of a newly available, vertically resolved aerosol data set in combination with precise temperature observations from RO. We focus on the tropical stratospheric region and accurately characterize natural atmospheric variability to investigate the imprint of volcanic signals on short-term temperature trends.

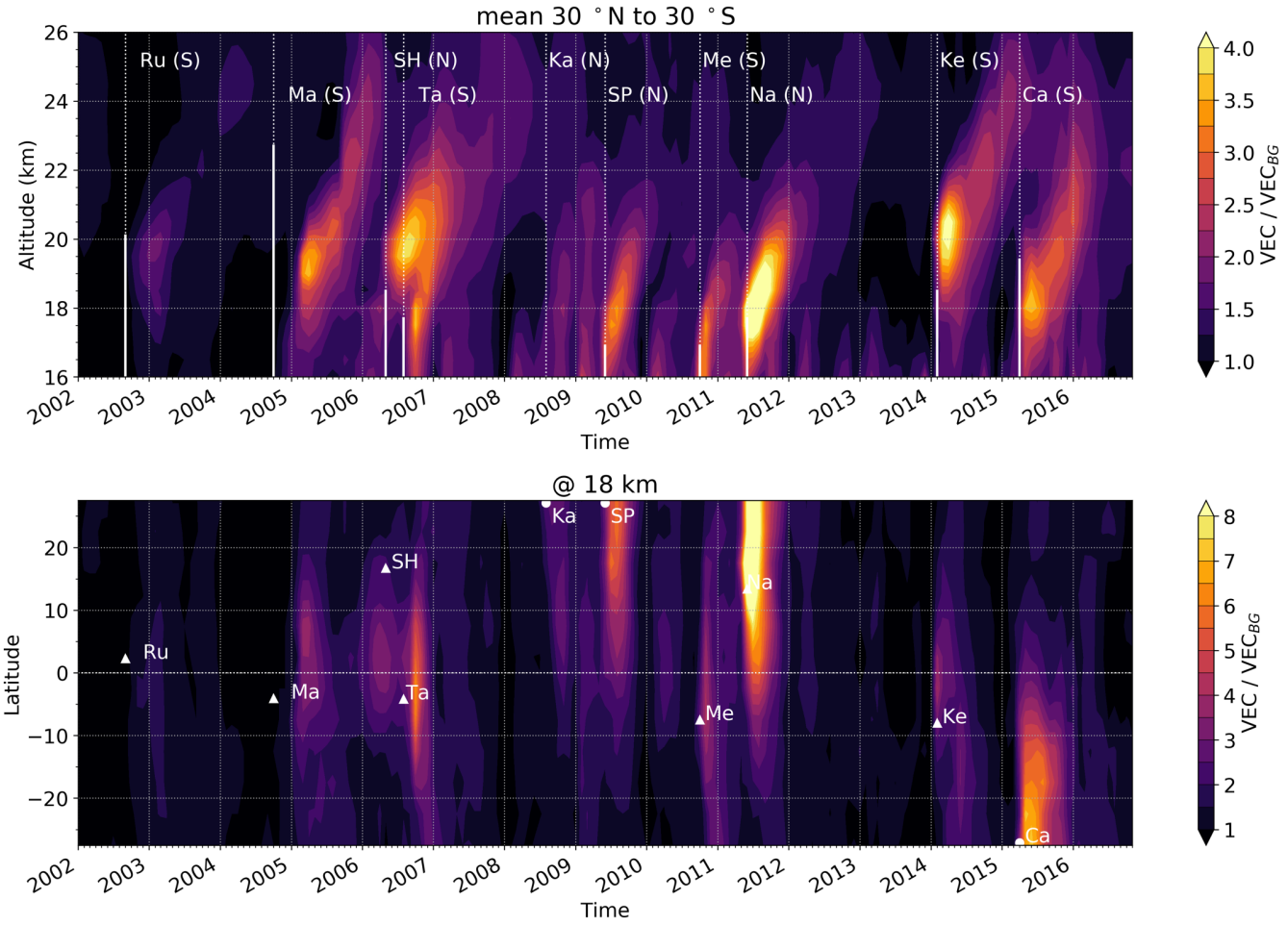

Figure 1. Altitude time pattern of the aerosol concentration divided by the background concentration (mean 30°N to 30°S; top) as well as the latitude time pattern of the aerosol concentration divided by the background concentration at 18 km (bottom). Vertical lines in the altitude time pattern mark the date of the eruptions as well as the maximum SO_2 altitude reported in the Global Volcanism Program (2013) database (solid lines). N and S in brackets indicate north and south of the equator. Triangles in the latitude time pattern mark the time of the eruption as well as the latitude of the eruption. Eruptions that occurred at latitudes not part of the plot range are marked with a semicircle. Note that, for example, for the Manam (Ma), the start date of the eruption does not coincide with the date of the main emission event.

2. Data and Method

2.1. Aerosol and Temperature Data

We use stratospheric aerosol data from the Global Space-based Stratospheric Aerosol Climatology (GloSSAC; Thomason, 2017; Thomason et al., 2018). GloSSAC is based on various aerosol measurement missions (e.g., SAGE, OSIRIS and CALIPSO; Thomason et al., 2018) and became available in 2017. We employ the vertically resolved Volume Extinction Coefficient measured at 525 nm with a latitudinal resolution of 5° zonal bands and a vertical resolution of 500 m. We inspect altitudes above 16 km as below this level, tropical data are not complete. Since the focus is on the tropical upper troposphere-lower stratosphere region, the upper limit is set to 26 km and we use data between 30°S to 30°N. From the original aerosol concentration data, we subtract the provided background aerosol concentration to create deseasonalized aerosol anomalies. The background aerosol concentration represents the state of the stratosphere without volcanic influence and is the monthly average concentration of the years 1999 to 2004, excluding 2002 since in this year the eruption of the Ruang occurred (Thomason, 2017; Thomason et al., 2018). The aerosol concentration divided by the background concentration is illustrated in Figure 1 and clearly shows a volcanic pattern of aerosols which are lofted into the middle stratosphere over time.

We take advantage of the vertically high resolved data from RO to analyze the spatiotemporal imprint of volcanoes on temperature. RO is a limb sounding technique exploiting signals from Global Navigation Satellite

Systems and provides long-term stability, global coverage, high accuracy, and vertical resolution in the upper troposphere and lower stratosphere (Steiner et al., 2011). We use temperature data from the Wegener Center OPSv5.6 RO multisatellite record (Angerer et al., 2017) on 5° latitudinal bands with a vertical gridding of 500 m to match the aerosol data. Temperature anomalies are created by subtracting the mean seasonal cycle for the investigated time series.

The GloSSAC data set is currently available from 1979 until the end of 2016. The RO temperature record is available from end of 2001 onward. Therefore, our investigated time period is from 2002 to 2016.

2.2. Regression Analysis

We estimate the volcanic signals in stratospheric temperature using multiple linear regression analysis. To account for autocorrelation in the monthly temperature data, we utilize a Generalized Least Squares with Autocorrelated AR(p) Errors model.

For the small eruptions in the study period, temperature signals are hard to detect because they are masked by natural variability. For large eruptions, volcanic signals can be estimated from the regression residuals when natural variability modes such as El Niño–Southern Oscillation (ENSO) or QBO are taken into account. Conventional variability indices, such as the Niño 3.4 SST or QBO winds at specific pressure levels, have been used in previous studies (Randel et al., 2009). This approach is less effective for smaller eruptions, because the residual variability is comparable to the volcanic signal amplitude (Mehta et al., 2015).

To separate the small post-2000 volcanic signals from other variability, we therefore take advantage of the temperature variability indices introduced by Wilhelmsen et al. (2018), which leave very small temperature residuals by construction. Compared to conventional indices these indices are of high vertical resolution and are created directly from the temperature anomalies derived from the RO measurements, using an empirical orthogonal function (EOF) analysis (Hannachi et al., 2007) on each separate altitude level in the data set. The leading principal components (PCs) are used as variability indices for the corresponding altitude level.

These variability indices do not only include QBO or ENSO, but all other main modes of variability such as aerosol-induced temperature changes, which leads to a nonzero correlation between the aerosol index and the variability indices. Additionally, the aerosol distribution itself is correlated to the QBO phase (Trepte & Hitchman, 1992). This means that a regression analysis, using only the regular aerosol anomalies as explanatory variable, would result in volcanic temperature signals that also include QBO related temperature variability. Therefore, when both the aerosol and the temperature variability indices are used in the multiple linear regression analysis, this results in collinearity between the regressors (see Santer et al., 2001).

To avoid collinearity, we remove in a first step the QBO signal from the aerosol index, and in a second step the resulting QBO-free aerosol signal from the variability indices.

In the first step, we subtract the QBO signal from the aerosol anomalies using linear regression. Hereby, we utilize QBO indices derived from the Singapore wind fields via EOF analysis. The reconstructed aerosol concentration for the leading two PCs derived from the wind field indicates a relatively weak QBO signal in the lower stratospheric aerosol concentration, which becomes stronger toward the middle stratosphere. Around 24 km, the impact of the QBO phases on the aerosol anomalies is reversed, changing from positive to negative, and vice versa. This agrees with the QBO-induced aerosol mixing ratio anomalies found by Hommel et al. (2015), who investigated the influence of the QBO on stratospheric aerosol distribution using an aerosol-coupled climate model.

After subtracting the QBO reconstructed aerosol concentration from the aerosol anomalies, primarily the volcanic pattern remains in the aerosol regressor, as verified by correlation analysis.

In the second step, we create the temperature variability indices from the residual temperature anomalies that remain after excluding the aerosol variability. This is done by subtracting a first estimate of the volcano-related temperature variability from the original temperature anomalies. The first estimate is computed using the Generalized Least Squares with Autocorrelated AR(p) Errors model on the temperature anomalies with the volcanic aerosols distribution, as the only explanatory variable. Since we removed the QBO signals from the aerosols distribution the first estimate of the volcanic temperature signals does not include QBO variability. Then we apply an EOF analysis on the residual temperature anomalies as explained above, and use the resulting variability indices in the following steps.

The final regression model then includes the QBO-free aerosol anomalies as well as the aerosol-free variability indices derived from the temperature anomalies after subtracting the estimated volcanic temperature signal. It can be written as

$$X^{\mathrm{Mod}}_{\phi,h,t} = \beta^{\mathrm{const}}_{\phi,h} + \beta^{\mathrm{linear}}_{\phi,h} t + \beta^{\mathrm{aer}}_{\phi,h} A^{\mathrm{anom}}_{\phi,h,t} + \beta^{\mathrm{PC1}}_{\phi,h} \mathrm{PC1}_{h,t} + \beta^{\mathrm{PC2}}_{\phi,h} \mathrm{PC2}_{h,t} + \beta^{\mathrm{PC3}}_{\phi,h} \mathrm{PC3}_{h,t} + \epsilon \quad (1)$$

where $X^{\mathrm{Mod}}_{\phi,h,t}$ represents the temperature anomalies as function of latitude (ϕ), altitude (h), and time (t), $A^{\mathrm{anom}}_{\phi,h,t}$ the QBO-free aerosol anomalies, $\mathrm{PC1}_{h,t}$, $\mathrm{PC2}_{h,t}$, and $\mathrm{PC3}_{h,t}$ the aerosol-free variability indices, and ϵ the residual.

3. Results and Discussion

Signals from several central tropical eruptions such as those of Manam, Soufrière Hills and Tavurvur, Merapi, Nabro, and Kelut are clearly visible in the aerosol data (Figure 1). Yet, also perturbations from higher-latitude eruptions such as those of Sarychev Peak and Calbuco can be identified. After the eruptions, the aerosols rise with roughly 4 km/year (cf. Vernier et al., 2011) in the lower to middle tropical stratosphere due to the vertical transport within the tropical pipe. However, a considerable amount of aerosols reaches higher altitudes only after particular eruptions such as that of Tavurvur and Soufrière Hills, respectively and also of Kelut and Calbuco. From Nabro, which emitted several times more aerosols than the other eruptions, seemingly only a small amount reached altitudes above 20 km.

This difference in the efficiency of the vertical transport of the aerosols not only depends on the injection height but also on the phase of the QBO during the time of the eruption, since the strength of the horizontal and vertical transport processes within the tropical pipe are connected to the phase of the QBO (Flury et al., 2013; Kremser et al., 2016). Flury et al. (2013) note that in the westerly shear zone of the QBO the transport out of the tropical pipe toward higher latitudes is enhanced while the vertical transport within the pipe is reduced. This means that during the QBO westerly shear volcanic aerosols are less likely transported to higher altitudes but are rather transported to the midlatitudes. Conversely, during the QBO easterly shear higher altitudes are more likely to be reached.

3.1. Volcanic Temperature Signals

In the reconstructed temperature for the volcanic aerosols (Figure 2), warming signals following the different eruptions are visible in the lowermost stratosphere up to around 20 km. Especially the Tavurvur (2006), Merapi (2010), Nabro (2011), and Calbuco (2015) eruptions show strong temperature impacts of about 0.5 K in the tropical mean. Weaker, but also visible signals of about 0.2 K can be associated with the Manam (2005), the Sarychev Peak (2009), and the Kelut (2014) eruptions. The warming at this altitude is most likely a result of absorption of solar and terrestrial long wave radiation by the volcanic sulfate aerosols (Robock, 2015, 2000; Mehta et al., 2015). The magnitude of the temperature increase following the Tavurvur and Soufrière Hills eruptions is consistent with the warming signal found by Mehta et al. (2015), who estimated the warming signal as the difference of averaged temperature residuals before and after the eruptions. Nabro emitted far more aerosols to this altitude, the subsequent warming, however, is only slightly stronger than for the Soufrière Hills and Tavurvur eruptions. This results from the Nabro aerosols being spread predominantly to the Northern hemisphere by the Asian monsoon (Bourassa et al., 2012). Thus, the main aerosol concentration is located at latitudes north of 10°N (Figure 1, bottom). For the Calbuco eruption, in contrast, a large amount of aerosols was transported toward the equator.

The altitude time cross section (Figure 2, top) further displays cooling signals of up to 0.3 K between 20 and 24 km. Since the signals follow the pattern of the volcanic aerosols as seen in Figure 1, we assume that they originate from the specific eruptions, which affected the aerosol concentration at altitudes between 20 and 24 km. Eruptions that have an impact on temperature at this height are those of Manam (2005) and Tavurvur and Soufrière Hills (2006; cf. Mehta et al., 2015), as well as Kelut (2014) and Calbuco (2015). Other eruptions such as Nabro (2011), which also caused a substantial temperature increase in the lower stratosphere (Biondi et al., 2017), appear to have nearly no cooling effect at higher altitudes. This correlates with the findings in Figure 1 (top), which indicates that the Merapi or the Nabro eruption did not substantially influence the aerosol concentration at altitudes above 20 km.

However, the cooling between 22 and 24 km is an interesting feature that cannot simply be explained by the radiative properties of the sulfate aerosols. A possible explanation for the cooling is given by Robock (2015)

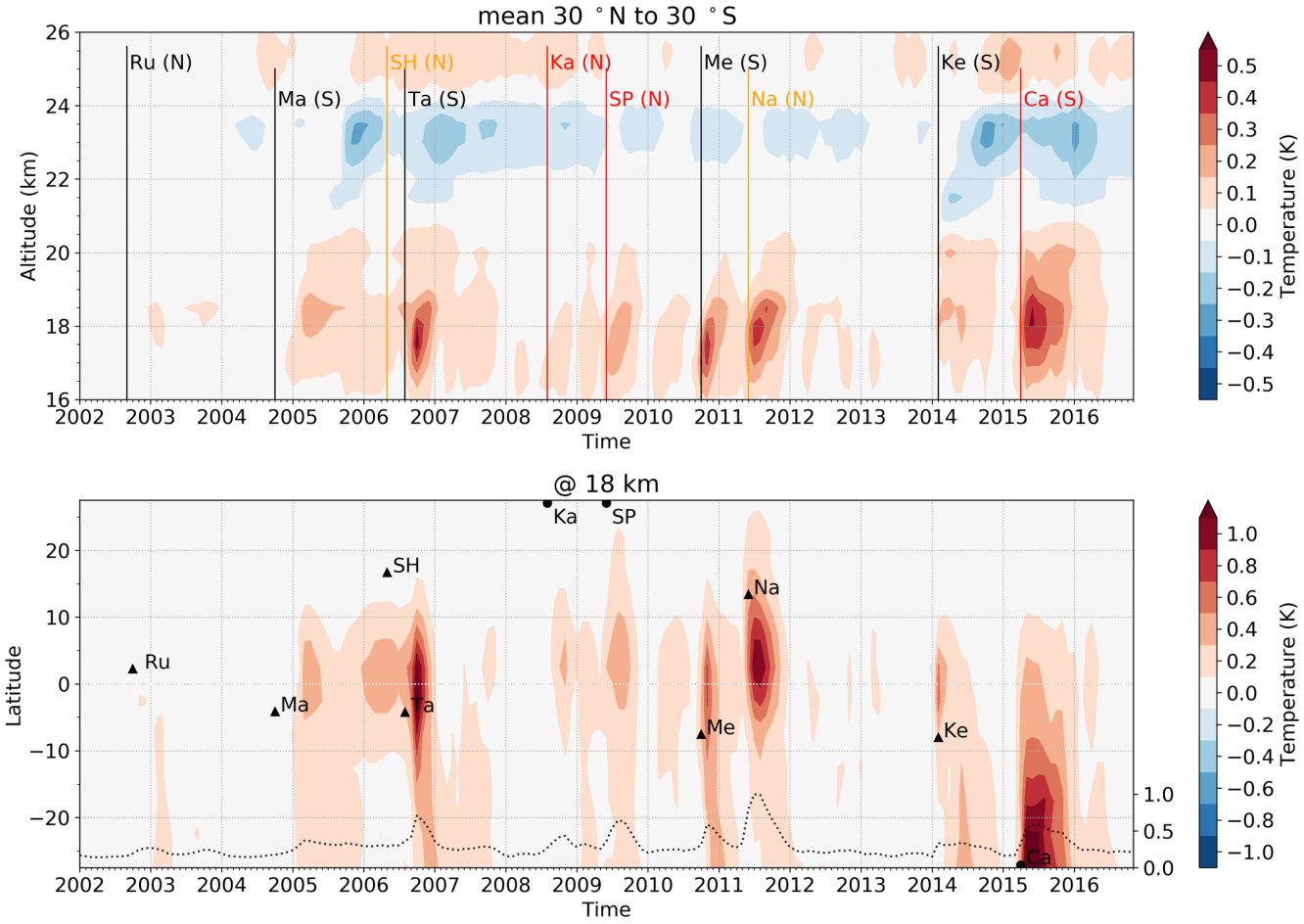

Figure 2. Altitude time cross section of the volcanic aerosol reconstructed temperature (mean 30°N to 30°S; top) as well as the latitude time cross section at 18 km (bottom). Vertical lines in the altitude time pattern mark the date of the eruptions. N and S in brackets indicate north and south of the equator. Line colors indicate the latitude of the eruption (red >30, orange >10, and black <10). Triangles in the latitude time pattern mark the date as well as the latitude of the eruption. Eruptions that occurred at latitudes not part of the plot range are marked with a semicircle. The dashed line represents the normalized VEC for the 18-km altitude level (mean 30°N to 30°S).

and Aquila et al. (2013). As described by Robock (2015), aerosols, in addition to their effects on the radiative flux, can also affect stratospheric dynamics and chemistry (especially ozone depletion). Robock (2015) also notes that in the tropics volcanic clouds enhance the tropical upwelling and hence bring low ozone concentration layers to higher altitudes, possibly causing cooling. Simulations by Aquila et al. (2013) showed a decrease in ozone shortly after the Pinatubo eruption, strongest at about 24 km, which was mainly due to increased tropical upwelling. For large eruptions, the warming effect due to the huge amount of aerosols is dominant (Free & Lanzante, 2009; Randel et al., 2009; Robock, 2015). However, for the small eruptions considered in this study, the dynamical ozone reduction could be more relevant and could explain the observed cooling signals.

A strong indication that the cooling signals are caused by changes in the ozone concentration is that they disappear when we include ozone variability (not shown). The warming signals in the lowermost stratosphere, however, remain robust. As the cooling is assumed to be an aerosol-induced effect, we do not further account for ozone.

Other possible explanations for cooling signals in the tropical stratosphere are ENSO-related changes in the ozone concentration due to increased tropical upwelling (Diallo et al., 2018; Domeisen et al., 2019; Randel et al., 2009). Diallo et al. (2018) found a strong reduction of tropical ozone related to the 2015/2016 ENSO event. We investigated the influence of ENSO on the volcano-induced temperature variability and found that it is negligible (consistent with Santer et al., 2015). Additionally, the midstratospheric cooling signals in

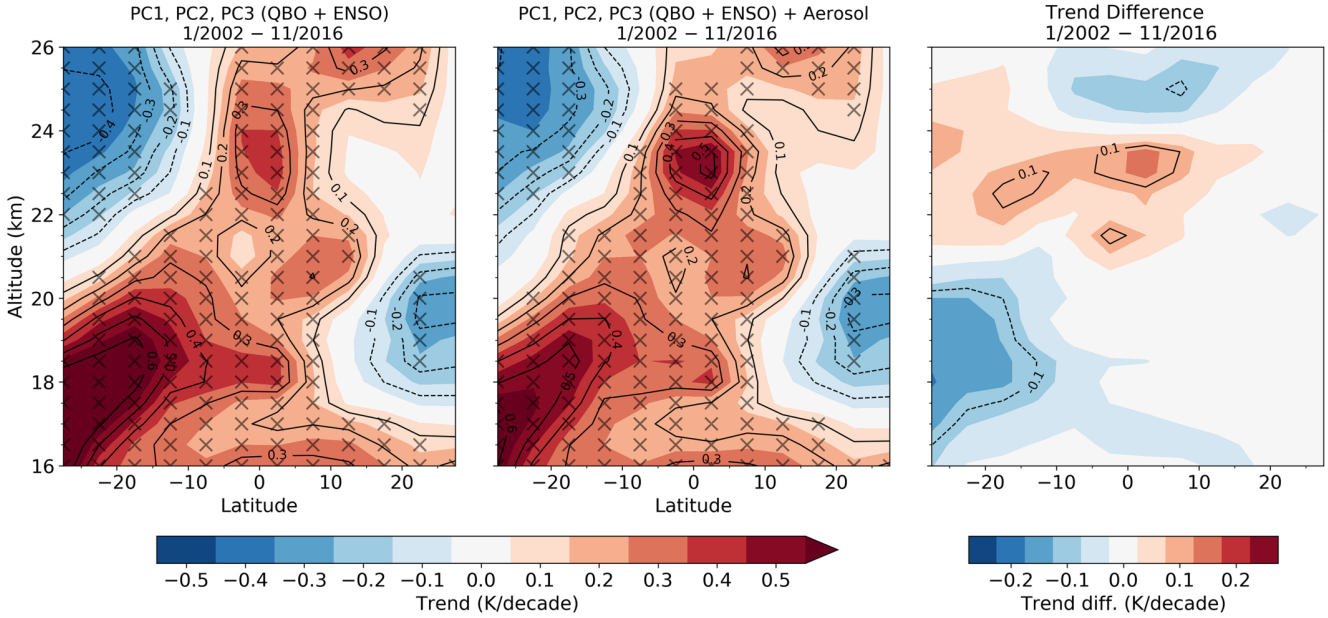

Figure 3. Altitude-latitude cross section of the linear trend for the time series from 2002 to 2016 considering only natural variability indices (left), and natural variability indices together with the volcanic aerosols (center); trend difference (right). Trend values that are significant at the 95% confidence level are indicated with an X mark. QBO = Quasi-biennial Oscillation; ENSO = El Niño–Southern Oscillation; PC = principal component.

2010 and 2014 do not coincide with ENSO events. Therefore, we assume that the cooling signals resulting from our approach are not related to an ENSO pattern in the stratospheric circulation.

The small positive temperature signals around 26 km presumably result from volcanic modulations of the aerosol concentration in the stratospheric aerosol layer, which has its strongest mixing ratio at this altitude (Hommel et al., 2015; Vernier et al., 2011).

Figure 2 (bottom) shows the latitudinal distribution of the warming signals maxima at 18 km, which reveals additional features. Except for the Calbuco, the warming signals appear to be limited to approximately 15°N to 15°S in latitude and are largest close to the equator. This even applies to eruptions that took place at high latitudes and of which only a small fraction of aerosols reached the tropical region, where their effect is more pronounced (Ferraro et al., 2011; Mehta et al., 2015).

In contrast to other higher-latitude eruptions, for the Calbuco eruption in the Southern Hemisphere, a strong warming is observed. As shown in Figure 1 (bottom), a large amount of the Calbuco aerosols was transported toward low latitudes. However, the latitude time cross section in Figure 2 (bottom) also shows that the Calbuco warming for this altitude level is largest outside the central tropics. This may be explained by the fact that at the time of the Calbuco eruption there was an extraordinary strong ENSO event (Stockdale et al., 2017). ENSO events cause a comparatively warm troposphere and also lead to reduced temperature in the lower stratosphere, not only in the tropics but also at midlatitudes (Free & Seidel, 2009). Such conditions increase the warming potential of the volcanic aerosols (Ferraro et al., 2011) and hence may explain why the Calbuco signal is strongest at midlatitudes.

3.2. Linear Trend Analysis

For analyzing the volcanic impacts on short-term climatological trends, we perform the regression with and without including aerosols. We find that including the aerosol index causes substantial changes in the resulting linear trend (Figure 3). The differences are more pronounced in the Southern Hemisphere between 30°S and 10°S where the trend is reduced by more than 0.1 K (approximately 20%). This is related to the Calbuco eruption, which occurred at the end of the investigated time series. A slightly increased trend is detected in the equatorial region between 22 and 24 km, presumably due to the cooling signals from the ozone reduction. In the central tropical lower stratosphere, where most of the eruptions show the strongest warming signals, the trend differences are small. This is because the eruptions with strong signals are distributed roughly uniformly in time over the investigated time period.

4. Conclusions

This is the first study addressing the precise quantification of the impact of recent minor volcanic eruptions on temperature variability and trends using a combination of vertically high resolved temperature and aerosol data, both from satellite measurements. This facilitates the accurate detection of signals of post-2000 volcanic eruptions in space and time and their imprint on stratospheric temperature.

We found robust warming signals in the lower stratosphere up to 20 km from the inspected explosive volcanoes. The strongest imprint was found for Tavurvur, Merapi, Nabro, and Calbuco. The latitudinal distribution of the volcanic imprints was clearly resolved and strongest in the central tropics, with the exception of Calbuco. The results for specific eruptions agree with findings of previous studies that used standard AOD to represent volcanic variability.

In the middle stratosphere we found small cooling signals for the investigated volcanic eruptions. A suggested explanation is an indirect aerosol effect on ozone due to an enhanced upwelling of ozone-poor air after the eruption. The results indicate that small eruptions may also be relevant when investigating stratospheric ozone in the tropics.

Compared to major variability modes such as the QBO, the overall variability due to post-2000 volcanic eruptions was found to be small; however, they are of importance for short-term trend analysis. For the investigated time series we found that the impact on linear trends can be up to 20%, depending on altitude and latitude. While the temperature trend is reduced in the lower stratosphere, an enhanced positive trend is observed in the middle stratosphere.

The results show that detailed knowledge of the vertical structure of volcanic temperature changes is crucial for comprehensive trend analysis, as their influence varies for different altitudes and latitudes. Exploiting the potential of the newly available, highly resolved data sets is beneficial for gaining better knowledge on the impacts of volcanic eruptions. This further helps to separate natural climate variability from anthropogenic influences in climate trend detection, and to improve climate models.

Acknowledgments

The authors express their gratitude to UCAR/CDAAC (Boulder, CO, USA) for providing access to RO phase and orbit data as well as to ECMWF (Reading, UK) for giving access to analysis and forecast data. We also thank the WEGC EOPAC team for providing the OPSv5.6 RO data, which are available online (https://doi.org/10.25364/WEGC/OPS5.6:2019.1). The GloSSAC data set was obtained from the NASA Langley Research Center Atmospheric Sciences Data Center. We acknowledge Global Volcanism Program, Smithsonian Institution (https://volcano.si.edu/) for providing data on the volcanic eruptions and FU Berlin (Berlin, DE) for providing Singapore wind data (https://www.geo.fu-berlin.de/met/ag/strat/produkte/qbo/). The authors want to particularly thank Harald Rieder (WEGC, AT), Jean-Paul Vernier (LARC, USA), and William Randel (NCAR, USA) for fruitful discussions and sharing their expertise. We thank two anonymous reviewers for their helpful comments. This work was funded by the Austrian Science Fund (FWF) under Research Grant P27724-NBL (VERTICLIM) and W1256-G15 (Doctoral Programme Climate Change-Uncertainties, Thresholds and Coping Strategies) as well as by the FFG-ALR project ATROMSAF1(ASAP-13 859771).

References

Angerer, B., Ladstädter, F., Scherllin-Pirscher, B., Schwärz, M., Steiner, A. K., Foelsche, U., & Kirchengast, G. (2017). Quality aspects of the WEGC multi-satellite GPS radio occultation record OPSv5.6. *Atmospheric Measurement Techniques*, *10*, 4845–4863. https://doi.org/10.5194/amt-10-4845-2017

Aquila, V., Oman, L. D., Stolarski, R., Douglass, A. R., & Newman, P. A. (2013). The response of ozone and nitrogen dioxide to the eruption of Mt. Pinatubo at southern and northern midlatitudes. *Journal of the Atmospheric Sciences*, *70*(3), 894–900. https://doi.org/10.1175/jas-d-12-0143.1

Baldwin, M. P., Gray, L. J., Dunkerton, T. J., Hamilton, K., Haynes, P. H., Randel, W. J., et al. (2001). The quasi-biennial oscillation. *Reviews of Geophysics*, *39*(2), 179–229. https://doi.org/10.1029/1999RG000073

Biondi, R., Steiner, A. K., Kirchengast, G., Brenot, H., & Rieckh, T. (2017). Supporting the detection and monitoring of volcanic clouds: A promising new application of global navigation satellite system radio occultation. *Advances in Space Research*, *60*(12), 2707–2722. https://doi.org/10.1016/j.asr.2017.06.039

Bourassa, A. E., Robock, A., Randel, W. J., Deshler, T., Rieger, L. A., Lloyd, N. D., et al. (2012). Large volcanic aerosol load in the stratosphere linked to Asian monsoon transport. *Science*, *337*, 78–81. https://doi.org/10.1126/science.1219371

Diallo, M., Riese, M., Birner, T., Konopka, P., Müller, R., Hegglin, M. I., et al. (2018). Response of stratospheric water vapor and ozone to the unusual timing of El Niño and the QBO disruption in 2015–2016. *Atmospheric Chemistry and Physics*, *18*(17), 13,055–13,073. https://doi.org/10.5194/acp-18-13055-2018

Domeisen, D. I., Garfinkel, C. I., & Butler, A. H. (2019). The teleconnection of El Niño Southern Oscillation to the stratosphere. *Reviews of Geophysics*, *57*, 5–47. https://doi.org/10.1029/2018rg000596

Ferraro, A. J., Highwood, E. J., & Charlton-Perez, A. J. (2011). Stratospheric heating by potential geoengineering aerosols. *Geophysical Research Letters*, *38*, L24706. https://doi.org/10.1029/2011GL049761

Flury, T., Wu, D. L., & Read, W. G. (2013). Variability in the speed of the Brewer–Dobson circulation as observed by Aura/MLS. *Atmospheric Chemistry and Physics*, *13*(9), 4563–4575. https://doi.org/10.5194/acp-13-4563-2013

Free, M., & Lanzante, J. (2009). Effect of volcanic eruptions on the vertical temperature profile in radiosonde data and climate models. *Journal of Climate*, *22*(11), 2925–2939. https://doi.org/10.1175/2008jcli2562.1

Free, M., & Seidel, D. J. (2009). Observed El Niño–Southern Oscillation temperature signal in the stratosphere. *Journal of Geophysical Research*, *114*, D23108. https://doi.org/10.1029/2009JD012420

Global Volcanism Program (2013). Volcanoes of the world, v. 4.3.4.https://doi.org/10.5479/si.gvp.votw4-2013 (Smithsonian Institution, Downloaded 08 Nov 2018).

Hannachi, A., Jolliffe, I. T., & Stephenson, D. B. (2007). Empirical orthogonal functions and related techniques in atmospheric science: A review. *International Journal of Climatology*, *27*(9), 1119–1152. https://doi.org/10.1002/joc.1499

Hommel, R., Timmreck, C., Giorgetta, M. A., & Graf, H. F. (2015). Quasi-biennial oscillation of the tropical stratospheric aerosol layer. *Atmospheric Chemistry and Physics*, *15*(10), 5557–5584. https://doi.org/10.5194/acp-15-5557-2015s.

Kremser, S., Thomason, L. W., von Hobe, M., Hermann, M., Deshler, T., Timmreck, C., et al. (2016). Stratospheric aerosol—Observations, processes, and impact on climate. *Reviews of Geophysics*, *54*, 278–335. https://doi.org/10.1002/2015RG000511

Mehta, S. K., Fujiwara, M., Tsuda, T., & Vernier, J. P. (2015). Effect of recent minor volcanic eruptions on temperatures in the upper troposphere and lower stratosphere. *Journal of Atmospheric and Solar-Terrestrial Physics*, *129*, 99–110. https://doi.org/10.1016/j.jastp.2015.04.009

Okazaki, I., & Heki, K. (2012). Atmospheric temperature changes by volcanic eruptions: GPS radio occultation observations in the 2010 Icelandic and 2011 Chilean cases. *Journal of Volcanology and Geothermal Research*, *245–246*, 123–127. https://doi.org/10.1016/j.jvolgeores.2012.08.018

Parker, D. E., Wilson, H., Jones, P. D., Christy, J. R., & Folland, C. K. (1996). The impact of Mount Pinatubo on world-wide temperatures. *International Journal of Climatology*, *16*(5), 487–497. https://doi.org/10.1002/(SICI)1097-0088(199605)16:5<487::AID-JOC39>3.0.CO;2-J

Randel, W. J., Garcia, R. R., Calvo, N., & Marsh, D. (2009). ENSO influence on zonal mean temperature and ozone in the tropical lower stratosphere. *Journal of Geophysical Research*, *36*, L15822. https://doi.org/10.1029/2009GL039343

Robock, A. (2000). Volcanic eruptions and climate. *Reviews of Geophysics*, *38*(2), 191–219. https://doi.org/10.1029/1998rg000054

Robock, A. (2015). *Climatic impacts of volcanic eruptions Edited by* H. Sigurdsson (pp. 935–942). https://doi.org/10.1016/B978-0-12-385938-9.00053-5

Santer, B. D., Solomon, S., Bonfils, C., Zelinka, M. D., Painter, J. F., Beltran, F., et al. (2015). Observed multivariable signals of late 20th and early 21st century volcanic activity. *Geophysical Research Letters*, *42*, 500–509. https://doi.org/10.1002/2014GL062366

Santer, B. D., Wigley, T. M. L., Doutriaux, C., Boyle, J. S., Hansen, J. E., Jones, P. D., et al. (2001). Accounting for the effects of volcanoes and ENSO in comparisons of modeled and observed temperature trends. *Journal of Geophysical Research*, *106*, 28,033–28,059. https://doi.org/10.1029/2000JD000189

Steiner, A. K., Lackner, B. C., Ladstädter, F., Scherllin-Pirscher, B., Foelsche, U., & Kirchengast, G. (2011). GPS radio occultation for climate monitoring and change detection. *Radio Science*, *46*, RS0D24. https://doi.org/10.1029/2010RS004614

Stockdale, T., Balmasedaand, M., & Ferranti, L. (2017). The 2015/2016 El Niño and beyond. ECMWF Newsletter. https://www.ecmwf.int/node/18187 https://doi.org/10.21957/m3c157

Thomason, L. W. (2017). GloSSAC Level 3 netCDF file—Version 1 [Data set]. https://doi.org/10.5067/glossac-l3-v1.0 (NASA Langley Atmospheric Science Data Center DAAC).

Thomason, L. W., Ernest, N., Millán, L., Rieger, L., Bourassa, A., Vernier, J. P., & Peter, T. (2018). A global space-based stratospheric aerosol climatology: 1979–2016. *Earth System Science Data*, *10*(1), 469–492. https://doi.org/10.5194/essd-10-469-2018

Timmreck, C. (2012). Modeling the climatic effects of large explosive volcanic eruptions. *WIREs Climate Change*, *3*, 545–564. https://doi.org/10.1002/wcc.192

Trepte, C. R., & Hitchman, M. H. (1992). Tropical stratospheric circulation deduced from satellite aerosol data. *Nature*, *355*(6361), 626–628. https://doi.org/10.1038/355626a0

Vernier, J. P., Thomason, L. W., Pommereau, J. P., Bourassa, A., Pelon, J., Garnier, A., et al. (2011). Major influence of tropical volcanic eruptions on the stratospheric aerosol layer during the last decade. *Geophysical Research Letters*, *38*, L12807. https://doi.org/10.1029/2011GL047563

Wang, K.-Y., Lin, S.-C., & Lee, L.-C. (2009). Immediate impact of the Mt Chaiten eruption on atmosphere from FORMOSAT-3/COSMIC constellation. *Geophysical Research Letters*, *36*, L03808. https://doi.org/10.1029/2008GL036802

Wilhelmsen, H., Ladstädter, F., Scherllin-Pirscher, B., & Steiner, A. K. (2018). Atmospheric QBO and ENSO indices with high vertical resolution from GNSS radio occultation temperature measurements. *Atmospheric Measurement Techniques*, *11*(3), 1333–1346. https://doi.org/10.5194/amt-11-1333-2018

Part III.

Supplementary Results

This part presents additional results that were found during the research process but were not published in form of a scientific paper.

In the first section, the increase in the stratospheric aerosol levels from 2002 to 2016 is discussed. Thereafter the effectiveness of regression indices based on Radio Occultation (RO) temperature compared to conventional indices for analyzing small volcanic signals in stratospheric temperature is outlined. Furthermore the regression results as well as the temperature variance explained by the different variability indices are presented.

Additionally, the results of a regression analysis where ozone is considered alongside Quasi-Biennial Oscillation (QBO) and El Niño–Southern Oscillation (ENSO) variability are presented.

The high vertically resolved temperature and aerosol data are also used to detect the temporal evolution of specific eruptions. Especially the Soufrière Hills and Tavurvur eruptions, which occurred in quick succession, as well as the Nabro and Calbuco eruptions are highlighted.

The last section demonstrates that the methods and data used in this study are also capable of detecting forest fire signals in the lower stratosphere.

Consistent with the published paper, the results presented here are based on the 15–year period beginning in 2002, the point to which the increased stratospheric aerosol concentration following the Pinatubo eruption in 1991 almost reached a background level again. At the same time a series of minor volcanic eruptions started (Vernier et al. 2011). The time-series analyzed ends in 2016, until when the high resolution Global Space-based Stratospheric Aerosol Climatology (GloSSAC) data are currently available. For investigating a possible trend a longer time series would be desirable. However, while GloSSAC data are available already from the year 1979 (Thomason 2017), comprehensive RO temperature data are obtainable only from 2001 onward (Angerer et al. 2017).

1. Linear Trend in the Aerosol Data

Figure 1 (left) illustrates the mean stratospheric aerosol concentration from 2002 to 2016. At first glance one can see that the aerosol concentration decreases rapidly with increasing altitude. However, when the aerosol concentration is divided by the background concentration (right) it becomes apparent that, especially at altitudes between 17 km and 22 km, aerosol levels are highly increased in relation to the stratospheric background due to the numerous volcanic eruptions during the investigated time-period.

Figure 2 illustrates the GloSSAC aerosol concentration in relation to the background concentration for different altitude levels as well as the calculated linear trend. It can be seen that the volcanic aerosols are brought to higher altitudes over time, which causes the volcanic peaks to lag behind the eruption date. For instance, the peak at 20 km associated with the Calbuco eruption appears a few months after the eruption while the peak associated with the Kelut lags behind the

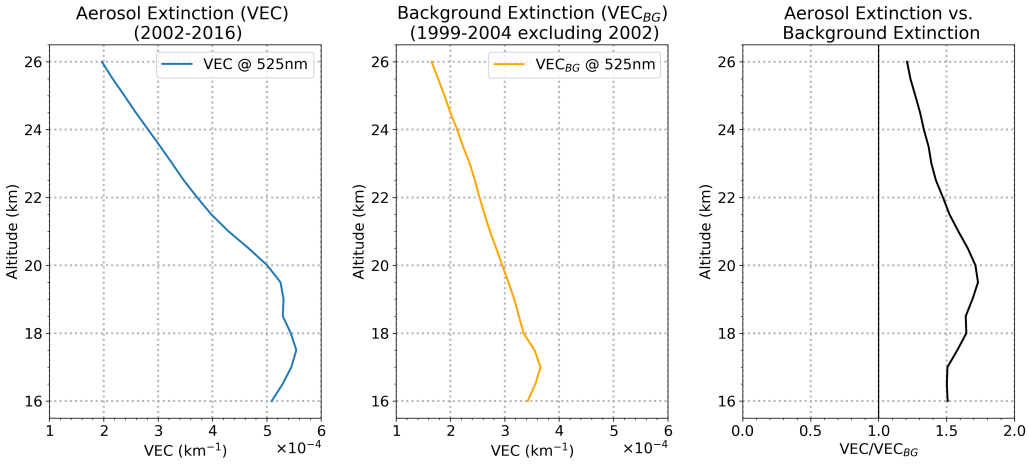

Figure 1.: Aerosol extinction for the time-period from 2002 to 2016 (left), background extinction (center) as well as the aerosol extinction divided by the background extinction (right) calculated for the tropical mean (30°N to 30°S).

eruption date by only a month. The difference here is that the Calbuco erupted at a higher latitude and a majority of the aerosols had to reach the tropical region before they could be lifted. The Kelut, however, erupted in the tropics and injected most of its aerosols directly to an altitude of approximately 20 km.

Studies such as Hofmann et al. (2009) reported an increase in the stratospheric aerosol concentration of about 4–7% per year above 20 km for the early 2000s. Hofmann et al. (2009) concluded that this trend was mainly due to increased coal burning in Southeast Asia. Vernier et al. (2011) in contrast, argued, that this increase was primarily caused by minor volcanic eruptions.

Even though the linear trend strongly depends on the time series analyzed, which in this study is substantially longer compared to (Vernier et al. 2011), a trend of approximately 1 % to 3 % per year can also be identified in Fig. 2 depending on the altitude. Fig. 1 in Stocker et al. (2019) and also Fig. 2 presented here, suggest that, at least in the tropics, the linear trend results from the strong volcanic peaks, especially since, after the Nabro eruption, the aerosol levels almost fell back to the background levels. This, however, supports the conclusions drawn by Vernier et al. (2011).

Since the trend in the aerosol concentration appears to be caused by the volcanic eruptions, the aerosol index (Volume Extinction Coefficient (VEC)) used was not detrended in the regression analysis as we are interested in the trend that can not be explained by natural processes.

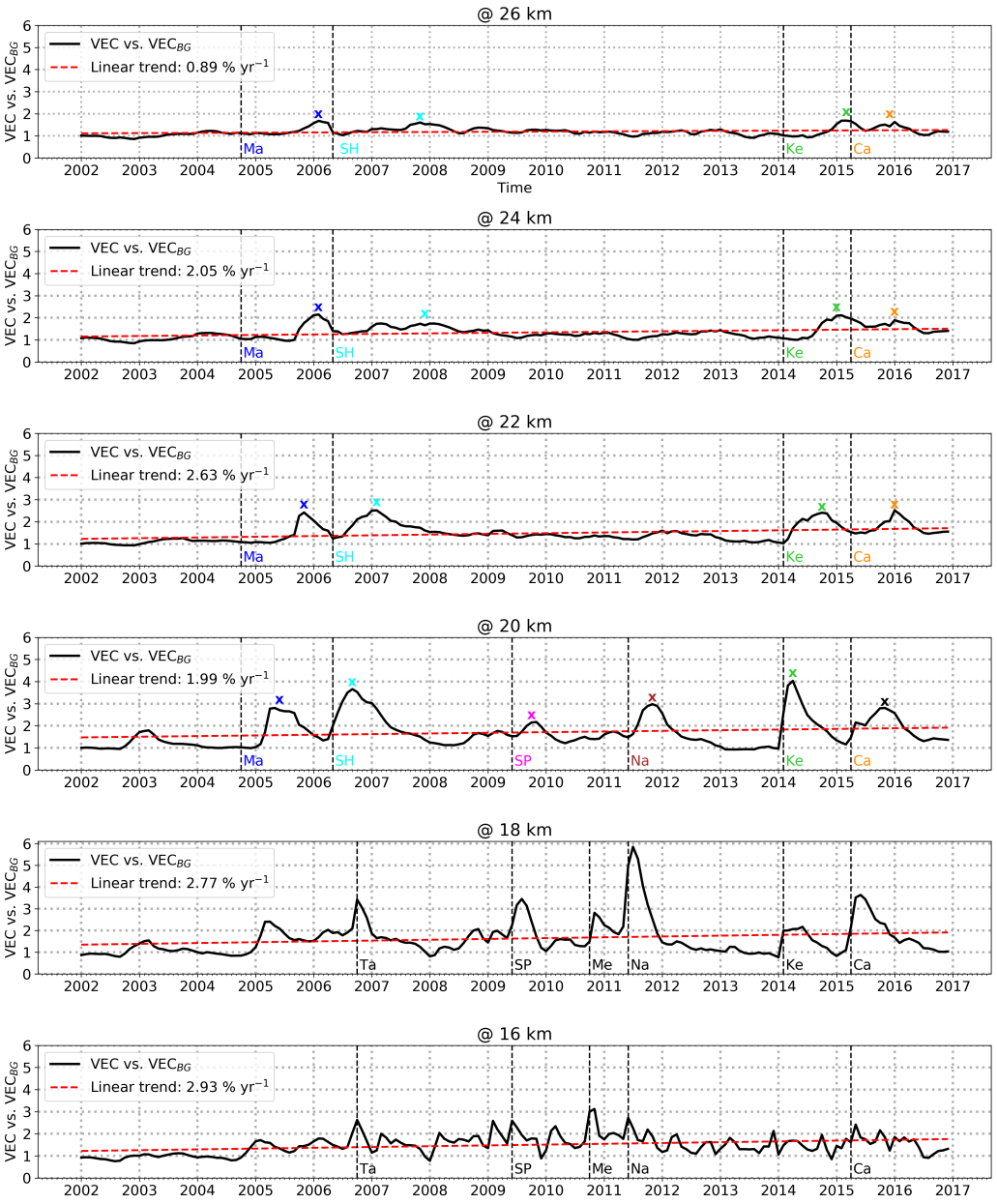

Figure 2.: Aerosol extinction vs. background extinction (mean 30°N to 30°S) at different altitude levels as well as the calculated linear trend (red). Vertical lines mark the date of the eruptions (abbreviations can be found in Table 1). With increasing altitude the peaks lag behind the eruption date. Above 26 km the different peaks can no longer be associated with volcanic activity.

2. Conventional Atmospheric Variability Indices vs. Indices Derived From RO Temperature

Studies such as Randel et al. (2009) applied a multiple linear regression model to investigate the lower stratospheric temperature variability using conventional QBO and ENSO indices. In the temperature residuals they found distinct signals that can be associated with the El Chichón and Pinatubo eruptions.

This raises the question whether the small signals from post-2000 eruptions can also be identified in the lower stratospheric temperature residuals when other natural variability is removed. Therefore two different approaches were used. For the first approach similar to Randel et al. (2009), QBO indices derived from the Singapore wind field and the ENSO 3.4 Sea Surface Temperature (SST) index were utilized while for the second approach the altitude resolved natural variability indices derived from the RO temperature anomalies were used.

For the conventional variability indices (Fig. 3) it is evident that the residual temperature varies greatly by about ±2 K. While major eruptions such as the Pinatubo can still be identified within the residuals (cf. Randel et al. 2009) it is almost impossible to identify smaller volcanic imprints such as those of the Soufrière Hills and Tavurvur eruptions in 2006, for which the stratospheric temperature changes are expected to range between 0.5 K to 0.8 K (Mehta et al. 2015).

For the second approach (Fig. 4), where the natural variability indices derived from RO temperature as described in Sect. 5.3 are used, the residual variability is greatly reduced and signals from eruptions such as the Tavurvur, Merapi or Nabro can clearly be identified.

3. Variability of the Stratospheric Temperature

This section presents the results of the multiple linear regression used to determine the volcanic imprints in the stratospheric temperature. Therefore the regression coefficients, indices as well as the reconstructed temperature fields are shown. Additionally, the variance explained by the different variability indices is discussed. The reconstructed temperature fields for the volcanic aerosols are omitted since they have already been presented in Stocker et al. (2019) (Fig. 2 therein).

The regression coefficients illustrated in Fig. 5 indicate that there is considerable aerosol variability in the temperature anomalies in the central tropics at an altitude of around 18 km and also between 20 km and 24 km as well as in the southern lowermost stratosphere where the Calbuco eruption dominates the arosol time-series. The coefficient for the first Principal Component (PC) is robust at all altitudes in the central tropical region and appears to be less important in the subtropics. Although the variability indices derived from RO temperature do not exclusively represent phenomena such as QBO or ENSO (Wilhelmsen et al. 2018), this implies that the first PC primarily represents the central tropical QBO. In contrast, the second PC is weak in the central tropics but stronger at latitudes

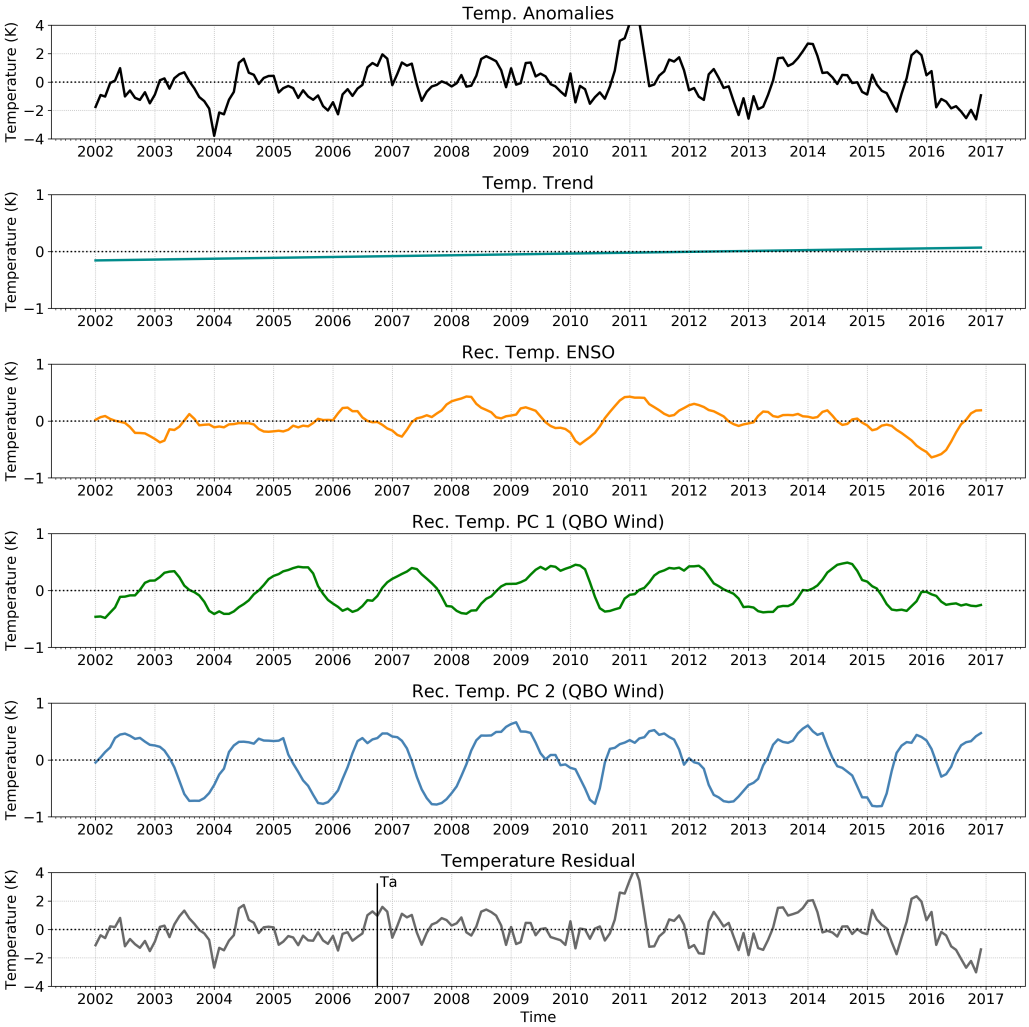

Figure 3.: Regression results for the central tropical lower stratosphere (mean 10°N to 10°S @ 18km) using ENSO 3.4 SST as well as the first two principal components (QBO-indices) derived from the Singapore wind field as regression indices. Note the different temperature scales on the y axis. The vertical line marks the date of the Tavurvur eruption.

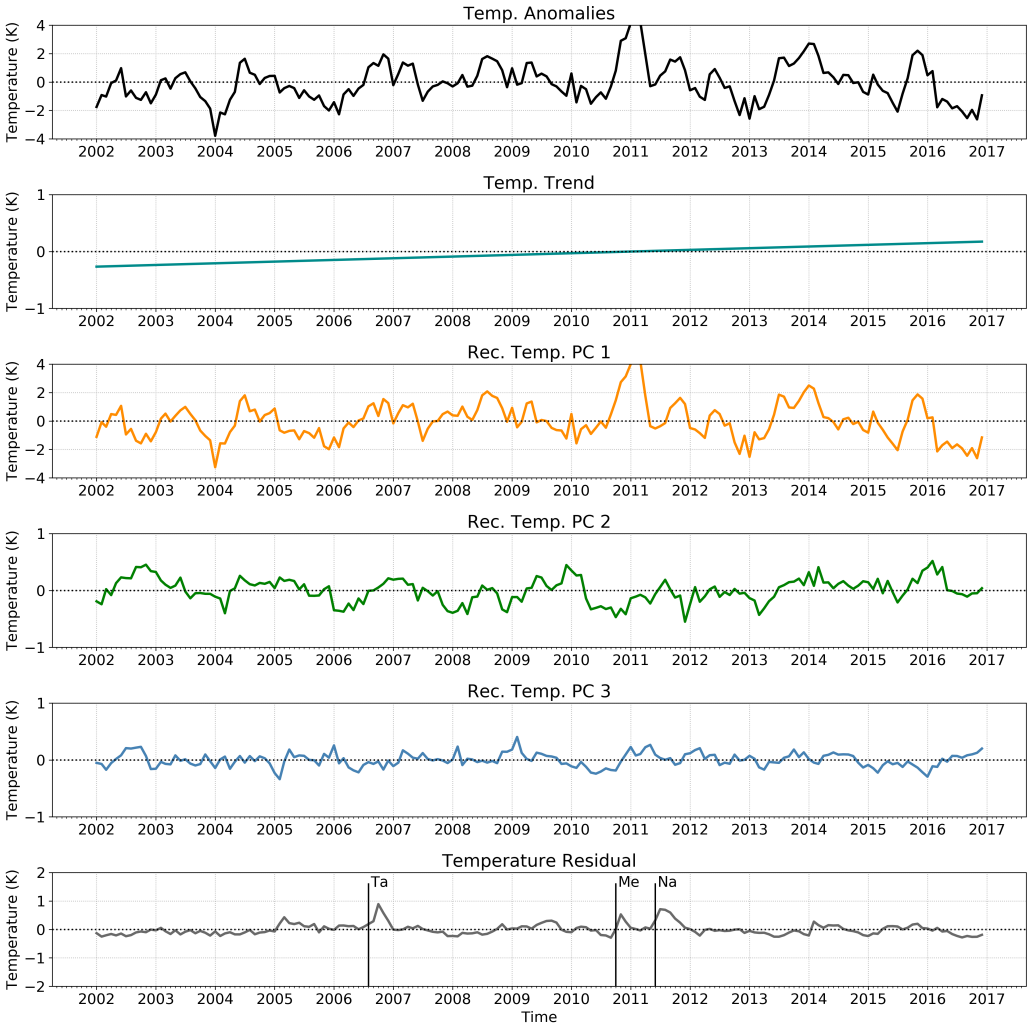

Figure 4.: Regression results for the central tropical lower stratosphere (mean 10°N to 10°S @ 18km) using variability indices derived from the volcanic aerosol cleared RO-temperature anomalies. Note the different temperature scales on the y axis. Vertical lines mark the date of the Tavurvur, Merapi and Nabro eruption.

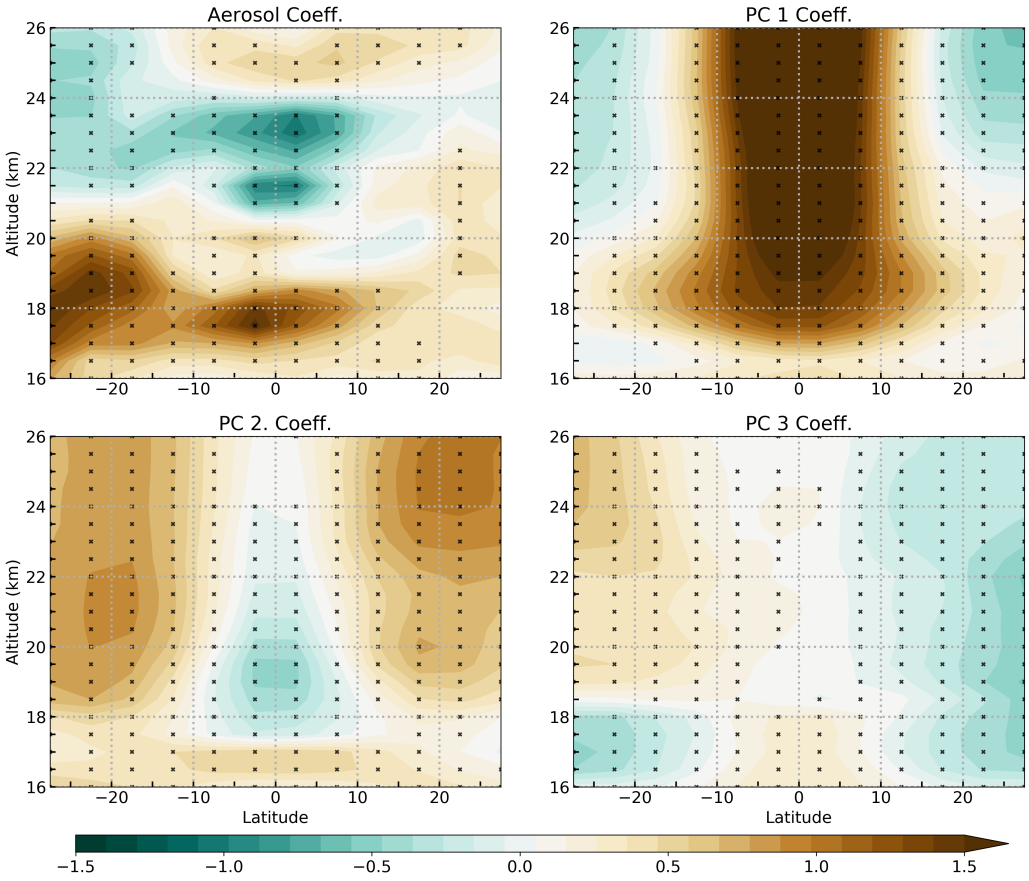

Figure 5.: Regression coefficients for the different normalized regression indices for the time-period from 2002 to 2017. Values which are significant at the 95% confidence level are marked with an X.

between 30°N and 10°N and also between 10°S and 30°S. Therefore the second PC predominantly accounts for temperature variability in the subtropics. The regression coefficient for the third PC is comparatively weak at all latitudes and altitudes.

The reconstructed temperature for the first PC shown in Fig. 6 clearly resembles the well known downward propagating pattern of the QBO. The second PC presented in Fig. 7, in contrast, does not show a distinct pattern. However, the latitude time cross section resembles a phase shifted QBO like pattern in the subtropics (c.f. Baldwin et al. 2001, Fig. 6). Fig. 8 reveals that the third PC explains parts of the temperature variability in the tropopause region around 17 km and below, while it basically has no influence at higher altitudes. This indicates a possible connection to the ENSO.

Although the indices shown here have been derived from temperature anomalies where the influence of stratospheric aerosol has been removed they highly agree with the indices created by Wilhelmsen et al. (2018). Correlations between the different indices used here and the regular QBO and ENSO indices are not shown but are similar to the ones reported by Wilhelmsen et al. (2018).

While the overall variability of the tropical stratospheric temperature presented in Fig. 9 is clearly dominated by the first two PCs, the effect of the aerosols and hence the volcanoes is almost negligible, since the eruptions occurred only episodically and with the exception of the Calbuco were only relevant close to the equator. However, as already shown in Stocker et al. (2019), at least for the investigated time-series, they do have an influence on the temperature trend.

4. Considering the Effect of Volcanoes on the Ozone Concentration

As discussed in Stocker et al. (2019), a possible explanation for the cooling signals is that they are caused by volcano-induced changes in the ozone concentration. Free and Lanzante (2009) compared the observed temperature changes induced by the Agung, El Chichón, and Pinatubo eruptions to climate model results. They found that in the tropical lowermost stratosphere the models tend to produce a stronger warming than observed. They argue that besides a misspecification of the aerosol forcing the difference may also be due to a competing ozone effect which is not represented in the climate models.

Consequently an additional regression where ozone variability is also considered was performed during the course of this study. Hereby, in a first step ozone[1] anomalies were created. Thereafter the ozone data was transferred to an altitude-latitude grid consistent with the aerosol and temperature data.

To avoid collinearity, QBO, similar to the aerosols, together with ENSO variability is removed from the ozone anomalies via linear regression. The resulting QBO

[1]Ozone data obtained from; http://dx.doi.org/10.17632/2mgx2xzzpk.2. Also see Ball et al. (2017)

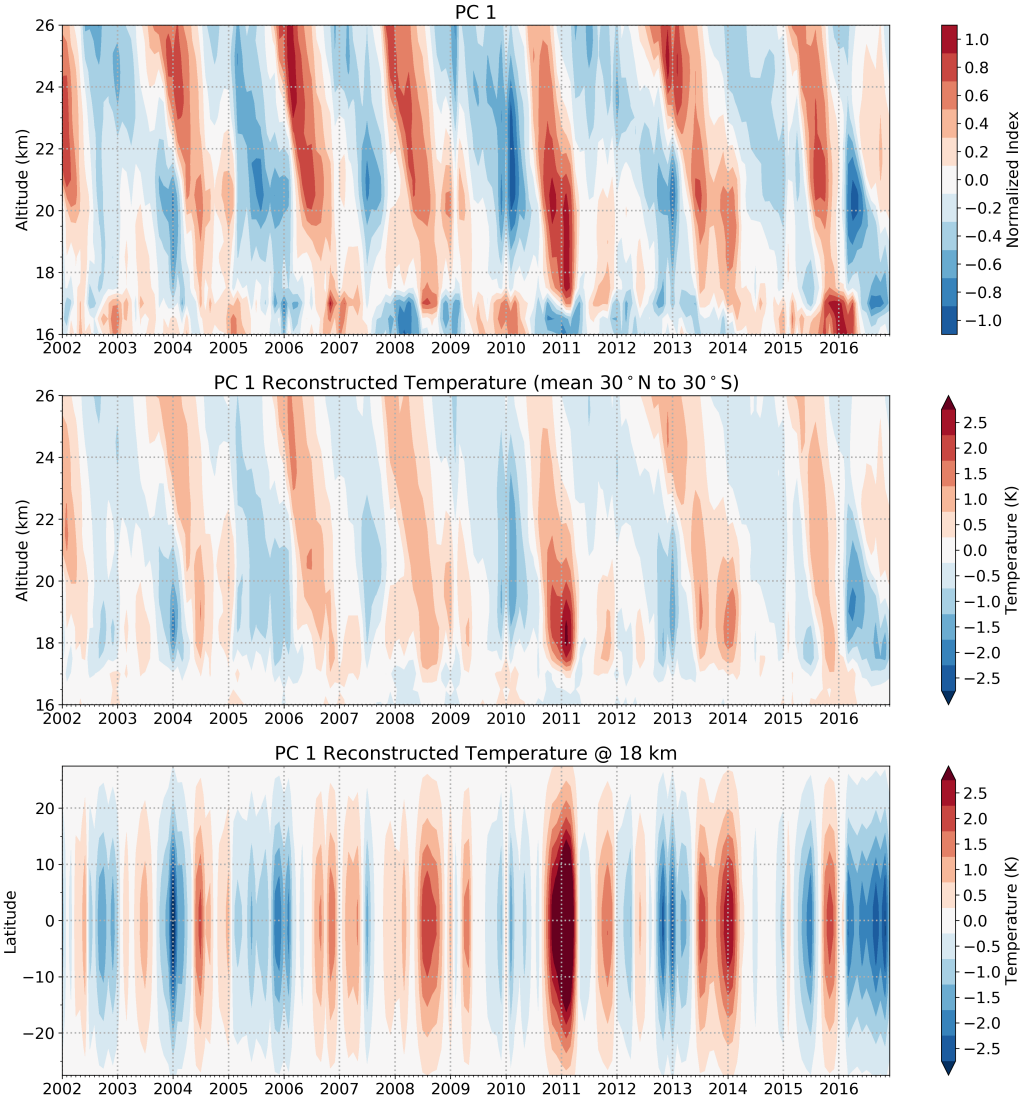

Figure 6.: Regression index (top), reconstructed tropical mean temperature field as well as the reconstructed temperature field at 18 km for the first PC.

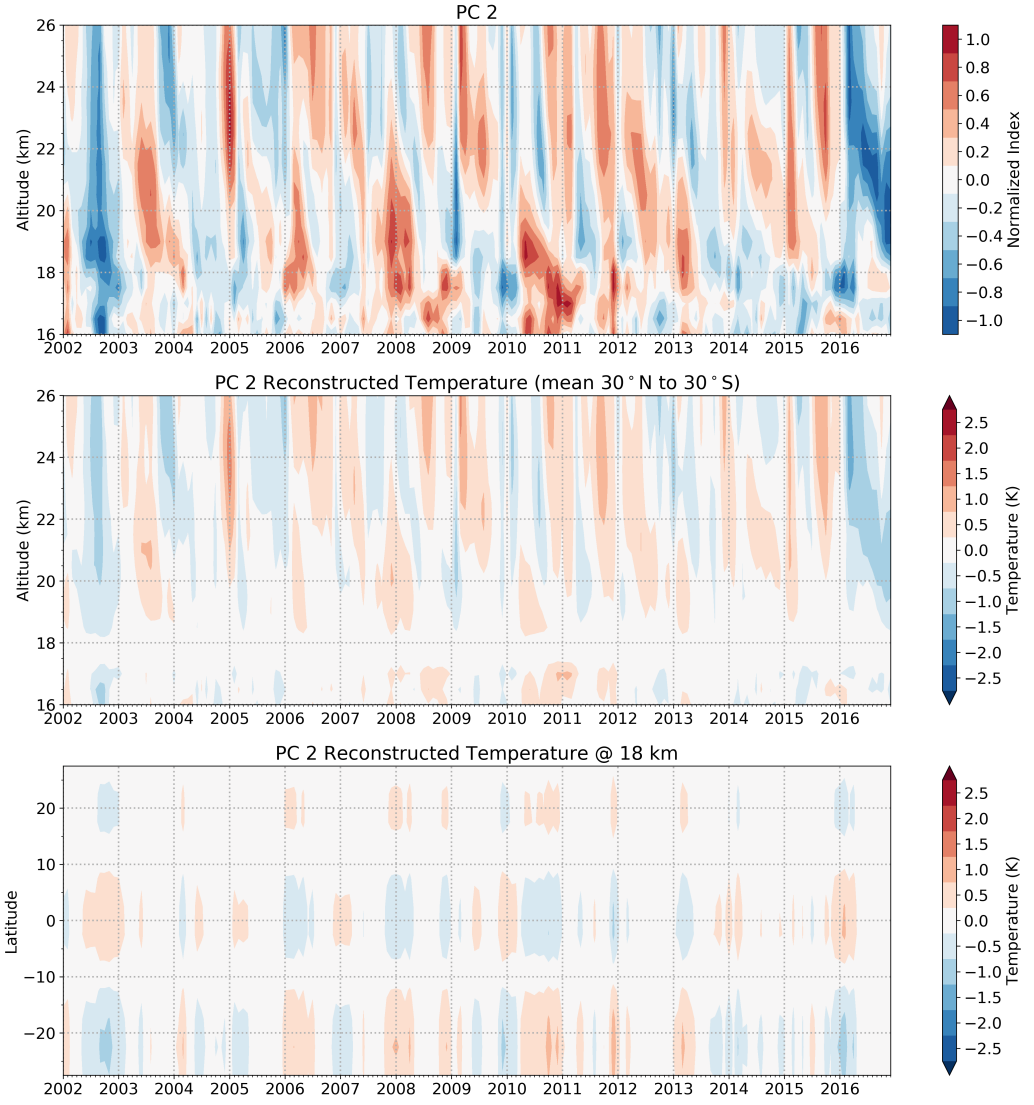

Figure 7.: Regression index (top), reconstructed tropical mean temperature field as well as the reconstructed temperature field at 18 km for the second PC.

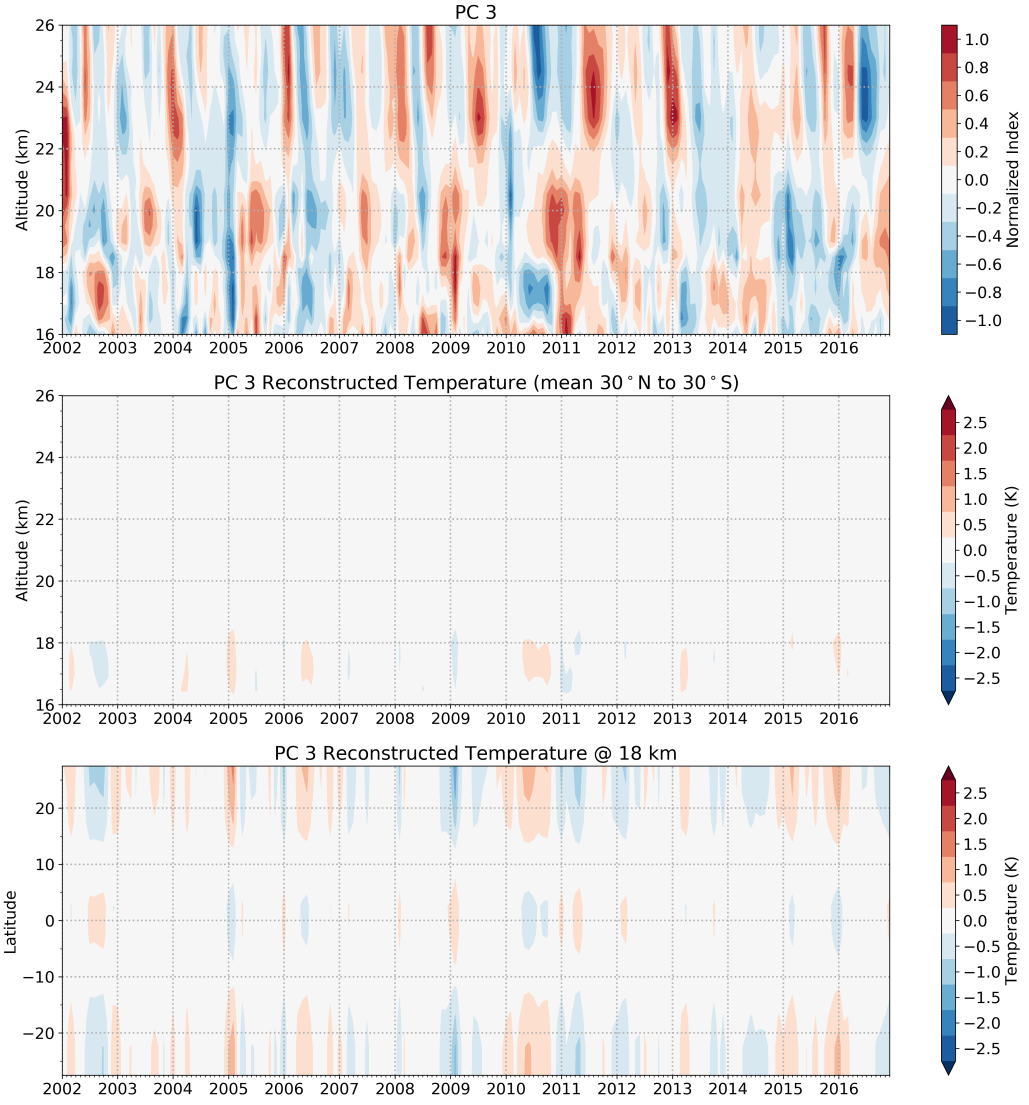

Figure 8.: Regression index (top), reconstructed tropical mean temperature field as well as the reconstructed temperature field at 18 km for the third PC.

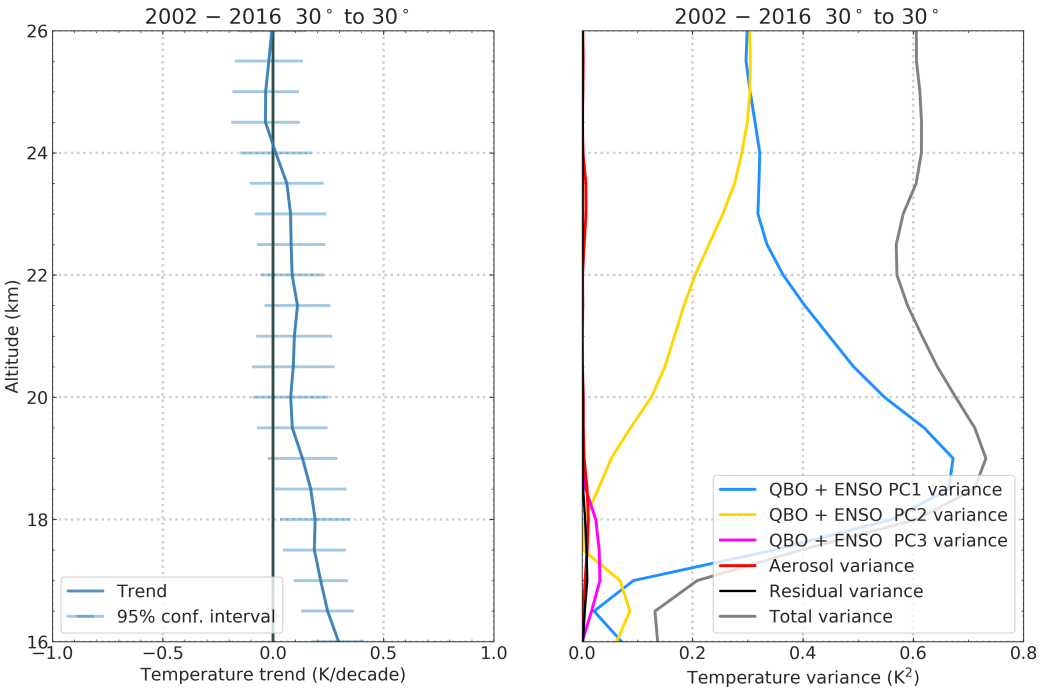

Figure 9.: Linear trend (left) and temperature variability (right) explained by the different regression indices (mean 30°S to 30°).

and ENSO free ozone anomalies are then considered in a linear regression model to create aerosol and ozone free temperature anomalies. In a second step new variability indices are created from the residual temperature anomalies. In the final regression model the ozone anomalies as well as aerosols and the aerosol- and ozone free variability indices are considered.

Figure 10 displays the resulting reconstructed temperature for the volcanic aerosols. While the warming signals due to the different volcanic eruptions are slightly enhanced but comparable to those presented in Stocker et al. (2019) it is clearly visible that the cooling signals in the mid stratosphere between 22 km and 24 km almost disappear when ozone variability is considered. Since we consider the cooling signals to be an indirect volcanic effect, we finally did not account for ozone in Stocker et al. (2019).

5. Temperature Signals From Specific Eruptions

This section presents the temporal evolution of three volcanic eruptions for the reason that each of them has special characteristics. The first ones are the Soufrière Hills and the Tavurvur eruptions. They took place within a relatively short period of time which makes it difficult to separate their effects. The Nabro eruption in 2011 is taken into account because it emitted the highest amount of aerosols.

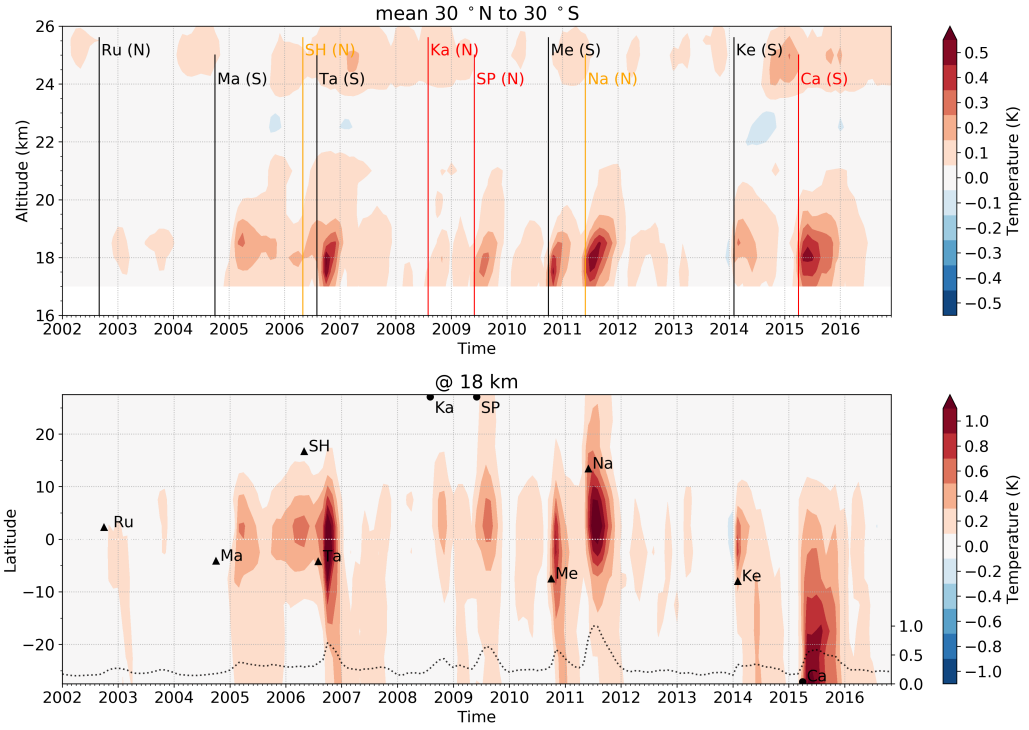

Figure 10.: Altitude time cross section of the volcanic aerosol reconstructed temperature (mean 30°N to 30°S; top) as well as the latitude time cross section at 18 km (bottom) when additionally ozone is considered in the regression model. Vertical lines in the altitude time pattern mark the date of the eruptions. N and S in brackets indicate eruptions north and south of the equator. Line colors indicate the latitude of the eruption (red >30, orange >10, and black <10). Triangles in the latitude time pattern mark the date as well as the latitude of the eruption. Eruptions that occurred at latitudes not part of the plot range are marked with a semicircle. The dashed line represents the normalized VEC for the 18 km altitude level (mean 30°N to 30°S).

Finally the Calbuco eruption is examined as it took place at a high latitude and, in contrast to other higher latitude eruptions such as the Nabro, affected temperatures also at high latitudes.

5.1. The Soufrière Hills and Tavurvur Eruption

According to the Global Volcanism Program (2013) the Soufrière Hills eruption started in April 2005. The main emission event, however, where the volcano emitted 200 kt of SO_2 to an altitude of about 20 km took place in May 2006. This emission is clearly visible in Fig. 11 and is strongest between August and October 2006. However, only a small warming signal, which developed between June and August 2006, can be detected.

In October 2006 a second signal appears in the lower stratospheric aerosol concentration. The signal can be associated with the Tavurvur eruption, which started in August 2006, and emitted about 300 kt to an altitude of 18 km in October 2006. A strong peak warming of roughly 1.5 K can be observed at this height. At an altitude of around 22 km a cooling, most likely associated with the aerosols from the Soufrière Hills eruption, develops.

In December 2006 the lower stratospheric warming from the Tavurvur has almost disappeared. Since the Tavurvur emitted most of its aerosols only to an altitude of 18 km during a QBO westerly shear, the aerosols are not confined to the central tropical region and therefore have been quickly removed. The aerosols from the Soufrière Hills in contrast seem to be further lifted within the tropical pipe and already reach an altitude of 22 km to 24 km between December and February 2006, causing a noticeable cooling.

5.2. The Nabro Eruption

Figure 12 shows the temporal evolution of the Nabro eruption in 2011, which emitted 3600 kt of SO_2 to an altitude of 18 km. The Nabro eruption took place 16°N of the equator and strongly influenced the aerosol concentration in the northern hemisphere. Only a small fraction of the aerosols reached the central tropical region and most of them were not transported to altitudes above 20 km since a majority of the aerosols was transported to higher latitudes within the shallow branch of the Brewer–Dobson Circulation (BDC). A warming signal of about 1 K that develops between July 2011 and September 2011 is only visible near the equator and already disappears in November 2011.

Although the Nabro erupted ten times more aerosols than the Tavurvur in 2006, the magnitude of their temperature signals is comparable. Additionally, both eruptions did not affect temperatures at higher altitudes as they occurred during a QBO westerly shear which causes lower vertical transport within and a higher meridional transport out of the tropical pipe (Flury et al. 2013).

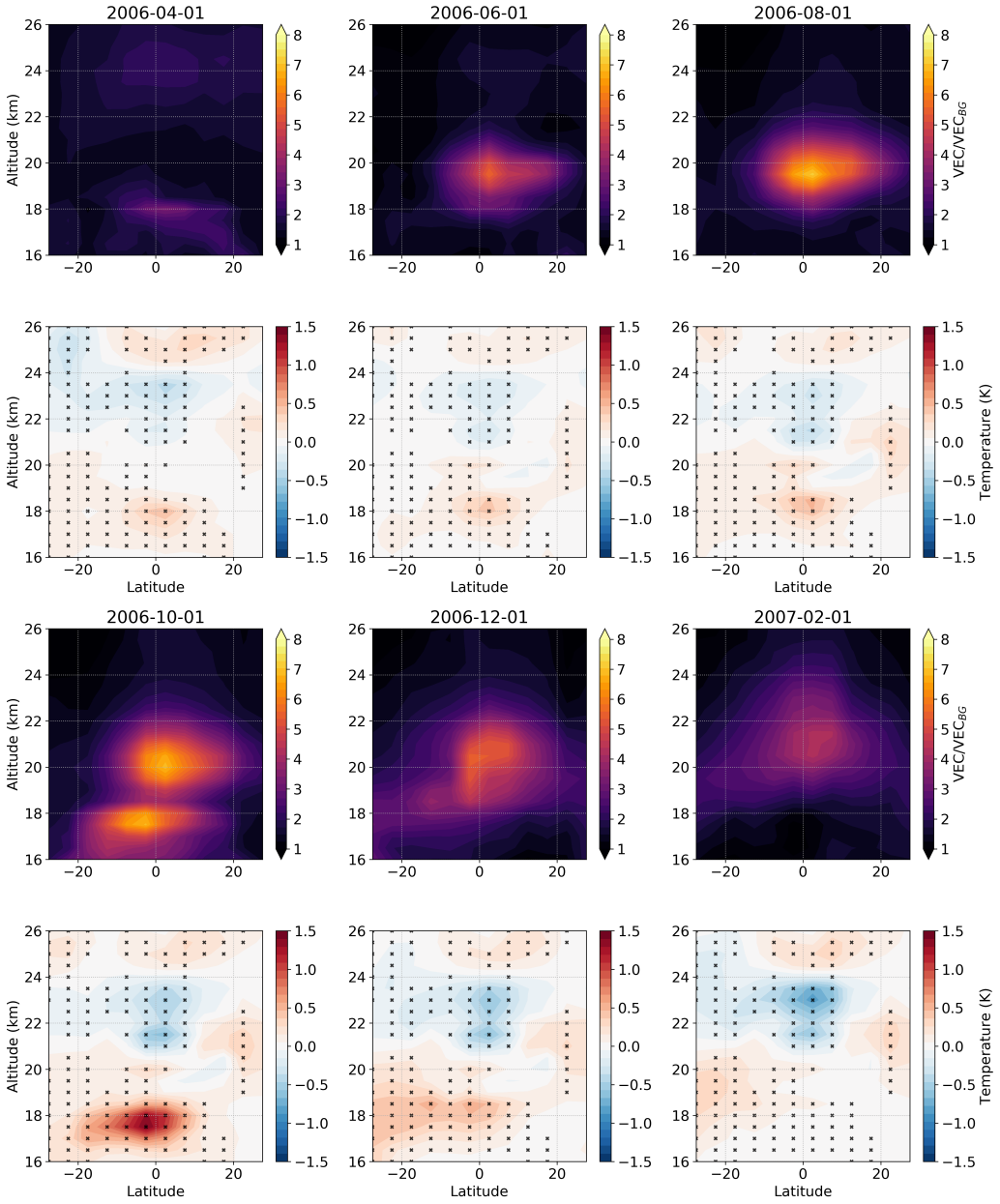

Figure 11.: Temporal evolution of the aerosol concentration (first and third row) as well as the temperature signal (second and fourth row) associated with the Soufrière Hills and Tavurvur eruption, respectively. Regions where the aerosol regression coefficient for the time period 2002 to 2017 (compare Fig. 5) is significant at the 95% level are marked with an X for reference.

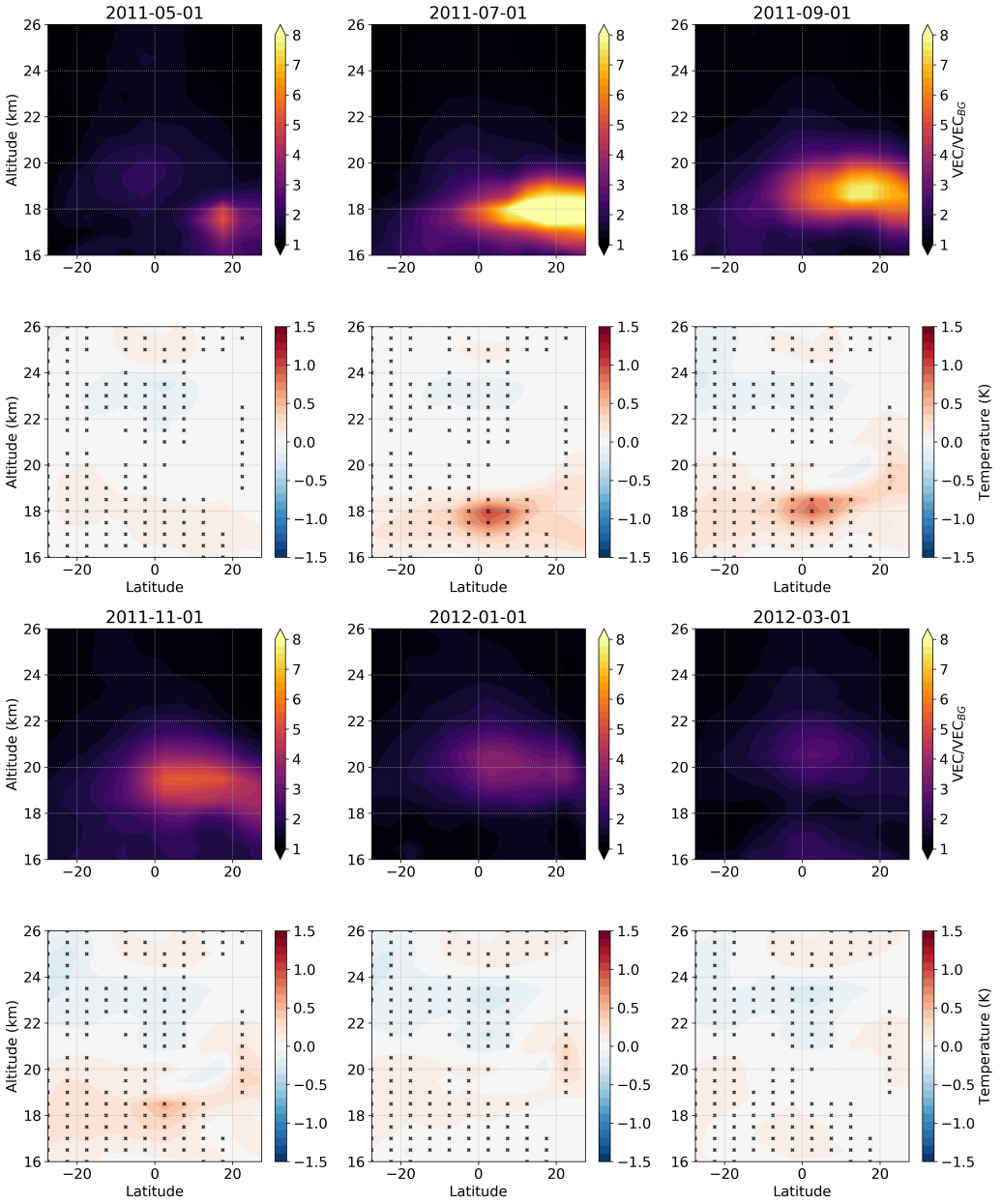

Figure 12.: Temporal evolution of the aerosol concentration (first and third row) as well as the temperature signal (second and fourth row) associated with the Nabro eruption. Regions where the aerosol regression coefficient for the time period 2002 to 2017 (compare Fig. 5) is significant at the 95% level are marked with an X for reference.

5.3. The Calbuco Eruption

The Calbuco Eruption took place in April 2015 at a latitude of 41.33° south of the equator. It emitted an SO_2 mass of 400 kt directly to an altitude of 20 km. As can be observed in Fig. 13, before the eruption the aerosol concentration in the lower stratosphere almost fall back to a background state, until in May 2015 a strong peak in the aerosol concentration appears. While at higher latitudes the Calbuco plume initially reaches an altitude of around 20 km a lower branch of the aerosols is transported towards the equator. In July 2015 the top of the plume is also transported equator-wards. Compared to other eruptions such as the Nabro there is a distinct warming visible at higher latitudes which is strongest from May to September 2015. This can be explained by the fact that during the Calbuco eruption there was a strong ENSO event which caused a warmer troposphere and hence led to more long-wave emission in the southern hemisphere. Between November 2015 and January 2016 the Calbuco aerosols already reached altitudes between 20 km and 22 km, causing a cooling.

6. Detecting Forest Fire Signals

A closer look at Fig. 1 in Stocker et al. (2019) reveals that not all of the peaks in the aerosol concentration can be associated with volcanic eruptions. They rather come from other anthropogenic or natural sources such as forest fires. The highly resolved GloSSAC aerosol and RO temperature data offer the possibility to investigate such events as well. For example, according to Siddaway and Petelina (2011), in February 2009, a large bush fire in Australia injected a smoke plume and perturbed the stratospheric aerosol levels in the subtropical Upper Troposphere–Lower Stratosphere (UTLS) between 5°S and 25°S for the period from February to June. To investigate this event they compared the limb-scattered spectral solar radiance of the plume to the background radiance in 2008.

A small perturbation in the aerosol concentration for the corresponding region can also be detected in the GloSSAC data used in this study. However, the signal is by far less evident compared to those of volcanic eruptions in the southern subtropics. Nevertheless, the approach used in this study suggests a peak warming of approximately 0.1 K following the 2009 bush fire. The GloSSAC data as well as the resulting temperature signals from the method used in this study are displayed in Fig. 14, computed for the region from 5°S to 25°S.

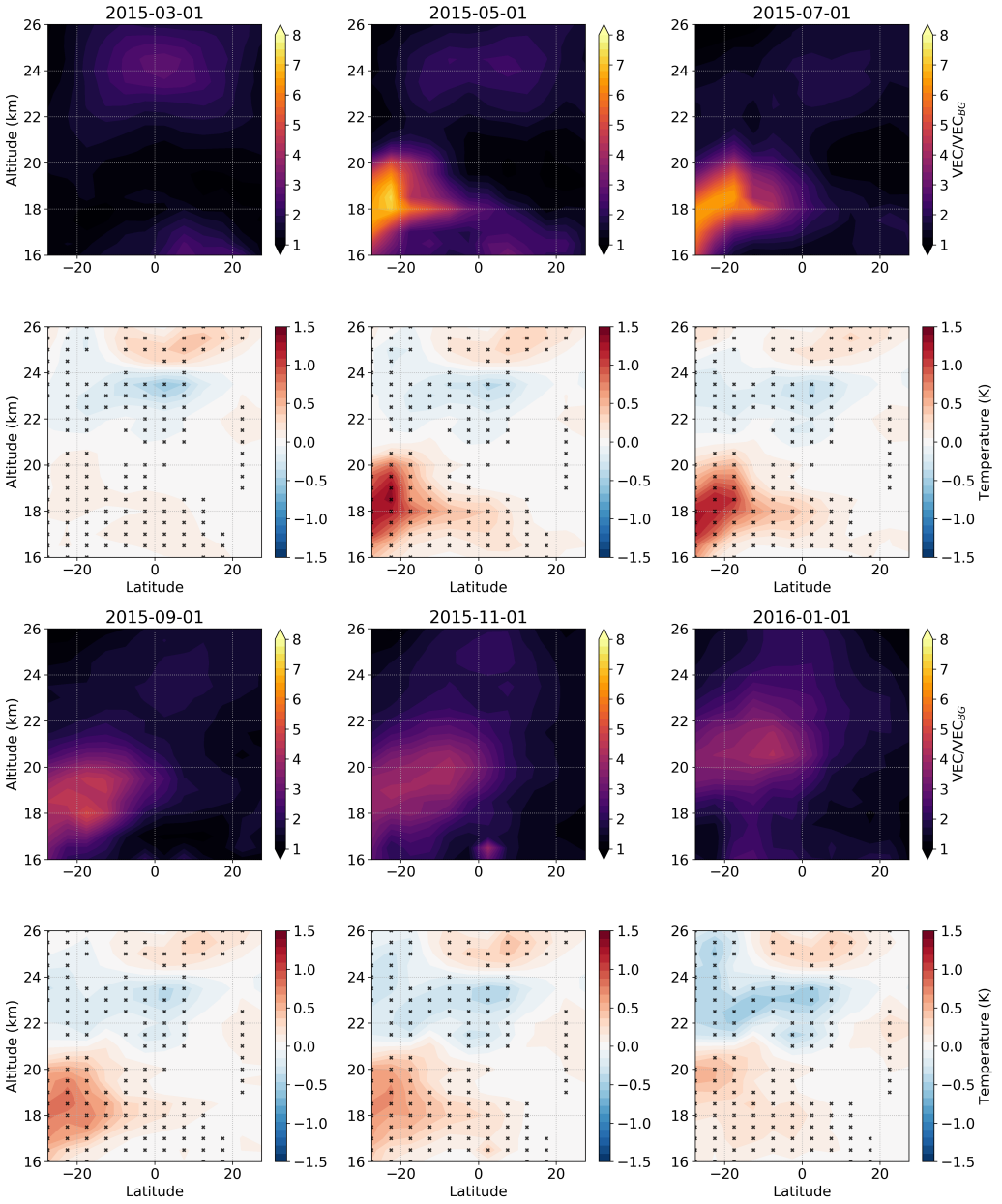

Figure 13.: Temporal evolution of the aerosol concentration (first and third row) as well as the temperature signal (second and fourth row) associated with the Calbuco eruption. Regions where the aerosol regression coefficient for the time period 2002 to 2017 (compare Fig. 5) is significant at the 95% level are marked with an X for reference.

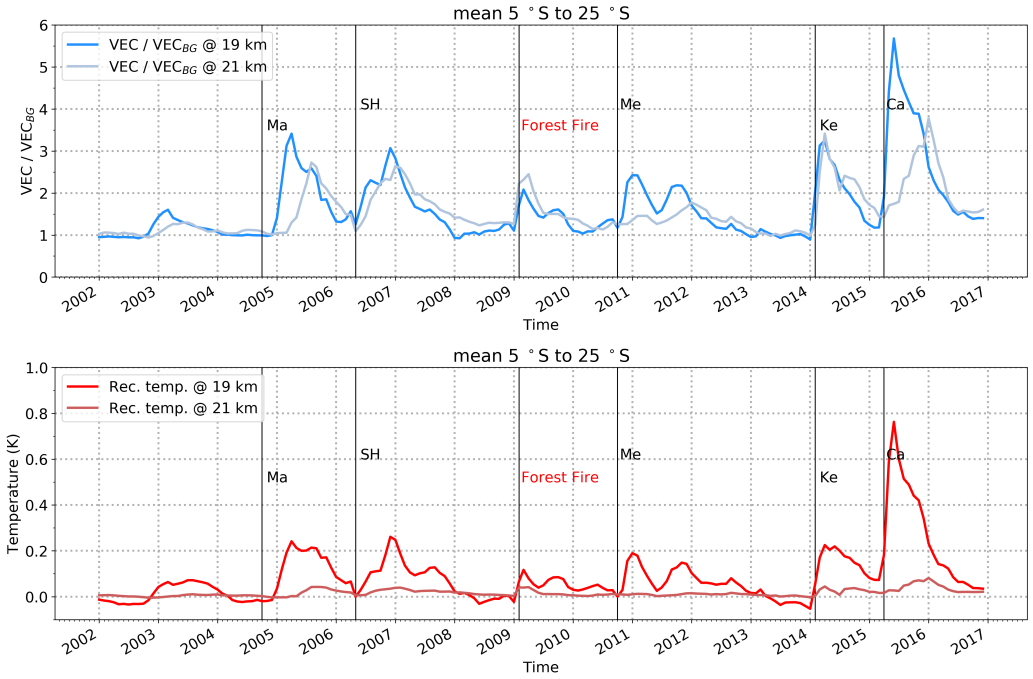

Figure 14.: Time-series of the stratospheric aerosol concentration compared to the background concentration (top) as well as the reconstructed temperature (bottom) for the region between 5°S and 25°S. Volcanic eruptions as well as the 2009 Australian Bush fire are marked by vertical lines.

Acronyms

AOD Aerosol Optical Depth.

AR(1) First-order Autoregressive process.

BDC Brewer–Dobson Circulation.

ENSO El Niño–Southern Oscillation.

EOF Empirical Orthogonal Function.

GloSSAC Global Space-based Stratospheric Aerosol Climatology.

GLS Generalized Least Squares.

GNSS Global Navigation Satellite System.

LEO Low Earth Orbit.

OLS Ordinary Least Squares.

OPS Occultation Processing System.

OPSv5.6 Occultation Processing System version 5.6.

PC Principal Component.

QBO Quasi-Biennial Oscillation.

RO Radio Occultation.

SAOD Stratospheric Aerosol Optical Depth.

SST Sea Surface Temperature.

UG University of Graz.

UTLS Upper Troposphere–Lower Stratosphere [region].

VEC Volume Extinction Coefficient.

VEI Volcanic Explosivity Index.

WEGC Wegener Center for Climate and Global Change [University of Graz].

WMO World Meteorological Organization.

List of Figures

Part I. Synopsis

Part II. Published Paper

Part III. Supplementary Results

List of Tables

Part I. Synopsis

Part II. Published Paper

Bibliography

Angerer, B., F. Ladstädter, B. Scherllin-Pirscher, M. Schwärz, A. K. Steiner, U. Foelsche, and G. Kirchengast (2017). "Quality aspects of the WEGC multi-satellite GPS radio occultation record OPSv5.6". *Atmos. Meas. Tech.* 10, pp. 4845–4863. DOI: 10.5194/amt-10-4845-2017.

Anthes, R. A. (2011). "Exploring Earth's atmosphere with radio occultation: contributions to weather, climate, and space weather". *Atmos. Meas. Tech.* 4, pp. 1077–1103. DOI: 10.5194/amt-4-1077-2011.

Aquila, V., L. D. Oman, R. Stolarski, A. R. Douglass, and P. A. Newman (2013). "The Response of Ozone and Nitrogen Dioxide to the Eruption of Mt. Pinatubo at Southern and Northern Midlatitudes". *J. Atmos. Sci.* 70.3, pp. 894–900. DOI: 10.1175/jas-d-12-0143.1.

Baldwin, M. P., L. J. Gray, T. J. Dunkerton, K. Hamilton, P. H. Haynes, W. J. Randel, J. R. Holton, M. J. Alexander, I. Hirota, T. Horinouchi, D. B. A. Jones, J. S. Kinnersley, C. Marquardt, K. Sato, and M. Takahashi (2001). "The Quasi-Biennial Oscillation". *Rev. Geophys.* 39.2, pp. 179–229. DOI: 10.1029/1999rg000073.

Ball, W. T., J. Alsing, D. J. Mortlock, E. V. Rozanov, F. Tummon, and J. D. Haigh (2017). "Reconciling differences in stratospheric ozone composites". *Atmos. Chem. Phys.* 17.20, pp. 12269–12302. DOI: 10.5194/acp-17-12269-2017.

Barkley, M. P., P. I. Palmer, C. D. Boone, P. F. Bernath, and P. Suntharalingam (2008). "Global distributions of carbonyl sulfide in the upper troposphere and stratosphere". *Geophys. Res. Lett.* 35.14. DOI: 10.1029/2008gl034270.

Barry, R., R. Chorley, R. Barry, and T. Chorley (2004). *Atmosphere, Weather and Climate*. 8th ed. London: Routledge. DOI: 10.4324/9780203428238.

Biondi, R., A. K. Steiner, G. Kirchengast, H. Brenot, and T. Rieckh (2017). "Supporting the detection and monitoring of volcanic clouds: A promising new application of Global Navigation Satellite System radio occultation". *Adv. Space Res.* 60.12, pp. 2707–2722. DOI: 10.1016/j.asr.2017.06.039.

Birner, T. and H. Bönisch (2011). "Residual circulation trajectories and transit times into the extratropical lowermost stratosphere". *Atmos. Chem. Phys.* 11.2, pp. 817–827. DOI: 10.5194/acp-11-817-2011.

Bönisch, H., A. Engel, T. Birner, P. Hoor, D. W. Tarasick, and E. A. Ray (2014). "On the structural changes in the Brewer-Dobson circulation after 2000". *Atmos. Chem. Phys.* 11.8, pp. 3937–3948. DOI: 10.5194/acp-11-3937-2011.

Boucher, O., D. Randall, P. Artaxo, C. Bretherton, G. Feingold, P. Forster, V.-M. Kerminen, Y. Kondo, H. Liao, U. Lohmann, P. Rasch, S. K. Satheesh, S. Sherwood, B. Stevens, and X. Y. Zhang (2013). "Clouds and aerosols". In: *Climate*

Change 2013: The Physical Science Basis. Contribution of Working Group I to the Fifth Assessment Report of the Intergovernmental Panel on Climate Change. Ed. by T. F. Stocker, D. Qin, G.-K. Plattner, M. Tignor, S. K. Allen, J. Doschung, A. Nauels, Y. Xia, V. Bex, and P. M. Midgley. Cambridge, UK: Cambridge University Press, pp. 571–657. DOI: 10.1017/CBO9781107415324.016.

Bourgeois, Q., A. M. L. Ekman, J.-B. Renard, R. Krejci, A. Devasthale, F. A.-M. Bender, I. Riipinen, G. Berthet, and J. L. Tackett (2018). "How much of the global aerosol optical depth is found in the boundary layer and free troposphere?" *Atmos. Chem. Phys.* 18.10, pp. 7709–7720. DOI: 10.5194/acp-18-7709-2018.

Butchart, N. (2014). "The Brewer-Dobson circulation". *Rev. Geophys.* 52, pp. 157–184. DOI: 10.1002/2013RG000448.

Dettling, M. (2016). *Applied Time Series Analysis*. URL: https://stat.ethz.ch/education/semesters/ss2016/atsa/ATSA_Script_v160527.pdf.

Domeisen, D. I., C. I. Garfinkel, and A. H. Butler (2019). "The Teleconnection of El Niño Southern Oscillation to the Stratosphere". *Rev. Geophys.* 57.1, pp. 5–47. DOI: 10.1029/2018rg000596.

DWD (2020). *Aerosol optical depth*. Ed. by Deutscher Wetterdienst. https://www.dwd.de/EN/research/observing_atmosphere/composition_atmosphere/aerosol/cont_nav/aod_node.html. Accessed: 03.02.2020.

Ebmeier, S. K., A. M. Sayer, R. G. Grainger, T. A. Mather, and E. Carboni (2014). "Systematic satellite observations of the impact of aerosols from passive volcanic degassing on local cloud properties". *Atmos. Chem. Phys.* 14.19, pp. 10601–10618. DOI: 10.5194/acp-14-10601-2014.

Flury, T., D. L. Wu, and W. G. Read (2013). "Variability in the speed of the Brewer–Dobson circulation as observed by Aura/MLS". *Atmos. Chem. Phys.* 13.9, pp. 4563–4575. DOI: 10.5194/acp-13-4563-2013.

Foelsche, U., S. Syndergaard, J. Fritzer, and G. Kirchengast (2011). "Errors in GNSS radio occultation data: relevance of the measurement geometry and obliquity of profiles". *Atmos. Meas. Tech.* 4, pp. 189–199. DOI: 10.5194/amt-4-189-2011.

Free, M. and J. Lanzante (2009). "Effect of Volcanic Eruptions on the Vertical Temperature Profile in Radiosonde Data and Climate Models". *J. Climate* 22.11, pp. 2925–2939. DOI: 10.1175/2008jcli2562.1.

Free, M. and D. J. Seidel (2009). "Observed El Niño–Southern Oscillation temperature signal in the stratosphere". *J. Geophys. Res.* 114, D23108. DOI: 10.1029/2009JD012420.

Fueglistaler, S., A. E. Dessler, T. J. Dunkerton, I. Folkins, Q. Fu, and P. W. Mote (2009). "Tropical tropopause layer". *Rev. Geophys.* 47, RG1004. DOI: 10.1029/2008RG000267.

Geller, M. A., T. Zhou, and W. Yuan (Aug. 2016). "The QBO, gravity waves forced by tropical convection, and ENSO". *J. Geophys. Res.: Atmos* 121.15, pp. 8886–8895. ISSN: 2169-8996. DOI: 10.1002/2015JD024125.

Global Volcanism Program (2013). *Volcanoes of the World, v. 4.3.4*. Ed. by E. Venzke. Smithsonian Institution, Downloaded 08 Nov 2018. URL: https://doi.org/10.5479/si.gvp.votw4-2013.

Gorbunov, M. E., H.-H. Benzon, A. S. Jensen, M. S. Lohmann, and A. S. Nielsen (2004). "Comparative analysis of radio occultation processing approaches based on Fourier integral operators". *Radio Sci.* 39, RS6004. DOI: 10.1029/2003RS002916.

Hanck, C., M. Arnold, A. Gerber, and M. Schmelzer (2019). "Omitted Variable Bias". In: *Introduction to Econometrics with R*. University of Duisburg-Essen. URL: https://www.econometrics-with-r.org/index.html.

Hannachi, A., I. T. Jolliffe, and D. B. Stephenson (July 2007). "Empirical orthogonal functions and related techniques in atmospheric science: A review". *Int. J. Climatol.* 27.9, pp. 1119–1152. ISSN: 08998418, 10970088. DOI: 10.1002/joc.1499.

Hofmann, D., J. Barnes, M. O'Neill, M. Trudeau, and R. Neely (2009). "Increase in background stratospheric aerosol observed with lidar at Mauna Loa Observatory and Boulder, Colorado". *Geophys. Res. Lett.* 36. DOI: 10.1029/2009GL039008.

Hommel, R., C. Timmreck, M. A. Giorgetta, and H. F. Graf (2015). "Quasi-biennial oscillation of the tropical stratospheric aerosol layer". *Atmos. Chem. Phys.* 15.10. DOI: 10.5194/acp-15-5557-2015.

Junge, C. E., C. W. Chagnon, and J. E. Manson (1961). "A World-wide Stratospheric Aerosol Layer". *Science* 133.3463, pp. 1478–1479. DOI: 10.1126/science.133.3463.1478-a.

Karl, T. R., S. J. Hassol, C. D. Miller, and W. L. Murray, eds. (2006). *Temperature Trends in the Lower Atmosphere: Steps for Understanding and Reconciling Differences*. Climate Change Science Program and the Subcommittee on Global Change Research, Washington, DC.

Kasting, J. F. and D. Catling (2003). "Evolution of a Habitable Planet". *Annu. Rev. Astron. Astrophys.* 41.1, pp. 429–463. DOI: 10.1146/annurev.astro.41.071601.170049.

Kraus, H. (2004). *Die Atmosphäre der Erde. Eine Einführung in die Meteorologie*. 3rd ed. Berlin: Springer-Verlag. ISBN: 978-3-540-20656-9. DOI: 10.1007/3-540-35017-9.

Kremser, S., L. W. Thomason, M. von Hobe, M. Hermann, T. Deshler, C. Timmreck, M. Toohey, A. Stenke, J. P. Schwarz, R. Weigel, S. Fueglistaler, F. J. Prata, J.-P. Vernier, H. Schlager, J. E. Barnes, J.-C. Antuña-Marrero, D. Fairlie, M. Palm, E. Mahieu, J. Notholt, M. Rex, C. Bingen, F. Vanhellemont, A. Bourassa, J. M. C. Plane, D. Klocke, S. A. Carn, L. Clarisse, T. Trickl, R. Neely, A. D. James, L. Rieger, J. C. Wilson, and B. Meland (2016). "Stratospheric aerosol—Observations, processes, and impact on climate". *Rev. Geophys.* 54.2, pp. 278–335. DOI: 10.1002/2015RG000511.

Kursinski, E. R., G. A. Hajj, J. T. Schofield, R. P. Linfield, and K. R. Hardy (1997). "Observing Earth's atmosphere with radio occultation measurements using the Global Positioning System". *J. Geophys. Res.* 102.D19, pp. 23429–23465. DOI: 10.1029/97JD01569.

Lacis, A., J. Hansen, and M. Sato (1992). "Climate forcing by stratospheric aerosols". *Geophys. Res. Lett.* 19, pp. 1607–1610. DOI: 10.1029/92GL01620.

Langmann, B. (2014). "On the Role of Climate Forcing by Volcanic Sulphate and Volcanic Ash". *Adv. Meteorol.* 2014, pp. 1–17. DOI: 10.1155/2014/340123.

Mather, T. A. (2015). "Volcanoes and the environment: Lessons for understanding Earth's past and future from studies of present-day volcanic emissions". *J. Volcanol. Geotherm. Res.* 304, pp. 160–179. DOI: 10.1016/j.jvolgeores.2015.08.016.

McCormick, P. M., L. W. Thomason, and C. R. Trepte (1995). "Atmospheric effects of the Mt Pinatubo eruption". *Nature* 373, pp. 399–404. DOI: 10.1038/373399a0.

Mehta, S. K., M. Fujiwara, T. Tsuda, and J.-P. Vernier (2015). "Effect of recent minor volcanic eruptions on temperatures in the upper troposphere and lower stratosphere". *J. Atmos. Solar-Terr. Phys.* 129, pp. 99–110. DOI: 10.1016/j.jastp.2015.04.009.

Mirabel, P. J. and A. Jaecker-Voirol (1988). "Binary homogeneous nucleation". In: *Atmospheric Aerosols and Nucleation. Lecture Notes in Physics*. Ed. by P. Wagner and G. Vali. Vol. 309. Springer Berlin Heidelberg, pp. 1–14. DOI: 10.1007/3-540-50108-8_1004.

Murphy, D. M., K. D. Froyd, J. P. Schwarz, and J. C. Wilson (2013). "Observations of the chemical composition of stratospheric aerosol particles". *Quart. J. Roy. Meteor. Soc.* 140.681, pp. 1269–1278. DOI: 10.1002/qj.2213.

Naujokat, B. (Sept. 1986). "An Update of the Observed Quasi-Biennial Oscillation of the Stratospheric Winds over the Tropics". *J. Atmos. Sci.* 43.17, pp. 1873–1877. DOI: 10.1175/1520-0469(1986)043<1873:AUOTOQ>2.0.CO;2.

Newhall, C. G. and S. Self (1982). "The volcanic explosivity index (VEI) an estimate of explosive magnitude for historical volcanism". *J. Geophys. Res.: Oceans* 87.C2, pp. 1231–1238. DOI: 10.1029/JC087iC02p01231.

Niemeier, U. and H. Schmidt (2017). "Changing transport processes in the stratosphere by radiative heating of sulfate aerosols". *Atmos. Chem. Phys.* 17.24, pp. 14871–14886. DOI: 10.5194/acp-17-14871-2017.

Okazaki, I. and K. Heki (2012). "Atmospheric temperature changes by volcanic eruptions: GPS radio occultation observations in the 2010 Icelandic and 2011 Chilean cases". *J. Volcanol. Geotherm. Res.* 245–246, pp. 123–127. DOI: 10.1016/j.jvolgeores.2012.08.018.

Parker, D. E., H. Wilson, P. D. Jones, J. R. Christy, and C. K. Folland (1996). "The impact of Mount Pinatubo on world-wide temperatures". *Int. J. Climatol.* 16.5, pp. 487–497. DOI: 10.1002/(SICI)1097-0088(199605)16:5<487::AID-JOC39>3.0.CO;2-J.

Pirscher, B. (2010). *Multi-satellite climatologies of fundamental atmospheric variables from radio occultation and their validation (Ph.D. thesis)*. Sci. Rep. 33-2010. Austria: Wegener Center Verlag Graz. ISBN: 978-3-9502940-3-3.

Pitari, G., G. Di Genova, E. Mancini, D. Visioni, I. Gandolfi, and I. Cionni (2016). "Stratospheric Aerosols from Major Volcanic Eruptions: A Composition-Climate Model Study of the Aerosol Cloud Dispersal and e-folding Time". *Atmosphere* 7.6. DOI: 10.3390/atmos7060075.

Plumb, R. A. (1996). "A "tropical pipe" model of stratospheric transport". *J. Geophys. Res.: Atmos* 101.D2, pp. 3957–3972. DOI: 10.1029/95JD03002.

– (2002). "Stratospheric Transport". *J. Meteor. Soc. Japan* 80.4B, pp. 793–809. DOI: 10.2151/jmsj.80.793.

Randel, W. J., R. R. Garcia, N. Calvo, and D. Marsh (2009). "ENSO influence on zonal mean temperature and ozone in the tropical lower stratosphere". *J. Geophys. Res.* 36, L15822. DOI: 10.1029/2009GL039343.

Randel, W. J., F. Wu, R. Swinbank, J. Nash, and A. O'Neill (1999). "Global QBO circulation derived from UKMO stratospheric analyses". *J. Atmos. Sci.* 56.4, pp. 457–474.

Ridley, D. A., S. Solomon, J. E. Barnes, V. D. Burlakov, T. Deshler, S. I. Dolgii, A. B. Herber, T. Nagai, R. R. Neely III, A. V. Nevzorov, C. Ritter, T. Sakai, B. D. Santer, M. Sato, A. Schmidt, O. Uchino, and J. P. Vernier (2014). "Total volcanic stratospheric aerosol optical depths and implications for global climate change". *Geophys. Res. Lett.* 41.22, pp. 7763–7769. DOI: 10.1002/2014GL061541.

Robock, A. (2000). "Volcanic eruptions and climate". *Rev. Geophys.* 38.2, pp. 191–219. DOI: 10.1029/1998rg000054.

– (2015). "Climatic Impacts of Volcanic Eruptions". In: *The Encyclopedia of Volcanoes (Second Edition)*. Ed. by H. Sigurdsson. 2nd ed. Amsterdam: Academic Press, pp. 935–942. ISBN: 978-0-12-385938-9. DOI: 10.1016/B978-0-12-385938-9.00053-5.

Rosenfeld, D. and W. Woodley (2001). "Pollution and clouds". *Phys. World* 14.2, pp. 33–38. DOI: 10.1088/2058-7058/14/2/30.

Samset, B. H. (2016). "Aerosols and Climate". In: *Oxford Research Encyclopedia of Climate Science*. Oxford University Press. DOI: 10.1093/acrefore/9780190228620.013.13. URL: https://oxfordre.com/climatescience/view/10.1093/acrefore/9780190228620.001.0001/acrefore-9780190228620-e-13.

Santer, B. D., T. M. L. Wigley, C. Doutriaux, J. S. Boyle, J. E. Hansen, P. D. Jones, G. A. Meehl, E. Roeckner, S. Sengupta, and K. E. Taylor (2001). "Accounting for the effects of volcanoes and ENSO in comparisons of modeled and observed temperature trends". *J. Geophys. Res.* 106, pp. 28033–28059. DOI: 10.1029/2000JD000189.

Santer, B. D., S. Solomon, C. Bonfils, M. D. Zelinka, J. F. Painter, F. Beltran, J. C. Fyfe, G. Johannesson, C. Mears, D. A. Ridley, J.-P. Vernier, and F. J. Wentz (2015). "Observed multivariable signals of late 20th and early 21st century volcanic activity". *Geophys. Res. Lett.* 42.2, pp. 500–509. DOI: 10.1002/2014GL062366.

Santer, B. D., T. M. L. Wigley, J. S. Boyle, D. J. Gaffen, J. J. Hnilo, D. Nychka, D. E. Parker, and K. E. Taylor (2000). "Statistical significance of trends and trend differences in layer-average atmospheric temperature time series". *J. Geophys. Res.* 106.D6, pp. 7337–7356. DOI: 10.1029/1999JD901105.

Sato, M., J. E. Hansen, M. P. McCormick, and J. B. Pollack (1993). "Stratospheric aerosol optical depths, 1850–1990". *J. Geophys. Res.* 98.D12, p. 22987. DOI: 10.1029/93jd02553.

Scaife, A., E. Guilyardi, M. Cain, and A. Gilbert (2019). "What is the El Niño-Southern Oscillation?" *Weather* 74.7, pp. 250–251. DOI: 10.1002/2013GL059160.

Schaller, N., T. Griesser, A. Fischer, A. Stickler, and S. Brönnimann (2009). "Climate effects of the 1883 Krakatoa eruption: Historical and present perspectives". *Vierteljahresschr. Naturforsch. Ges. Zürich* 154, pp. 31–40.

Scherllin-Pirscher, B., A. K. Steiner, G. Kirchengast, Y.-H. Kuo, and U. Foelsche (2011). "Empirical analysis and modeling of errors of atmospheric profiles from GPS radio occultation". *Atmos. Meas. Tech.* 4, pp. 1875–1890. DOI: 10.5194/amt-4-1875-2011.

Schwärz, M., G. Kirchengast, B. Scherllin-Pirscher, J. Schwarz, F. Ladstädter, and B. Angerer (2016). *Multi-Mission Validation by Satellite Radio Occultation – Extension Project*. Final report for ESA/ESRIN No. 01/2016. University of Graz, Austria: WEGC. 164 pp.

Schwärz, M., B. Scherllin-Pirscher, G. Kirchengast, J. Schwarz, F. Ladstädter, J. Fritzer, and J. Ramsauer (2013). *Multi-Mission Validation by Satellite Radio Occultation*. Final report for ESA/ESRIN No. 01/2013. University of Graz, Austria: WEGC. 187 pp.

Seinfeld, J. H. and S. N. Pandis (1997). *Atmospheric Chemistry and Physics. From Air Pollution to Climate Change*. 1st ed. Wiley-Interscience. ISBN: 0-471-17816-0.

Siddaway, J. M. and S. V. Petelina (2011). "Transport and evolution of the 2009 Australian Black Saturday bushfire smoke in the lower stratosphere observed by OSIRIS on Odin". *J. Geophys. Res.: Atmos* 116.D6. DOI: 10.1029/2010JD015162.

Sokolik, I. N. (2009). *The Beer-Bouguer-Lambert law. Concepts of extinction (scattering plus absorption) and emission. Schwarzschild's equation.* Lecture. URL: http://irina.eas.gatech.edu/EAS8803_Fall2009/Lec2.pdf.

Solomon, S., J. S. Daniel, R. R. Neely, J.-P. Vernier, E. G. Dutton, and L. W. Thomason (2011). "The Persistently Variable "Background" Stratospheric Aerosol Layer and Global Climate Change". *Science* 333.6044, pp. 866–870. DOI: 10.1126/science.1206027.

Steiner, A. K., B. C. Lackner, F. Ladstädter, B. Scherllin-Pirscher, U. Foelsche, and G. Kirchengast (2011). "GPS radio occultation for climate monitoring and change detection". *Radio Sci.* 46, RS0D24. DOI: 10.1029/2010RS004614.

Stocker, M., F. Ladstädter, H. Wilhelmsen, and A. K. Steiner (2019). "Quantifying Stratospheric Temperature Signals and Climate Imprints From Post-2000 Volcanic Eruptions". *Geophys. Res. Lett.* 46.21, pp. 12486–12494. DOI: 10.1029/2019GL084396.

Storch, H. von and F. W. Zwiers (1999). *Statistical Analysis in Climate Research*. Cambridge University Press. DOI: 10.1017/CBO9780511612336.

Textor, C., H.-F. Graf, C. Timmreck, and A. Robock (2004). "Emissions from volcanoes". In: *Emissions of Atmospheric Trace Compounds*. Ed. by C. Granier, P. Artaxo, and C. E. Reeves. Springer Netherlands, pp. 269–303. DOI: 10.1007/978-1-4020-2167-1_7.

Thomason, L. W. (2017). *GloSSAC Level 3 netCDF file - Version 1 [Data set]*. NASA Langley Atmospheric Science Data Center DAAC. URL: https://doi.org/10.5067/glossac-l3-v1.0.

Thomason, L. W., N. Ernest, L. Millán, L. Rieger, A. Bourassa, J.-P. Vernier, G. Manney, B. Luo, F. Arfeuille, and T. Peter (2018). "A global space-based stratospheric aerosol climatology: 1979–2016". *Earth Sys. Sci. Data* 10.1, pp. 469–492. DOI: 10.5194/essd-10-469-2018.

Timmermann, A. et al. (2018). "El Niño–Southern Oscillation complexity". *Nature* 559, pp. 535–545. DOI: 10.1038/s41586-018-0252-6.

Timmreck, C. (2012). "Modeling the climatic effects of large explosive volcanic eruptions". *WIRes. Clim. Change* 6, pp. 545–564. DOI: 10.1002/wcc.192.

Trenberth, K. (2020). *The Climate Data Guide: Nino SST Indices (Nino 1+2, 3, 3.4, 4; ONI and TNI).* Ed. by National Center for Atmospheric Research Staff. URL: https://climatedataguide.ucar.edu/climate-data/nino-sst-indices-nino-12-3-34-4-oni-and-tni. (visited on 01/21/2010).

Trepte, C. R. and M. H. Hitchman (1992). "Tropical stratospheric circulation deduced from satellite aerosol data". *Nature* 355.6361, pp. 626–628. DOI: 10.1038/355626a0.

University of East Anglia (2020). *Climate change increases the risk of wildfires confirms new review.* URL: https://www.sciencedaily.com/releases/2020/01/200114074046.htm (visited on 01/20/2020).

Vernier, J. P., J. P. Pommereau, A. Garnier, J. Pelon, N. Larsen, J. Nielsen, T. Christensen, F. Cairo, L. W. Thomason, T. Leblanc, and I. S. McDermid (2009). "Tropical stratospheric aerosol layer from CALIPSO lidar observations". *J. Geophys. Res.: Atmos* 114.D4. DOI: 10.1029/2009JD011946.

Vernier, J.-P., L. W. Thomason, J.-P. Pommereau, A. Bourassa, J. Pelon, A. Garnier, A. Hauchecorne, L. Blanot, C. Trepte, D. Degenstein, and F. Vargas (2011). "Major influence of tropical volcanic eruptions on the stratospheric aerosol layer during the last decade". *Geophys. Res. Lett.* 38.12. DOI: 10.1029/2011GL047563.

Vorob'ev, V. V. and T. G. Krasil'nikova (1994). "Estimation of the accuracy of the atmospheric refractive index recovery from Doppler shift measurements at frequencies used in the NAVSTAR system". *Izv. Atmos. Ocean. Phys.* 29, pp. 602–609.

Wallace, P. (2001). "Volcanic SO_2 emissions and the abundance and distribution of exsolved gas in magma bodies". *J. Volcanol. Geotherm. Res.* 108.1, pp. 85–106. DOI: 10.1016/S0377-0273(00)00279-1.

Wang, L. and M. J. Alexander (2009). "Gravity wave activity during stratospheric sudden warmings in the 2007–2008 Northern Hemisphere winter". *J. Geophys. Res.* 114, D18108. DOI: 10.1029/2009JD011867.

Wilhelmsen, H., F. Ladstädter, B. Scherllin-Pirscher, and A. K. Steiner (2018). "Atmospheric QBO and ENSO indices with high vertical resolution from GNSS radio occultation temperature measurements". *Atmos. Meas. Tech.* 11.3, pp. 1333–1346. DOI: 10.5194/amt-11-1333-2018.

Wirakusumah, A. D. and H. Rachmat (2017). "Impact of the 1815 Tambora Eruption to global climate change". *IOP Conf. Ser.: Earth Environ. Sci.* 71. DOI: 10.1088/1755-1315/71/1/012007.

Abstract:
Explosive volcanic eruptions, such as Pinatubo in 1991, can inject sulfur dioxide, ash and other aerosols into the stratosphere causing temperature changes and affecting climate in the short term. Recently, also small post-2000 volcanic eruptions and their effects have come into research focus. While the effects of large eruptions are well known, the impacts of smaller eruptions are hard to quantify because their signals are easily masked by natural variability. In this thesis, the temperature signals from small volcanic eruptions between 2002 and 2016 are quantified, by using new vertically resolved aerosol data and precise temperature observations from radio occultation. Applying regression analysis, we find that conventional indices used to account for natural variability, such as the El Niño–Southern Oscillation and the Quasi-Biennial Oscillation, leave large temperature residuals. This further complicates a precise quantification of the small volcanic temperature signals. Therefore, we use here variability indices, which are vertically resolved and derived directly from radio occultation temperature. Additionally, we account for collinearity between these indices and the aerosol index for a precise quantification of the volcanic temperature signals. Results show characteristic space-time signals that can be clearly associated with specific volcanic eruptions. In the lower stratosphere, robust warming signals are observed, while in the mid-stratosphere also cooling signals of some eruptions appear, possibly from upwelling of ozone poor air. We find that the volcanic contribution to the stratospheric temperature trend 2002 to 2016 is up to 20%, depending on latitude and altitude. Therefore, we conclude that detailed knowledge of the vertical structure of volcanic temperature impacts is crucial for comprehensive trend analysis to separate natural from anthropogenic driven temperature changes.

Zum Inhalt:
Explosive Vulkanausbrüche, wie des Pinatubo 1991, können Schwefeldioxid, Asche und andere Aerosole bis in die Stratosphäre einbringen und Temperaturänderungen verursachen sowie das Klima kurzfristig beeinflussen. Seit Kurzem stehen auch die Auswirkungen kleiner Vulkanausbrüche, die sich seit dem Jahr 2000 ereignet haben, im Fokus der Forschung. Während die Auswirkungen großer Eruptionen gut erforscht sind, sind jene kleinerer Eruptionen nur schwer zu quantifizieren, da ihre Signale oft durch natürliche Variabilität überlagert werden. In dieser Arbeit werden die Temperatursignale kleinerer Vulkanausbrüche zwischen 2002 und 2016 anhand von neuen, vertikal aufgelösten, Aerosoldaten und präzisen Temperaturbeobachtungen aus der Radio-Okkultation detektiert. Mittels Regressionsanalyse wurde festgestellt, dass bei Verwendung konventioneller Indizes zur Charakterisierung der natürlichen Variabilität, wie El Niño–Southern Oscillation und Quasi-Biennale Oszillation, ein großes Residuum bleibt. Dies erschwert eine genaue Quantifizierung der vulkanischen Temperatursignale. Daher werden in dieser Arbeit vertikal aufgelöste Variabilitätsindizes verwendet, welche direkt aus den Temperaturmessungen berechnet werden. Auch wird zur genauen Quantifizierung der vulkanischen Temperatursignale die Kollinearität zwischen diesen Indizes und den Aerosolen berücksichtigt. Unsere Ergebnisse zeigen charakteristische Signale im Temperaturfeld, welche eindeutig Vulkanausbrüchen zugeordnet werden können. In der unteren Stratosphäre detektieren wir robuste Erwärmungssignale während in der mittleren Stratosphäre auch Abkühlungssignale nach bestimmten Eruptionen auftreten. Der Temperaturtrend in der unteren Stratosphäre wird im Zeitraum von 2002 bis 2016 durch Vulkanausbrüche um bis zu 20% beeinflusst. Daraus schließen wir, dass für eine umfassende Analyse von Klimatrends auch der Einfluss von kleinen Vulkanen miteinbezogen werden muss.

Wegener Center for Climate and Global Change
University of Graz
Brandhofgasse 5
A-8010 Graz, Austria
www.wegcenter.at
ISBN 978-3-9504717-5-5